1990

The interactions of water and perfluorodiethyl ether with Ru(100)

Pamela Kaye Leavitt
Iowa State University

Order Number 9035091

The interactions of water and perfluorodiethyl ether with Ru(100)

Leavitt, Pamela Kaye, Ph.D.

Iowa State University, 1990

U·M·I
300 N. Zeeb Rd.
Ann Arbor, MI 48106

The interactions of water and perfluorodiethyl ether with Ru(100)

by

Pamela Kaye Leavitt

A Dissertation Submitted to the
Graduate Faculty in Partial Fulfillment of the
Requirements for the Degree of
DOCTOR OF PHILOSOPHY

Department: Chemistry
Major: Analytical Chemistry

Approved:

Signature was redacted for privacy.

In Charge of Major Work

Signature was redacted for privacy.

For the Major Department

Signature was redacted for privacy.

For the Graduate College

Iowa State University
Ames, Iowa
1990

TABLE OF CONTENTS

DEDICATION

To my family for their love and support

GENERAL INTRODUCTION

Lubrication has become an important topic of study in recent years as technological advances have moved toward smaller components with very stringent compositional requirements. With this move toward smaller and more well-characterized components, the need for very thin and uniform coats of lubricants has become more important. As a result of this rapidly advancing technology, research has been undertaken in many areas, from bench-top ellipsometry to ultra-high vacuum (UHV) surface science, to characterize the properties of lubricants and their interactions with surfaces. One class of lubricants that is commercially important is perfluoropolyether (PFPE) lubricants. These lubricants are widely used particularly in the computer and aerospace industries due to their high thermal stability and their low volatility.

Let us consider a few examples of current research in the computer disk industry to illustrate the wide variety of techniques and approaches being used to advance the understanding of lubrication. It is necessary to apply a thin layer (typically 3-5 nm) of lubricant to computer disk surfaces to prevent direct contact between the disk and the head which can result in what we commonly term "disk crashes". Perfluoropolyether lubricants are often used in this application. The thickness of the lubricant must be carefully controlled for optimum performance. If the lubricant is too thick, an increase in stiction is observed during start-up. This results in mechanical failure at the head/disk interface. On the other hand, if the lubricant layer is too thin, insufficient

protection of the head/disk interface is provided. Techniques for measuring the lubricant thickness are readily available and currently in routine use industrially. Commonly used analysis techniques are X-ray photoelectron spectroscopy (XPS), Fourier-transform infra-red spectroscopy, radioactive tracer techniques, and ellipsometry. Ellipsometry is by far the easiest of these techniques to use because it is a bench-top technique. However, no methods are currently in use industrially to measure the lubricant thickness in situ. This is important since the lubricant layer spreads out and thins as the disk rotates. But research in this area is on-going (1).

As technology improves, these lubricant layers will undoubtedly become thinner, and new and improved methods for characterizing the thickness will be required. Once these lubricants have been applied to computer disk surfaces, it is important to understand how they are held there and how readily they decompose. One group of investigators has chosen to approach the question of decomposition by studying the interactions of perfluoroalkyl polyether oils with freshly cleaved stainless steel surfaces (2). In this study, they mechanically cleave the metal surface in UHV conditions in the presence of the oil and monitor the degree and the mechanism of decomposition of the oil using XPS and thermal desorption techniques.

Another important aspect in the lubrication of computer disk surfaces is the effect of contaminants on the surface-lubricant interactions. In particular, there is a great deal of interest in the effects of water contamination (humidity) on the performance of the

lubricant. One bench-top study on this particular problem involves coadsorbing the lubricant and water on a disk surface and studying the effects of the water on the lubricant layer using optical microscopy (3).

The intent of the research in this dissertation is to advance the understanding of the surface-lubricant bonding of perfluoropolyethers and the effects of humidity on this bonding. We have chosen to approach this problem by studying the interactions of perfluorodiethyl ether with a single-crystal Ru(100) surface. We believe that perfluorodiethyl ether is a good model of the back-bone structure of perfluoropolyether lubricants. Unfortunately, the polymeric ethers do not have a sufficiently high vapor pressure for the types of experiments we have undertaken. We hope to gain an understanding of the effects of surface morphology on this system by comparing the results obtained on the row-and-trough Ru(100) surface with results available on the hexagonally close-packed Ru(001) surface. Finally, we have studied the interactions of perfluorodiethyl ether coadsorbed with water in order to gain an understanding of the molecular-level interactions between these two Lewis bases.

We have chosen to use UHV techniques to study these systems. In particular, we have primarily used thermal desorption spectroscopy (TDS) to measure the bond strength of the ether on the surface and to observe the competition between the water and the ether on the surface. We have also characterized the interactions of the water on the surface using electron energy loss spectroscopy.

Explanation of Dissertation Format

This dissertation is arranged according to the alternate style format. Three papers are included. Paper I, "Adsorption of Water on Ru(100)", appears in volume 218 of Surface Science on pages 346-362, 1989. This paper is co-authored by Davis, Dyer and Thiel. Davis helped with the electron energy loss experiments, and Dyer helped with the thermal desorption experiments which are reported in this paper. Paper II is entitled "The Interactions of Hydrogen and Oxygen with Water on Ru(100): A thermal Desorption Study". Paper III, "The Interaction of a Fluorinated Ether with a Metal Surface: Effects of Surface Morphology and Water Coadsorption" is in press in the Journal of Vacuum Science and Technology A, 1990.

PAPER I.

ADSORPTION OF WATER ON RU(100)

Adsorption of Water on Ru(100)

P. K. Leavitt, J. L. Davis, J. S. Dyer and P. A. Thiel

Ames Laboratory and Department of Chemistry

Iowa State University

Ames, Iowa 50011

ABSTRACT

We have investigated the adsorption of water on Ru(100) using electron energy loss spectroscopy and thermal desorption spectroscopy. On this row-and-trough substrate, there is a single desorption state associated with the chemisorbed layer, which shifts down from 240 to 180 K as coverage increases. There is no isotope effect, i.e., desorption spectra of H_2O are the same as those of D_2O, within experimental error. Less than 0.1 monolayers of H_2O dissociate, and exchange between chemisorbed hydrogen and D_2O is not measurable. Pre-adsorbed oxygen and hydrogen cause distinctive changes in the shapes of the water desorption peaks on Ru(100). Electron energy loss spectroscopy indicates that the extent of hydrogen-bonding increases as water coverage increases at 85 K. Upon annealing and desorption, most changes in the vibrational spectra can be attributed to decreasing coverage, with the exception of some changes in the low-frequency modes. Comparison with previous studies of the hexagonally-close-packed Ru(001) surface reveals that surface morphology plays a major role in determining the properties of water adlayers on ruthenium surfaces.

INTRODUCTION

The interaction of water with Ru(001) has been studied extensively, using a wide variety of techniques (1-8). This surface appears to be unusual in its ability to stabilize hydrogen-bonded networks of water molecules to high temperatures, giving rise to a distinctive high-temperature state in thermal desorption spectroscopy (TDS) at about 220 K (1-6). The stability of the water clusters is thought to result from the very good lattice match between the atomically-smooth, hexagonal Ru(001) surface and bulk ice, which allows the water molecules to bond to the metal surface in favorable lattice sites, while simultaneously forming hydrogen-bonded clusters with little strain. Electron energy loss spectroscopy (EELS) has shown that two sharp and distinctive loss features due to librational modes, at 690-730 and 920-980 cm^{-1}, are associated with the hydrogen-bonded clusters on the (001) face.

An isotope effect has been observed in the thermal desorption of water. This effect - suppression of the high-temperature desorption state for D_2O - is attributed to conversion from large hydrogen-bonded aggregates at high coverages, to smaller, more stable clusters as coverage falls. Conversion is slower for the heavier isotope because the molecular motions necessary for rearrangement of the hydrogen-bonded aggregates are slower (6).

Thus, both the isotope effect and the unusual high-temperature desorption state are thought to be rooted in the particular structures of the water layer which are favored by the Ru(001) substrate morphology,

rather than by any particular chemical properties of Ru metal. However, this hypothesis has been untested, since no data have been reported for a Ru surface with different morphology, and so no comparisons could be drawn. We have therefore studied the adsorption of H_2O and D_2O on the atomically-rough Ru(100) surface. This surface is arranged in rows and troughs, much like an fcc(110) surface, and the clean surface is reportedly stable against reconstruction (9, 10). Its atomic arrangement is shown in Fig. 1. While an ice-like lattice can still form on such a surface (11, 12), the distortion from bulk ice would be considerably greater than that required on the (001) plane of Ru. This strain might be reflected in a lower stability of molecularly adsorbed water, if indeed surface morphology were a determining factor.

A second important factor comes into play when comparing the chemistry of water on these two ruthenium surfaces: the possibility that water may be more prone to dissociate on the rougher surface. There is little or no dissociation on the smooth (001) face [<0.05 monolayers (1-4)]. However, ruthenium is a metal for which bulk thermodynamic parameters do not predict a strong driving force, either for dissociative or non-dissociative adsorption of water (13). It thus belongs to a category of "borderline elements" (13), in which factors such as surface roughness may favor dissociation. Indeed, other "borderline" elements such as Ni, Co, and Re exhibit more tendency to adsorb water dissociatively when the surface is rougher (13 and references therein).

The purpose of this paper is twofold: to compare the desorption states of molecular water on the (100) and (001) Ru faces, and to

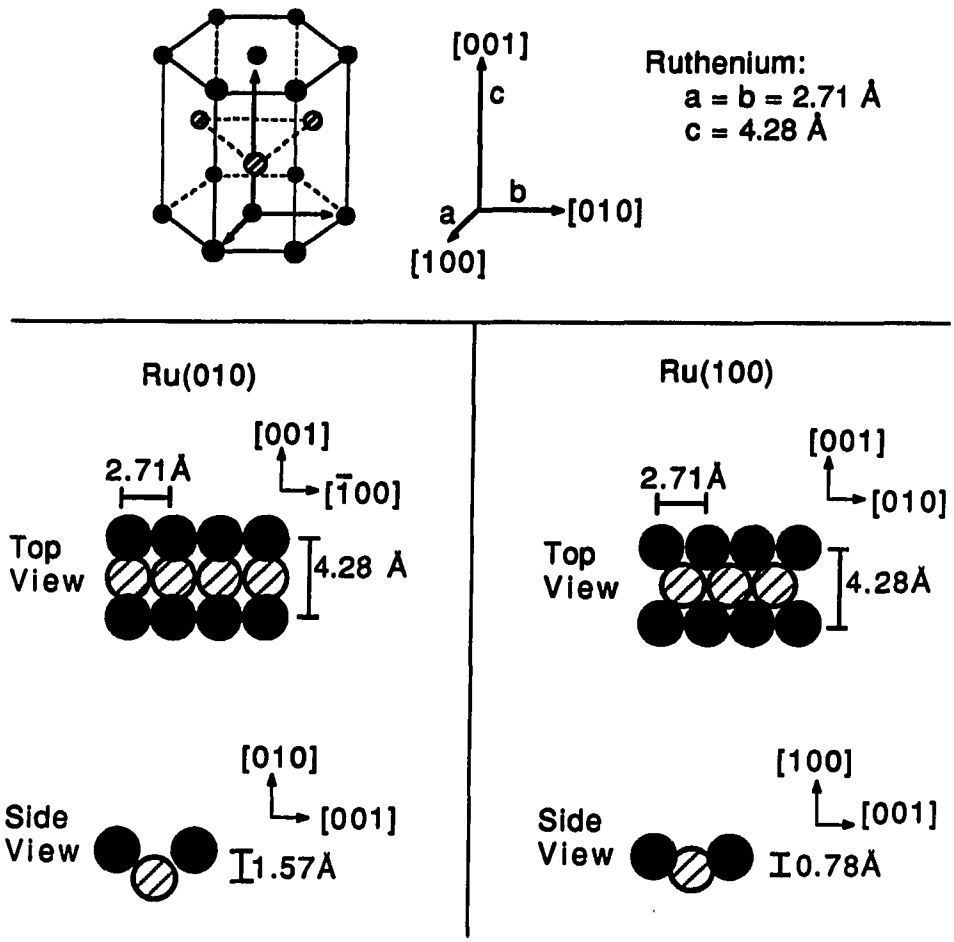

Figure 1. Arrangements of atoms, in and below, Ru(100) and (010) crystallographic planes

Both are row-and-trough arrangements, but the positions of atoms in the troughs differ. If a surface is nominally cut to the (100) plane, or the (010) plane, and if it contains a series of equally-spaced, or randomly-spaced, monatomic steps, then each arrangement shown is exposed equally. Presumably, surface free energies favor one over the other, but experimental data to this effect are unavailable. For brevity, we refer to the surface of our crystal as "(100)" in the text.

investigate the extent of dissociation on the (100) face. We find that, on the (100) face, there is a single desorption state which shifts down in temperature by 60 K as coverage increases, in contrast to the (001). There is no isotope effect in thermal desorption from Ru(100). There is little dissociation (less than 0.1 monolayer of H_2O) on the (100) surface. In addition, we show that oxygen and hydrogen strongly affect the shapes of the water desorption peaks on Ru(100). The differences between Ru(001) and (100), with respect to water chemisorption, are also reflected in the vibrational spectra of the adlayers.

EXPERIMENTAL DESCRIPTION

The experiments are performed in a stainless steel ultra-high vacuum chamber with a base pressure of ca. $1x10^{-10}$ torr. A typical base pressure during experiments is $2x10^{-10}$ Torr. The chamber is equipped with a quadrupole mass spectrometer, an electron energy loss spectrometer (EELS), and a single-pass cylindrical mirror analyzer (CMA) for Auger electron spectroscopy. There is also an ion gun for sample cleaning and a directional, effusive, molecular beam gas doser. The Ru(100) sample is cut from a single-crystal boule purchased from Materials Research Corporation. The sample, about 1 cm^2 in area, is cut and oriented to within one degree of the (100) face on both sides. The initial crystal cleaning involves a series of cycles consisting of argon ion bombardment, oxidation cycling, and high temperature annealing in vacuum to remove both silicon and oxygen until they are no longer detectable by Auger electron spectroscopy (AES). In addition, high concentrations of surface silicon are depleted by holding the sample at 700 K in 5×10^{-8} Torr H_2 for ca. 20 minutes. The extent of carbon contamination is monitored by exposing the surface to oxygen and recording the corresponding CO thermal desorption trace. When CO can no longer be detected by this procedure, the sample is annealed to 1630 K for 2 minutes and checked for complete oxygen removal with AES. The sample is heated resistively by two 0.020 inch Ta wires which are spotwelded to the sides. These same wires are attached to electrical feedthroughs in a liquid-nitrogen-coolable coldfinger (14). The sample can be cooled from 1600 to 80 K in about

five minutes. The sample temperature is measured with a thermocouple, 95% W-5% Re vs. 74% W-26% Re, spotwelded to the edge of the crystal.

The H_2O used in this study is obtained in-house. It is distilled, deionized twice on H^+/OH^- columns, passed over an organic exchange column to remove amine residues, and finally filtered for biological impurities. The D_2O, purchased from Norrell, Inc., is specified as 99.9% pure. After exchange in the dosing line, the D_2O used in the experiments is about 80% isotopically pure. Both the H_2O and D_2O are cycled through a series of freeze-pump-thaw cycles on the manifold to remove dissolved gases. Both are introduced into the UHV chamber via an all-metal doser with two apertures in series: a 2 μ conductance-limiting aperture followed by a 0.5 mm directional aperture. Exposures, ϵ, are reported in units of Torr-s, corresponding to pressure behind the 2 μ aperture multiplied by dosing time. Based on comparison between H_2O exposures obtained with the doser and exposures obtained by backfilling the chamber with H_2O, an exposure of 900 Torr-s through the doser corresponds to approximately 1 Langmuir.

The sample is cleaned between experiments by annealing to 1630 K for 2 minutes. There is no detectable oxygen signal in AES when this cleaning procedure is used.

The thermal desorption spectra are recorded using a UTI 100C quadrupole mass spectrometer located about 2.5 cm from the sample. The ionizer of the mass spectrometer is modified, after Johnson (15), to reduce the number of electrons which reach the sample surface. This modification reduces the electron current at the ~1 cm^2 sample from 10^{-5}

to 10^{-11} amps, thereby minimizing electron-stimulated desorption and dissociation. The temperature ramp is controlled by a feedback circuit (16) to obtain a heating rate of 10 K/s. The mass spectrometer and the temperature controller are both interfaced to an IBM-AT computer. This arrangement provides rapid multi-mass analysis during the temperature ramp.

The electron energy loss spectrometer is purchased from McAllister Technologies. It is a 127° sector design in a "double-C" configuration. In some situations, EELS data are acquired after heating the sample to elevated temperature (at a heating rate of 10 K/s), then cooling the sample back to $T \lesssim 100$ K.

EXPERIMENTAL RESULTS

Thermal Desorption

Thermal desorption spectra are shown in Fig. 2, for a wide range of initial exposures of H_2O and D_2O. Within experimental error, the spectra are identical for the two isotopes, at all exposures. At $\epsilon \lesssim 1500$ Torr-s, a single state (denoted "A") is visible, and at higher exposures a second state (denoted "C") develops. The A-state has two possible sources: (1) molecular water which is perturbed, relative to bulk ice, by its proximity to the metal surface; or (2) water which dissociates, but recombines to desorb in the A-state. For the reasons summarized in the discussion section, we believe that the first source predominates in the A-state. No desorption states of water are observed at T > 250 K.

The peak temperature of the A-state is shown as a function of exposure by the open circles in Fig. 3. These values are reproducible within about ±5 K, as shown by the error bar. The data of Figs. 2 and 3 show that the peak temperature of the A-state falls from ca. 240 to 180 K as coverage increases, with the majority of the drop occurring at exposures below 500 Torr-s. This range of peak temperature encompasses the full range of the <u>two</u> states (A_1 and A_2) of chemisorbed water on Ru(001), ca. 180 to 220 K (<u>1-7</u>). The C-state (not represented in Fig. 3) first appears at 160 K and increases in temperature with increasing exposure. This increase is in accord with the characteristics of zero-order desorption, i.e., of sublimation of bulk ice. In the low-coverage limit, the peak temperature of the C-state is within 10 K of that found

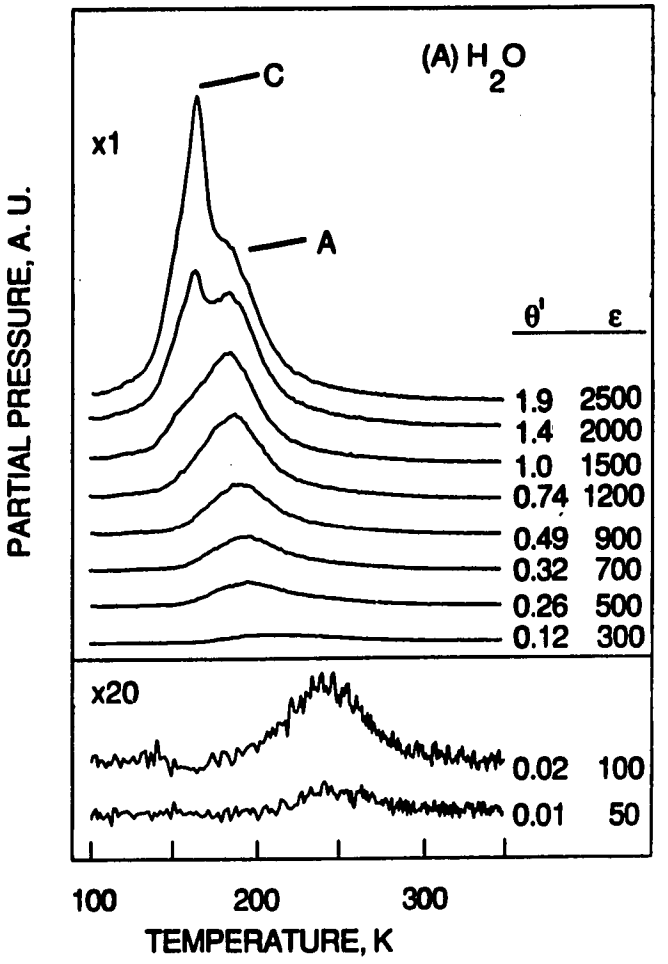

Figure 2. Thermal desorption spectra of H_2O and D_2O on Ru(100), following adsorption at 80 K

The heating rate is 10 K/s. The curves are labelled with values of the relative peak area, θ', and exposure, ϵ. A value of $\theta' = 1.0$ is arbitrarily chosen at $\epsilon = 1500$ Torr-s, where the C-state begins to appear.

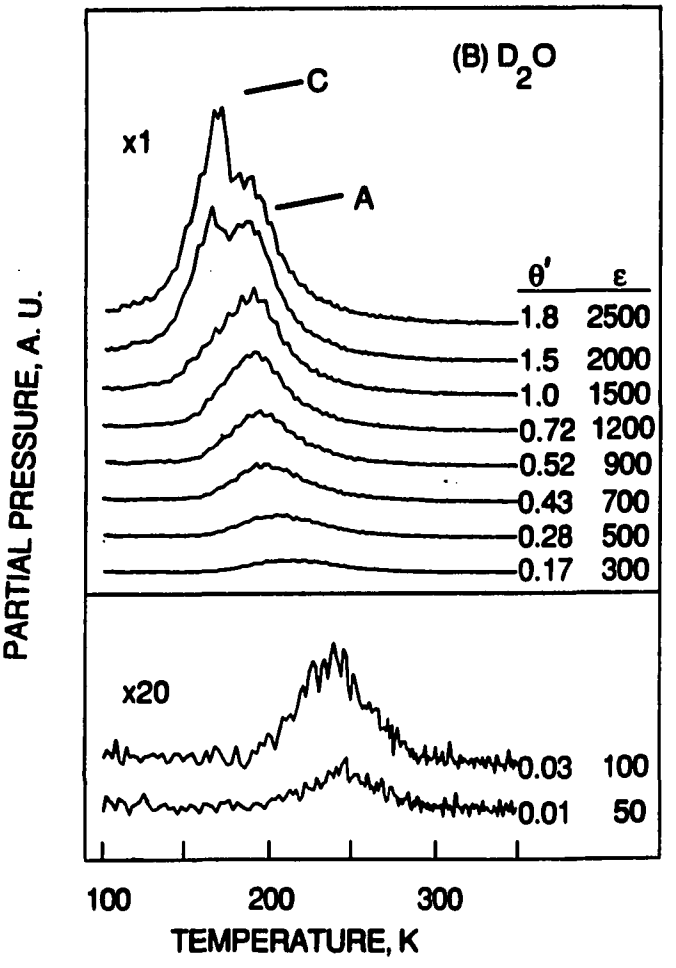

Figure 2 (Continued)

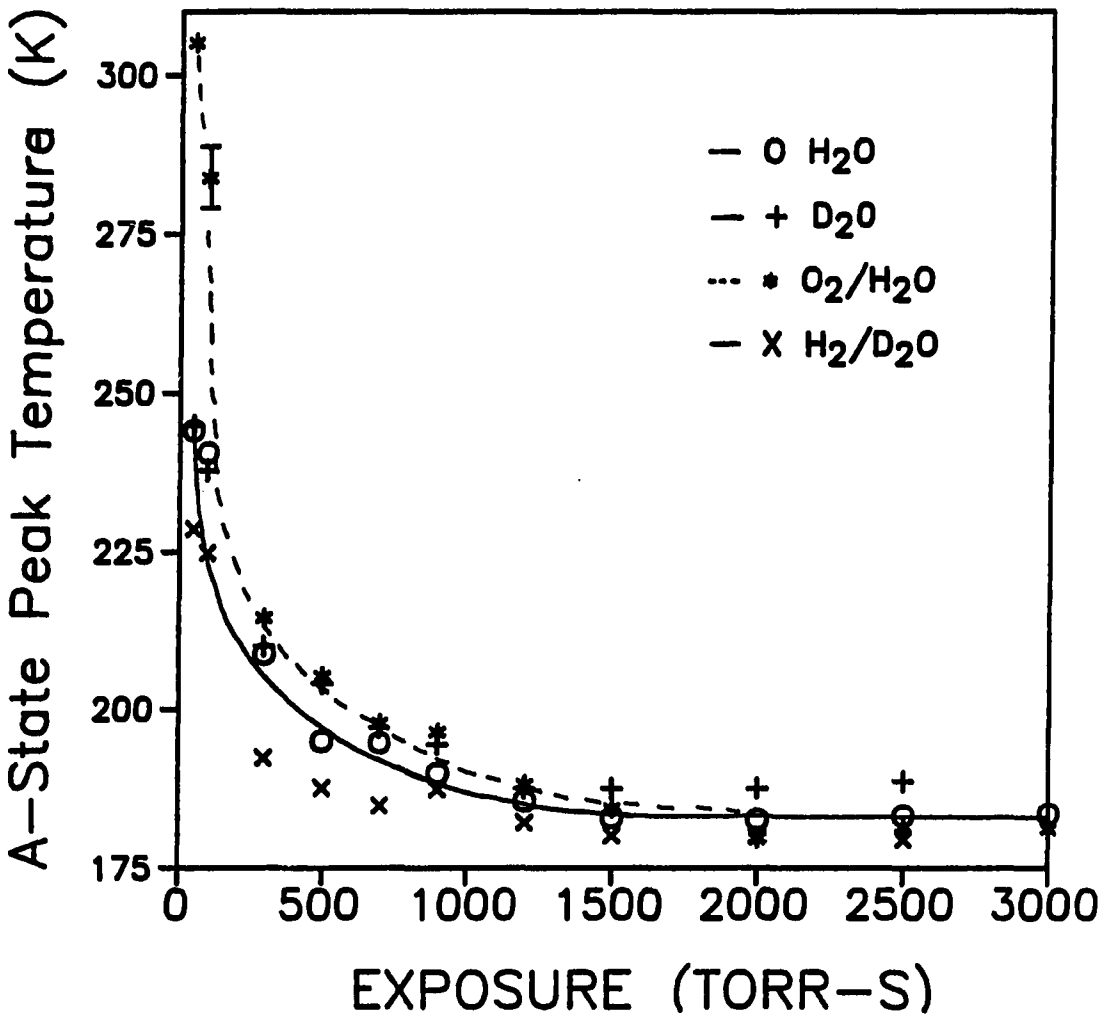

Figure 3. Peak temperatures in thermal desorption spectra of water

Open circles: H_2O peak following H_2O adsorption. Only the A-state is shown. The data are taken from Fig. 2. Stars: H_2O peak following oxygen + H_2O coadsorption. The data are taken from Fig. 6. Crosses: D_2O peak following H_2 + D_2O coadsorption. The data are taken from Fig. 6. Pluses: D_2O peak following D_2O adsorption. The data are taken from Fig. 2.

for the multilayer state on Ru(001) in many other laboratories (1-7), indicating that the multilayer is little perturbed by the metal structure.

The relative peak area, θ', of H_2O or D_2O, is shown as a function of exposure in Fig. 4. [We define $\theta' = 1$ as the point where the multilayer first appears, which is at $\epsilon \sim 1500$ Torr-s in Fig. 2.] Above 100 Torr-s, ($\theta' \gtrsim 0.05$), the data can be fit by a single straight line, with a correlation coefficient of 0.99. This indicates that the sticking coefficient (S) and the amount of dissociation are both coverage-invariant (to within at least 20%) for $\theta' \gtrsim 0.05$. The straight-line construction does not intersect the origin, indicating that most of the adsorbed water dissociates irreversibly at exposures below about 100 Torr-s ($\theta' \lesssim 0.05$).

The extent of irreversible dissociation is also reflected by the amount of H_2 evolved during the desorption ramp. As shown in Fig. 5, H_2O adsorption results in two desorption features for H_2, one centered at 170-195 K and one at 350 K. The former is probably due to desorption of H_2O followed by fragmentation in the ionizer of the mass spectrometer. We believe that the latter desorption state arises from dissociation of water and recombination of atomic hydrogen. The maximum integrated peak area of the 350 K state is approximately four times that of a background experiment (where the sample is held for the same time in vacuum prior to desorption), and is only 10% of the peak area of a saturation coverage of hydrogen on this surface. Because there is no information available regarding the absolute coverage of hydrogen at saturation on Ru(100), we

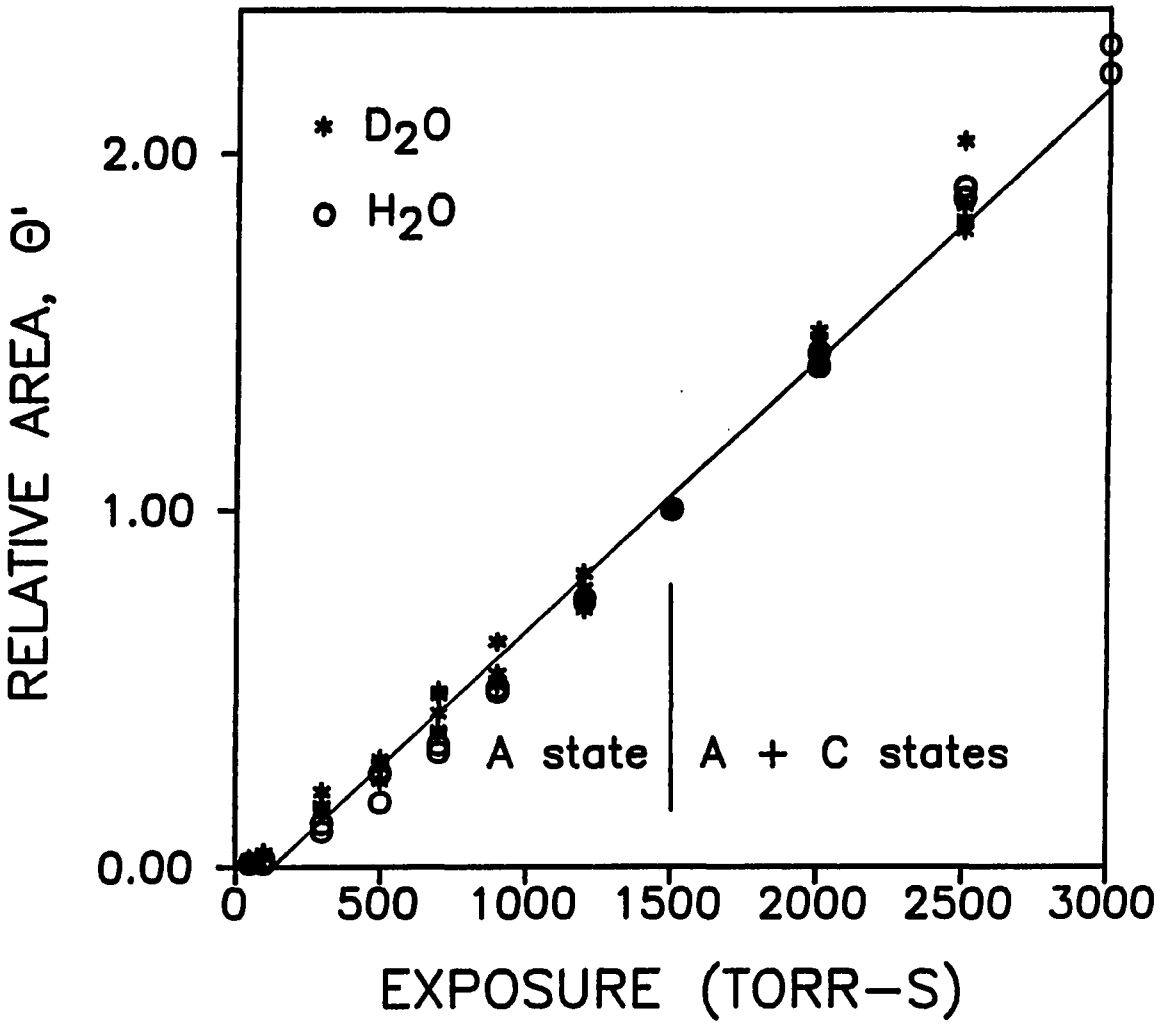

Figure 4. Relative peak area, θ′, as a function of exposure for H_2O and D_2O at 80 K

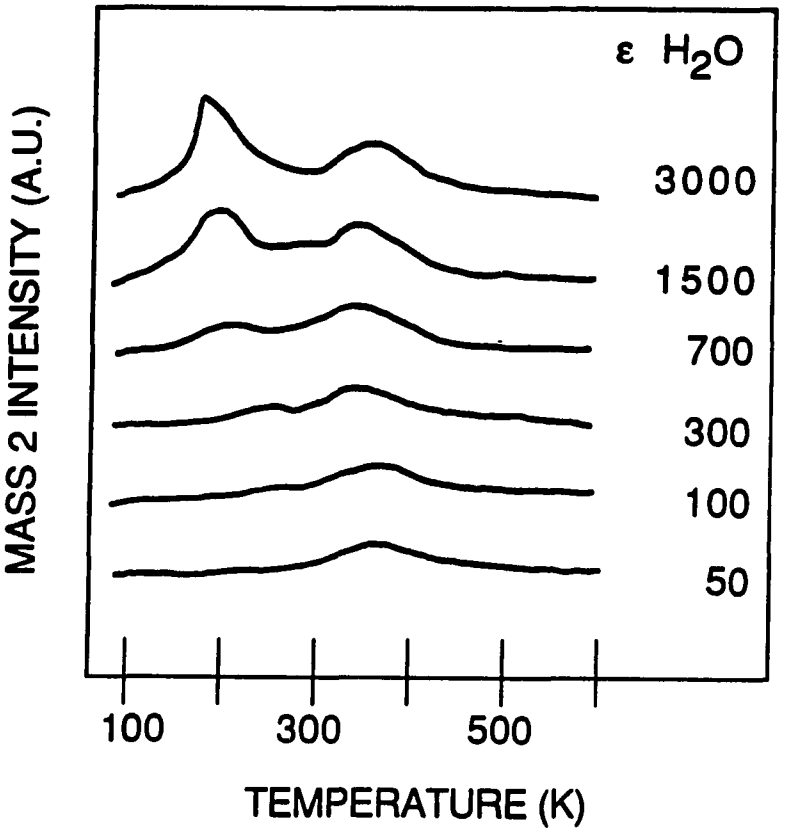

Figure 5. Thermal desorption spectra of H_2, following exposure to H_2O at 80 K

The curves are labelled with values of the water exposure, ϵ.

assume that its value lies between 1 and 2, i.e., that it lies somewhere in the range of values commonly reported for other transition metal surfaces (e.g., 17-20). Then the maximum amount of hydrogen which desorbs following water adsorption is between 0.1 and 0.2 monolayer of hydrogen, or between 0.05 and 0.1 monolayer of water. (We define one monolayer as one adsorbed particle per surface Ru atom, i.e., 9.6×10^{14} particles cm^{-2}.) We are unable to detect isotopic exchange between co-adsorbed D_2O and H_2, presumably because the amount of dissociation is so small.

Finally, the data of Fig. 6 indicate that the thermal desorption peak shape of water itself can be used as a test for gross amounts of co-adsorbed hydrogen or oxygen. Figure 6 shows thermal desorption spectra of water on a surface which is pre-treated with 2 L hydrogen or 0.5 L oxygen. The water desorption peak positions for these two sets of experiments are shown as a function of water exposure in Fig. 3. The coadsorbed hydrogen and oxygen exert two noteworthy effects on the water peak. First, at 50 and 100 Torr-s exposures of water, coadsorbed oxygen pushes the peak up close to room temperature, an increase of 50 to 65 K over the same exposure range in the absence of oxygen. Second, both hydrogen and oxygen change the shape of the peak at H_2O exposures above 1500 Torr-s. Comparison with data for this same exposure range in Fig. 2 reveals that the ice multilayer is absent in Fig. 6, or else shifted up in temperature so that it merges indistinguishably with the A-state. We favor the latter possibility, since the integrated $H_2O(D_2O)$ peak area

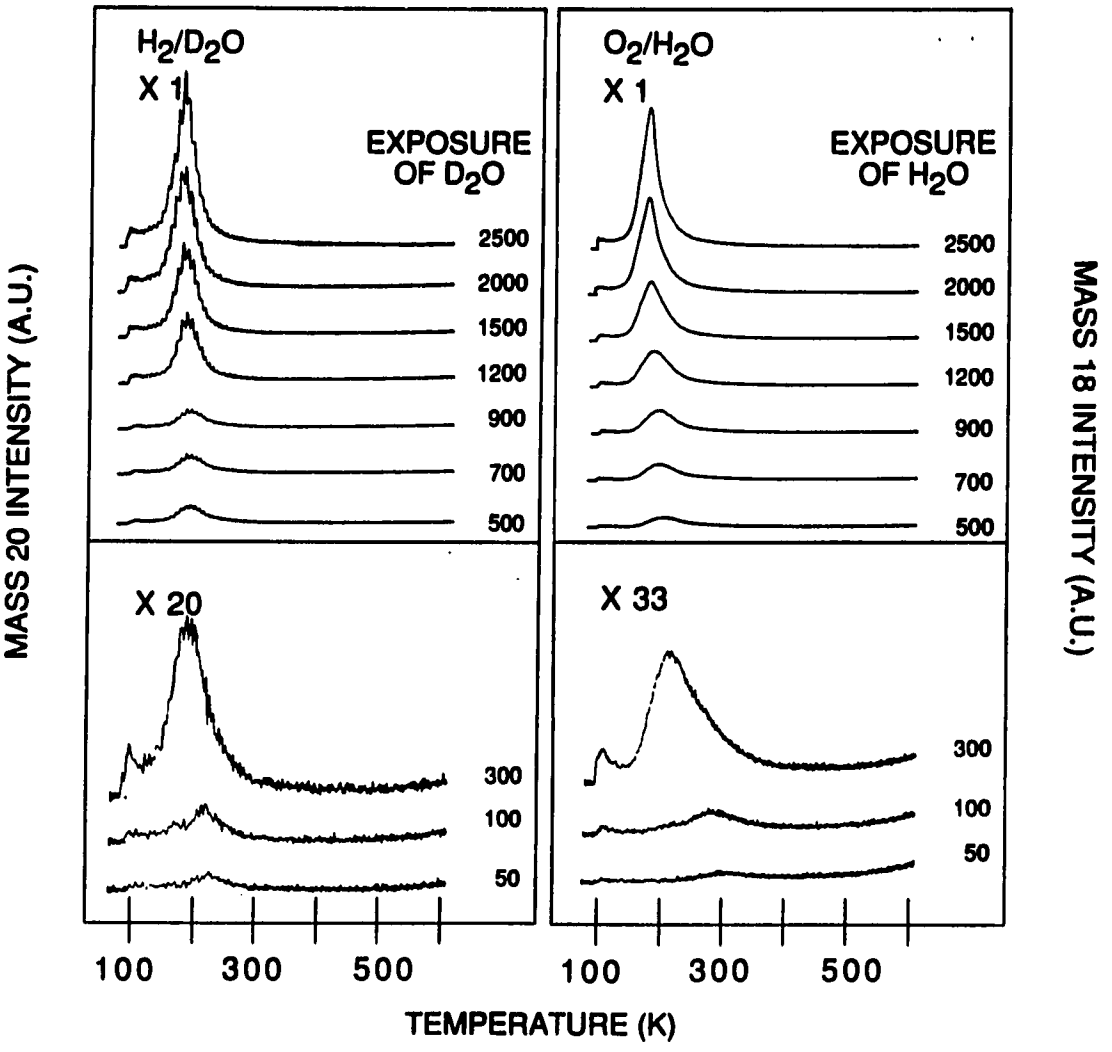

Figure 6. Thermal desorption of water (H_2O or D_2O) following exposure to H_2 or O_2

(A) 2 L H_2;
(B) 0.5 L O_2 at 80 K.
In (B), the oxygen-dosed surface is warmed to 345 K, to ensure dissociation, before exposure to water at 80 K.

increases almost linearly with exposure, much as it does in Fig. 4. This is indicative of multilayer condensation. Finally, the data of Fig. 6 indicate that a large amount of hydrogen or oxygen is not present in the spectra of Fig. 2. Otherwise, the spectra of Fig. 2 would not be so different from those of Fig. 6. Again, this is consistent with the idea that the extent of dissociation of chemisorbed water on the clean metal (as in Fig. 2) is quite small.

Electron Energy Loss Spectroscopy

Figure 7 shows EEL spectra obtained after four exposures of water on Ru(100) at 80 K. We assign the prominent features in these spectra largely by comparison with other vibrational studies of chemisorbed water (13 and references therein). The positions and assignments of the loss features, following the same four exposures at 80 K, are summarized in Table 1. Several trends can be seen in the data of Fig. 7 and Table 1. First, the O-H stretch shifts down by about 140 cm^{-1} as exposure (coverage) increases, probably due to an increasing degree of hydrogen-bonding. Second, the scissoring mode frequency shifts up by ca. 50 cm^{-1} as coverage increases. Its value at lowest coverage is essentially identical to that of the free molecule (1595 cm^{-1}), and its final value is identical to that of bulk ice (1620-1640 cm^{-1}). Again, this almost certainly reflects an increasing extent of hydrogen-bonding as coverage rises. Third, in the low-frequency region, a rather sharp, 560 cm^{-1}-feature is present after an exposure of 50 Torr-s. The assignment of this feature is discussed later. It is replaced by a broad feature at

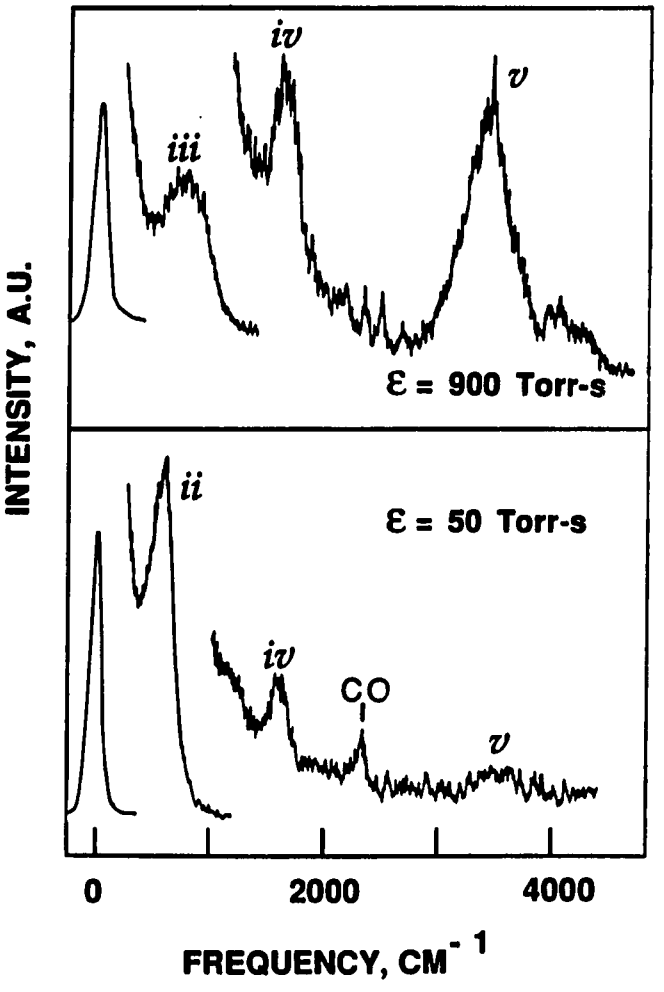

Figure 7. Electron energy loss spectra following four different H_2O exposures at 80 K

In each frame, the spectrum is successively magnified, from left to right, as follows:

50 Torr-s at 1x/100x/1000x; 1500 Torr-s at 1x/10x/100x;
900 Torr-s at 1x/30x/300x; 3000 Torr-s at 1x/30x/100x.

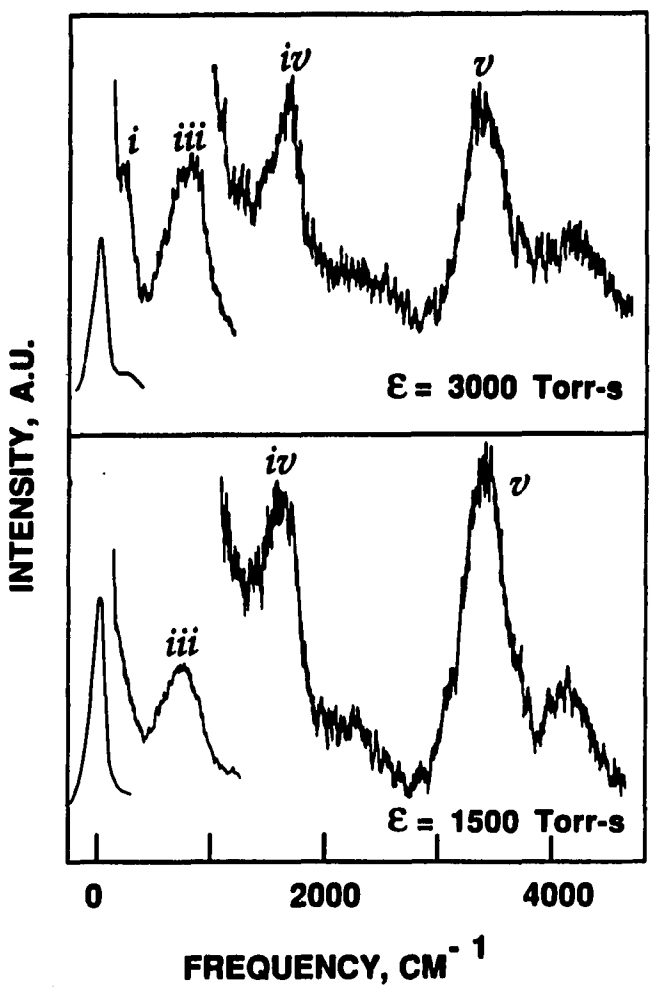

Figure 7 (Continued)

Table 1. Frequencies and assignments of loss features observed after increasing exposures of water at 80 K

Values of frequencies are quoted as $\bar{x}$ to within ± 1σ, where each set of $\bar{x}$ (the mean) and σ (the standard deviation) is obtained from three to five repetitive experiments.

	ϵ, Torr-s			
	50	900	1500	3000
(i) υ_{O-O}				190±10
(ii) $\upsilon_{H-O(H_2)}$		560±40		
(iii) δ_{lib}		715±45	735	775±20
(iv) δ_{HOH}	1590±20	1615±10	1625	1640±20
(v) υ_{OH}	3515±50	3415±45	3400	3375±35

715 to 775 cm^{-1} at higher coverage. The higher-coverage mode arises from librations (frustrated rotations). Fourth, in the low-frequency region, the oxygen-oxygen stretch of the ice lattice is visible at 190 cm^{-1}, after ice multilayers are well populated.

Figure 8 illustrates two sequences of EEL spectra taken after successive heating of water-covered surfaces. The frequencies corresponding to the peaks in these spectra are included in Table 2. The changes in the spectral features above 1000 cm^{-1} can all be attributed to H_2O desorption and decreasing coverage as the surface is heated. In contrast, the librational mode at 715 to 775 cm^{-1} *shifts* to 830-840 cm^{-1} when the temperature is raised. Also, a new feature at 345 cm^{-1} becomes apparent after heating to 160 K (see Fig. 8B). This is close to the position of the metal-water frustrated translation observed on Ru(001) at 390 to 400 cm^{-1} (2, 4). We thus assign the 345 cm^{-1} peak similarly. These latter two observations cannot be simply attributed to decreasing water coverage as the temperature rises.

The rather sharp loss feature at 555-590 cm^{-1} deserves discussion. In other H_2O/transition metal systems, EEL features in this region have been attributed to librational modes of chemisorbed water, or to metal-oxygen stretching vibrations of chemisorbed water, hydroxyl, or atomic oxygen (13 and references therein). In Fig. 8A, the peak is not readily apparent at 80 K but may be masked by the broad librational feature at 715 cm^{-1}. The 585 cm^{-1} peak emerges when the water-covered surface is heated to 185 K, and persists even after the sample is heated to 400 K and all other loss features have disappeared. In the 400 K spectra of

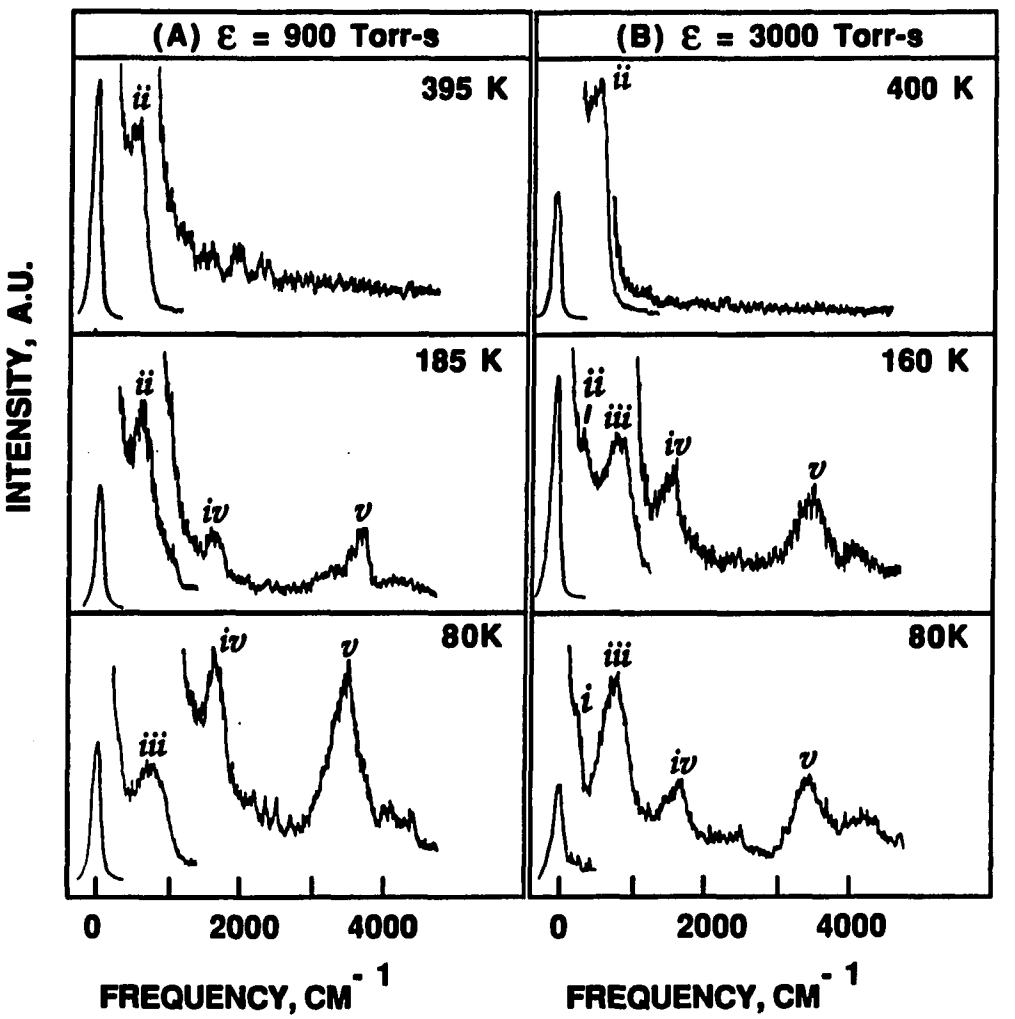

Figure 8. Electron energy loss spectra after 80 K exposure to two different H_2O coverages and successive annealing

For the corresponding desorption traces, see Fig. 2. The assignments and positions of the loss features are given in Table 2. Each spectrum is magnified, from left to right, as follows:

(A) - 80 K at 1x/30x/300x;
185K at 1x/100x/300x;
395K at 1x/100x/300x

(B) - 80 K at 1x/30x;
160K at 1x/30x/100x;
400K at 1x/300x/1000x.

Table 2. Frequencies and assignments of loss features observed when a water-covered surface is heated, following two different H_2O exposures at 80 K

Heating is accompanied by desorption, as indicated. Frequencies are quoted as $\bar{x} \pm 1\sigma$, where each set of $\bar{x}$ and σ is obtained from two experiments.

	ϵ = 900 Torr-s				ϵ = 3000 Torr-s		
	80 K	145 K (onset of desorption in C-state)	185 K (desorption peak maximum of A-state)	395 K (desorption complete)	80 K	160 K (onset of desorption in C-state)	400 K (desorption complete)
(i) ν_{O-O}					190±10		
(ii) $\nu_{M-O(H_2)}$			585	590±5		345±10	555±10
(iii) δ_{lib}	715±45	840±20			770±20	830±15	
(iv) δ_{HOH}	1615±10	1610±5	1575		1630±20	1575±10	
(v) ν_{OH}	3415±45	3460±15	3575		3345±35	3450±15	

Fig. 8, this feature undoubtedly represents the metal-oxygen stretch of atomic chemisorbed oxygen, thus indicating that some of the molecular water completely dissociates upon heating. There is never evidence for the existence of adsorbed hydroxyl, which would typically produce a distinctive M-OH bending mode in the 930 - 1190 cm^{-1} region (13) in addition to the metal-oxygen stretching mode.

A 560 cm^{-1} feature also appears after low exposures of water to Ru(100) at 80 K (see 50 Torr-s spectrum of Fig. 7). This feature is virtually identical to the peak which remains after annealing the water-covered surface to 400 K; thus, one possible interpretation is that it is due to the presence of oxygen adatoms. Furthermore, the 50 Torr-s spectrum of Fig. 7 includes features associated with molecular water, most notably the scissoring mode at 1590 cm^{-1}, but lacks features in the 930 to 1190 cm^{-1} region indicative of an adsorbed hydroxyl species. Therefore, if the foregoing assignment of the 560 cm^{-1} feature is correct, then some of the water molecules completely dissociate during the initial chemisorption of water on clean Ru(100) at 80 K, thus producing oxygen and hydrogen adatoms in addition to molecularly adsorbed water. The atomic hydrogen is presumably invisible in our EEL spectra due to its low scattering cross section (22).

Alternatively, the 560 cm^{-1} peak in Fig. 7 could be assigned to the metal-oxygen stretch and/or librational modes of molecularly chemisorbed water. Comparison with other systems does support such an assignment, since the metal-oxygen stretch varies from 390 to 660 cm^{-1}, and the librational modes range from 530 to 835 cm^{-1} (13, and references

therein). For instance, the metal-water stretch is observed at 500 - 530 cm^{-1}, for low coverages of H_2O on Rh(111) (23), very similar to the circumstances under which we observe the 560 cm^{-1} peak. However, this assignment conflicts with our interpretation of the high-coverage EEL spectra, where the 345 cm^{-1} band is attributed to the metal-oxygen stretching vibration of chemisorbed H_2O and the 700 cm^{-1} band is assigned to librations. The conflict between the low and high coverage assignments can be resolved if it is assumed that the frequency of one or both of these modes is strongly coverage-dependent on Ru(100). In other systems, it is known that librational modes can shift upward as much as 200 cm^{-1} as coverage varies from small values up to the ice multilayer (e.g., 2). Although we cannot disprove this assignment, we are skeptical that the 560 cm^{-1} features at 80 K and 400 K could coincidentally bear such a close resemblance, yet arise from entirely different adsorbates. Rather, we favor assigning the 560 cm^{-1} feature to atomic oxygen under both conditions.

In summary, the EELS data show that the extent of hydrogen-bonding increases as coverage increases at 80 K. When high coverages of water are annealed to 145-160 K, the librational feature shifts up to 830-840 cm^{-1}, an increase of at least 60 cm^{-1}, and the metal-oxygen stretch of molecular water becomes evident at 345 cm^{-1}. There is no evidence of adsorbed hydroxyl. When the water-covered surface is heated to 400 K, all of the EEL features of molecularly adsorbed water disappear, leaving only the metal-oxygen stretching vibration of atomic oxygen at 555-585 cm^{-1}. An identical feature is apparent following an exposure of

50 Torr-s at 80 K, suggesting that some water may dissociate completely to oxygen and hydrogen even at this low temperature.

DISCUSSION

Dissociation

The extent of dissociation on this surface is quite small. This statement rests upon four pieces of evidence:

(1) We cannot detect isotopic exchange between H_2 and D_2O.

(2) The shapes of the water thermal desorption peaks are affected quite strongly when atomic hydrogen or oxygen is deliberately pre-adsorbed, as in Fig. 6.

(3) The amount of hydrogen which desorbs, following adsorption of water, corresponds to an absolute coverage of 0.05 to 0.1 monolayers of water. This is small relative to the probable saturation coverage of a chemisorbed water layer, 0.50 to 1.0 monolayer. The latter numbers are obtained by assuming that the saturation coverage of water on Ru(100) is the same as that on Ni(110) (22, 11) or on Cu(110) (12), both of which are row-and-trough surfaces similar to Ru(100). The saturation coverage on Cu(110) is reportedly 1.0 (12), whereas that on Ni(110) is in question: Bange et al. report a value of 1.0 (11), whereas Griffiths et al. report 0.50 (24).

(4) The desorption yield of water as a function of coverage (Fig. 4) also reflects dissociation. The data indicate that most of the adsorbed water dissociates irreversibly at exposures below ca. 100 Torr-s. In order to use this in a quantitative way, let us assume that the absolute amount of dissociation is

constant above 100 Torr-s and that S is coverage-invariant. Then an exposure of 100 Torr-s corresponds to a coverage of 0.03 or 0.07 monolayers, depending upon whether the absolute coverage is 0.50 or 1.0 when the multilayer (C) state first appears, at ϵ = 1500 Torr-s. This value, 0.03 to 0.07, is comparable to the amount of dissociation derived from the maximum H_2 desorption yield, 0.05 to 0.1 monolayers.

We conclude, therefore, that the atomic roughness of this ruthenium surface does not act strongly to favor dissociation over molecular adsorption. The extent of dissociation is sufficiently low, in fact, that it may be attributed simply to the activity of surface defects. We estimate that $\lesssim$5% of the surface sites are defect sites, based on the quality of the crystal orientation. If dissociation occurs preferentially at defect sites, this would account for dissociation of ca. 0.05 monolayers, as observed.

Finally, the EELS data do not show evidence for formation of adsorbed hydroxyl species, under any conditions. This may result simply because the amount of adsorbed hydroxyl is smaller than our detection limit. Alternatively, one possible interpretation of the low-coverage data is that some water dissociates to atomic oxygen and hydrogen even upon adsorption at 80 K. This would be unusual, since dissociation on other transition metal surfaces is an activated process, requiring temperatures of 150 to 200 K. Further, dissociation proceeds through an adsorbed hydroxyl species on these other surfaces (13 and references therein).

Desorption States

We observe a single chemisorption state, the A-state, with a peak temperature which shifts down by 60 K as coverage increases. Its range of values, 240 to 180 K, encompasses the full range of the two states (A_1 and A_2) of chemisorbed water on Ru(001), ca. 180 to 220 K (1-7). Also, there is no isotope effect in desorption from the (100) surface. This contrasts the (001) face as well, leading us to conclude that surface morphology plays a very important role in the desorption kinetics of H_2O on Ru.

Recombination of dissociation fragments contributes little to desorption in the A-state, based upon our inability to detect isotopic mixing between H_2 and D_2O. Rather, the high peak temperatures at low coverage probably represent a relatively strong interaction between molecular water and the metal substrate. It is well-established that water acts as an electron donor (Lewis base) in bonding to metal surfaces, and as such it may be particularly attracted to the acidic on-top sites at the crests of the Ru(100) ridges. The peak temperature may decrease as coverage increases because the formation of a hydrogen-bonded network forces water molecules out of preferred adsorption sites, thus reducing the strength of the metal-water bond. In short, we propose that increasing hydrogen-bonding on this surface acts to destabilize the chemisorbed layer. The EELS data support the idea that the extent of hydrogen-bonding increases as coverage increases.

It is also interesting to compare the desorption spectra of Ru(100) with those of two other corrugated surfaces, Ni(110) and Cu(110).

Ni(110) exhibits a multiplicity of states (11, 24, 25), two of which (A_1 and A_2) fall in the range of the A-state on Ru(100). However, the positions of these peaks are invariant with coverage. Cu(110) exhibits a single chemisorption state of H_2O, at 165-175, but it shifts upward with increasing coverage (12), an effect which is also attributed to increasing hydrogen-bonding. It appears that the desorption states of H_2O on the atomically-corrugated, transition metal surfaces are very metal-specific, in contrast to the atomically-smooth, close-packed faces. In the latter case, a single chemisorption state at 170-190 K, which shifts slightly upward with increasing coverage, is the norm.

Vibrational Properties

The energy loss features, and the ways in which they change with coverage, are generally similar to those which have been observed on other metal surfaces (13). On Ru(001), strong changes in the shapes and positions of the librational modes occur when the sample is annealed to ca. 165 K (2, 4). On the (100) surface, we observe less dramatic changes when the sample is annealed to comparable temperatures. As shown by Fig. 8 and Table 2, the librational mode shifts up by ca. 60 cm^{-1}, and the metal-oxygen stretch of H_2O becomes visible at 345 cm^{-1}. Although these changes are somewhat similar to those found for Ru(001), the dramatic splitting of the librational feature into two sharp peaks is missing for Ru(100). Because these two sharp features are associated with particularly stable hydrogen-bonded clusters on the (001) face, we conclude that similar clusters cannot form on Ru (100). This is

consistent with the observation, from TDS, that water on Ru(100) becomes less stable against desorption with increasing coverage, i.e., as hydrogen-bonding becomes more extensive.

CONCLUSIONS

We have studied the interaction of water with the (100) surface of Ru. We observe only a small amount of water decomposition on Ru(100), 0.05-0.1 monolayers. Preadsorbed oxygen and hydrogen change the chemisorption peak shape drastically from that seen on the clean surface indicating that any decomposition must be a very small amount. Previous studies indicate that a similar amount of decomposition occurs on Ru(001) (1). Therefore, the atomically-rough Ru(100) substrate is not more active than the smooth (001) surface for water dissociation.

Desorption of water from the row-and-trough surface is quite dissimilar to that which has been previously observed from the hexagonally-close-packed Ru(001) surface. We observe only one chemisorption state in thermal desorption which shifts down in temperature from 240-180 K as coverage increases. This temperature range encompasses the desorption temperatures of both of the chemisorption states observed on Ru(001). Our EELS data indicate that the extent of hydrogen-bonding increases as coverage increases on Ru(100). These data, combined with the thermal desorption data - which show a shift to lower desorption temperatures as coverage is increased - suggest that hydrogen-bonding destabilizes chemisorption on this surface. This is in contrast to the situation on Ru(001). Hence, we conclude that surface morphology strongly affects the stability of water on Ru surfaces.

ACKNOWLEDGMENTS

We thank D. C. Johnson and L. Larew for supplying the purified H_2O used in this work. This research is supported by the Director for Energy Research, Office of Basic Energy Sciences. Ames Laboratory is operated for the U.S. Department of Energy by Iowa State University under Contract No. W-7405-ENG-82.

REFERENCES

1. T.E. Madey and J.T. Yates, Jr., Chem. Phys. Letters 51 (1977) 77.
2. P.A. Thiel, F.M. Hoffmann and W.H. Weinberg, J. Chem. Phys. 75 (1981) 5556.
3. D.L. Doering and T.E. Madey, Surface Sci. 123 (1982) 305.
4. P.A. Thiel, R.A. DePaola and F.M. Hoffmann, J. Chem. Phys. 80 (1984) 5326.
5. J.A. Polta, D.K. Flynn and P.A. Thiel, J. Catalysis 99 (1986) 88.
6. P.J. Schmitz, J.A. Polta, S.-L. Chang and P.A. Thiel, Surface Sci. 186 (1987) 219.
7. K. Kretzschmar, J.K. Sass, A.M. Bradshaw and S. Holloway, Surface Sci. 115 (1982) 183.
8. E.D. Williams and D.L. Doering, J. Vac. Sci. Technol. A 1 (1983) 1188.
9. R. Ku, N.A. Gjostein and H.P. Bonzel, Surface Sci. 64 (1977) 465.
10. T.W. Orent and R.S. Hansen, Surface Sci. 67 (1977) 325.
11. C. Nöbl, C. Benndorf and T.E. Madey, Surface Sci. 157 (1985) 29.
12. K. Bange, D.E. Grider, T.E. Madey and J.K. Sass, Surface Sci. 136 (1984) 38.
13. P.A. Thiel and T.E. Madey, Surface Sci. Reparts 7 (1987) 211.
14. P.A. Thiel and J.W. Anderegg, Rev. Sci. Instrum. 55 (1984) 1669.
15. A.L. Johnson, Ph.D. Dissertation, Univ. of California at Berkeley (1986).
16. H. Herz, H. Conrad and J. Küppers, J. Phys. E 12 (1979) 369.
17. K. Christmann, R.J. Behm, G. Ertl, M.A. Van Hove and W.H. Weinberg, J. Chem. Phys. 70 (1979) 4168.
18. A. Winkler and K.D. Rendulic, Surface Sci. 118 (1982) 19.
19. H. Froitzheim, H. Ibach and S. Lehwald, Phys. Rev. Letters 36 (1976) 1549.

20. T.E. Jackman, J.A. Davies, P.R. Norton, W.N. Unertl and K. Griffiths, Surface Sci. 141 (1984) L313.

21. P.A. Thiel, Ph.D. Dissertation, California Institute of Technology (1980).

22. H. Conrad, R. Scala, W. Stenzel and R. Unwin, J. Chem. Phys. 81 (1984) 6371.

23. F.T. Wagner and T.E. Moylan, Surface Sci. 191 (1987) 121.

24. K. Griffiths, U. Memmert, B.W. Callen and P.R. Norton, J. Vac. Sci. Technol. A 7 (1989) 2001.

25. J.L. Falconer and R.J. Madix, J. Catalysis 51 (1978) 47.

PAPER II.

THE INTERACTIONS OF HYDROGEN AND OXYGEN WITH WATER ON RU(100): A THERMAL DESORPTION STUDY

The Interactions of Hydrogen and Oxygen with Water on Ru(100): A Thermal Desorption Study

P. K. Leavitt and P. A. Thiel

Ames Laboratory, and Department of Chemistry
Iowa State University
Ames, Iowa 50011

ABSTRACT

We have investigated the interactions of hydrogen and oxygen coadsorbed with water on Ru(100). Low exposures of water desorb from clean Ru(100) at 240 K and this peak temperature shifts to 180 K as exposure is increased. The multilayer appears at 160 K. Pre-adsorbed oxygen moves the low exposure H_2O peak temperature up by as much as 65 K. Both coadsorbed hydrogen and oxygen force the peak temperature of the multilayer up in temperature to a point where it is no longer distinguishable from the monolayer chemisorption feature. Oxygen pre-dose experiments indicate that oxygen exhibits its greatest influence on the desorption of water from Ru(100) at an exposure of 0.25 L. The results from the oxygen pre-dosed surface are compared to results on other metal surfaces including Ru(001). The effect of surface morphology is discussed for this system.

INTRODUCTION

The interactions of water with metal surfaces have been studied extensively. The influence of coadsorbates on these systems has also been a topic of some interest. Previously, we have studied the interactions of water with Ru(100) (1). Water adsorbs primarily molecularly on this surface. One chemisorption feature is observed at 240 K at low exposures. As exposure increases the peak temperature shifts down to 180 K, and at high exposures a second feature due to desorption from a water multilayer appears at 160 K. A small amount of dissociation is observed--5 to 10% of a monolayer. No isotope effect is observed in this system when D_2O is adsorbed rather than H_2O.

In this paper we discuss the interactions of coadsorbed hydrogen with D_2O and coadsorbed oxygen with H_2O on the Ru(100) surface. The effects of coadsorbed hydrogen on the chemisorption of water on metal surfaces have not been studied extensively, but the interactions of coadsorbed oxygen with water have been a topic of some interest on various metal surfaces. Pre-dosed oxygen induces dissociation of water on several metal surface which allow molecular adsorption when clean. Among these are Ag, Cu, Ni, Pt and Pd(2 and references therein). The presence of coadsorbed oxygen on these surfaces leads to formation of adsorbed OH species. These species generally recombine with adsorbed hydrogen and desorb at ~250 K (2). This peak temperature compares to desorption temperatures of water from clean metal surfaces which generally occur below ~200 K. Other high temperature desorption features

are also observed on oxygen pre-dosed surfaces which are due to desorption of molecular water. These peaks are usually observed below 300 K under ultra-high vacuum conditions.

Low coverages of oxygen appear to be more effective in inducing the effects discussed above. The most intense features resulting from recombination and desorption of adsorbed OH species appear for oxygen pre-exposure values of ~0.25 L (2, and references therein). This exposure corresponds to an oxygen coverage of approximately 1/8 monolayer, indicating that one oxygen atom will influence the chemistry of several neighboring water molecules. Evidence of adsorbed oxygen atoms influencing the bonding of multiple water molecules is reported for many systems (3-7). Bange et al. report that 6-8 water molecules interact with a single adsorbed oxygen atom on Cu(110) (4). On this oxygen pre-dosed surface, five desorption features are observed, three of which are observed above the temperature at which molecular desorption occurs on the clean surface. The lower two of these are due to oxygen-stabilized, tightly-bound molecular water. Furthermore, the feature representative of molecular desorption from the clean surface disappears above 0.25 L oxygen pre-exposure.

The influence of preadsorbed oxygen on the desorption of water from Ru(001) is quite different from the systems discussed above. Preadsorbed oxygen does not induce dissociation and formation of an adsorbed OH species on this surface (8, 9). However, preadsorbed oxygen does force the adsorbed water molecules into their more tightly-bound state on this surface. Water desorbs from clean Ru(001) in two states, A1 and A2,

which are due to small and large hydrogen-bonded clusters on the surface, respectively. The A1 state appears at higher temperatures, and the presence of preadsorbed oxygen increases the population of this state as well as its temperature. A critical coverage of oxygen occurs at 0.5 L. At this point a maximum occurs in the conversion of water molecules from the A2 to the A1 state. Doering and Madey propose that the preadsorbed oxygen inhibits formation of the large hydrogen-bonded clusters (found in the A2 state) due to site-blocking effects (8).

In this paper, we will discuss the results obtained for coadsorption of hydrogen and oxygen with water on Ru(100) in light of the discussion above. Interestingly, preadsorption of oxygen on Ru(100) does not closely resemble any of the systems presented above.

EXPERIMENTAL PROCEDURES

The experimental apparatus and the initial sample cleaning procedure have been discussed extensively elsewhere (1). In short, the stainless steel chamber has a base pressure of 1 X 10^{-10} Torr, and is equipped with a UTI 100C mass spectrometer, a cylindrical mirror analyzer Auger spectrometer, an ion gun, and an effusive-flow gas doser. The oxygen and the hydrogen used in these experiments are purchased from Matheson Gas Co., and are specified as 99.6 and 99.99% pure, respectively. They are admitted to the chamber via variable leak valves. The water, admitted through the gas doser, has exposure units of Torr seconds corresponding to the product of pressure of water in Torr behind the conductance-limiting aperture and the dose time. As a point of reference, a 900 Torr-sec dose of H_2O using this doser corresponds to approximately 1L exposure achieved by backfilling the chamber. The H_2O is obtained in-house. The procedure used for its purification is described elsewhere (1). The D_2O is also admitted via the gas doser. It is obtained from Norrell, Inc., and is specified as 99.9% pure.

Between experiments, the sample is cleaned by a one-minute anneal to 1650 K in vacuum, to remove adsorbed oxygen. After this procedure, no oxygen is observable in the Auger spectrum.

The sample is cooled to about 90 K prior to its exposure to water, D_2O, or the coadsorbates. Following oxygen exposure, the sample is warmed to 340 K to induce dissociation of the oxygen. A heating rate of approximately 10 K/sec is used to induce desorption. Typically, masses 2

and 18 are monitored in the oxygen pre-dose experiments and either masses 2, 3, 4 and 20 or 4, 18, 19 and 20 are monitored for the hydrogen coadsorption experiments.

The D_2O is only about 70% pure as it enters the chamber. Apparently, this is a result of exchange with hydrogen on the walls of the gas manifold lines, since the D_2O itself is much purer. The purity of the D_2O prior to its entry into the gas manifold and chamber is determined by proton nmr using the method of standard additions. The method of standard additions is actually used to determine the percent water in a freshly opened D_2O standard. In this manner, the accuracy of the method can be determined. Figure 1A is a standard additions plot of integrated area under the proton nmr peak for a 1000 μl sample of a freshly opened bottle of D_2O vs. μl H_2O added. Analysis of this plot shows that there is no H_2O in the 1000 μl sample of D_2O within the accuracy of this method. The fact that the linear fit of the data crosses the x-axis on the positive side indicates that the amount of H_2O in this D_2O sample is actually negative! We know this can not be true, though, so we take this value as a measure of the uncertainty in the method. The linear fit of the data in Fig. 1A intersects the y-axis at an area of -5.3. Plugging the corresponding positive value into the linear equation, we obtain a volume of 3.9 μl, which corresponds to an uncertainty in the method of 0.4%. Figure 1B is a plot of percent H_2O vs. area of the proton nmr peak for each of the standard addition samples. The area under the unknown D_2O peak is indicated on the graph. This area corresponds to a D_2O purity of $98.1 \pm 0.4\%$.

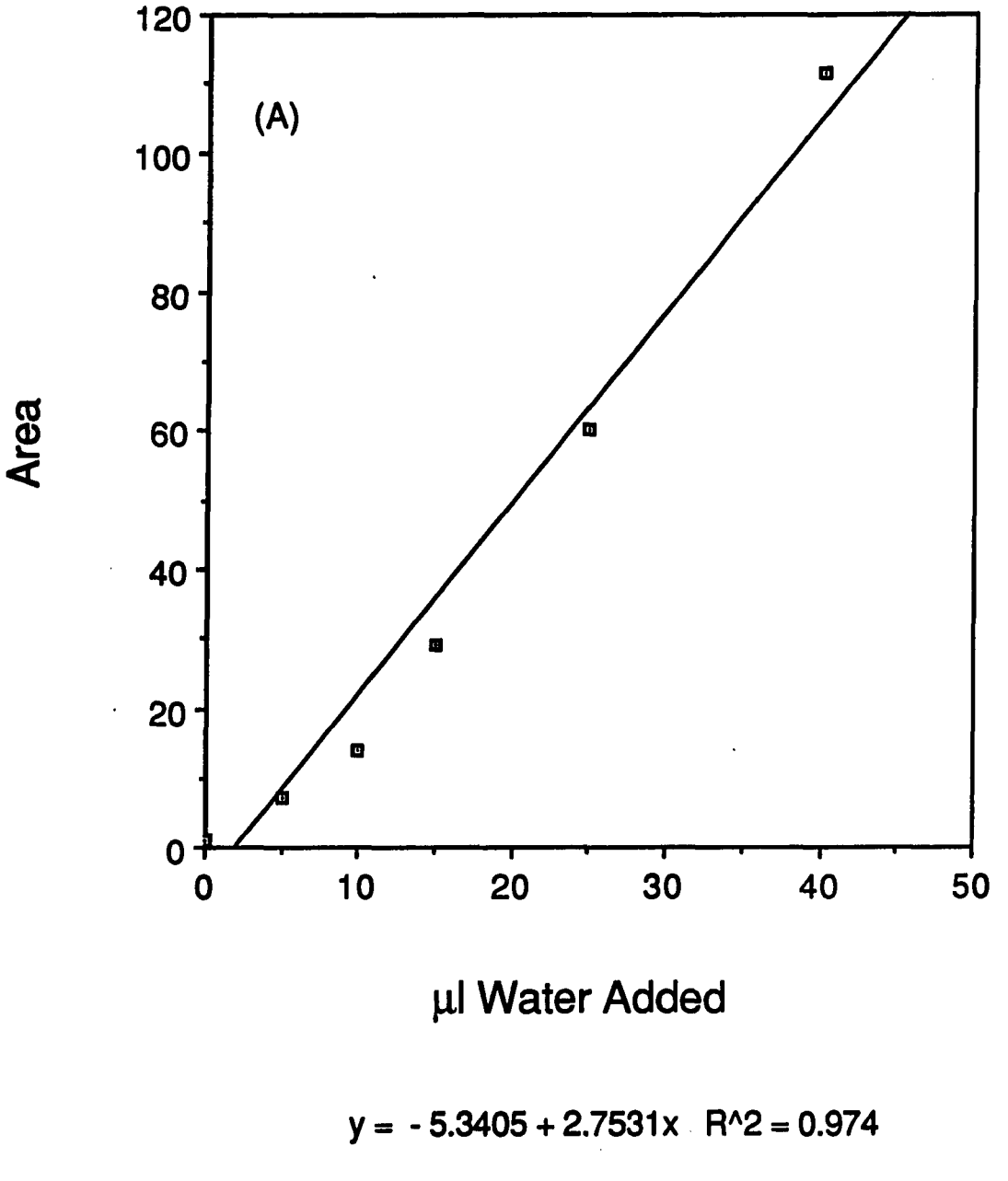

Figure 1. Standard additions plots for D_2O purity using proton nmr

Fig. 1A: μl H_2O added vs. proton nmr peak area.
Fig. 1B: Percent H_2O vs. proton nmr peak area.

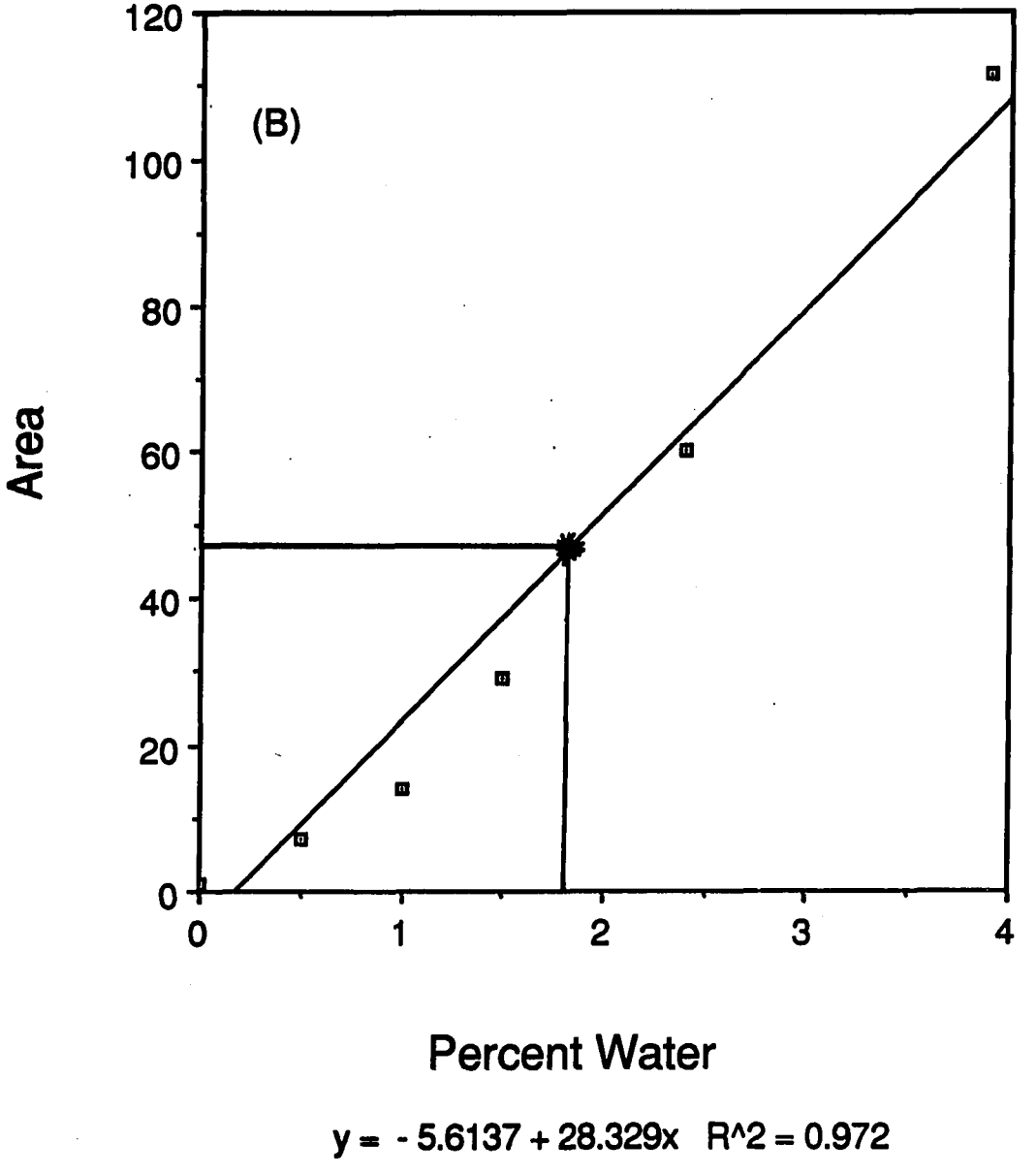

Figure 1 (Continued)

EXPERIMENTAL RESULTS

Hydrogen Coadsorption

Thermal desorption results for D_2O coadsorbed with 2 L hydrogen on Ru(100) are presented in Fig. 2. Hydrogen post-dose results are presented in Fig. 2A and hydrogen pre-dose results are plotted in Fig. 2B. Notice that the multilayer peak is indistinguishable from the monolayer desorption feature in the pre-exposure data, but appears as a separate feature in the post-dose data at the same temperature as it does on clean Ru(100). There are no other significant differences between the hydrogen pre-dose and post-dose data. Note that the hydrogen post-dose data are essentially identical to the desorption results of water from clean Ru(100), indicating that the influence of this adsorbate on the water thermal desorption is minimal to nonexistent when it is adsorbed second.

Oxygen Coadsorption

The oxygen coadsorption results are considerably more complicated than those of the hydrogen coadsorption studies. Several differences are observed in the thermal desorption of water from Ru(100) due to the presence of an oxygen coadsorbate. The most noticeable effect is the increase in the desorption temperature of water at low exposures by as much as 65 K. This effect is presented in Fig. 3 where the peak temperature of the chemisorbed state is plotted vs. H_2O exposure in Torr s for H_2O, D_2O, H_2O with oxygen pre-exposure and D_2O with hydrogen pre-

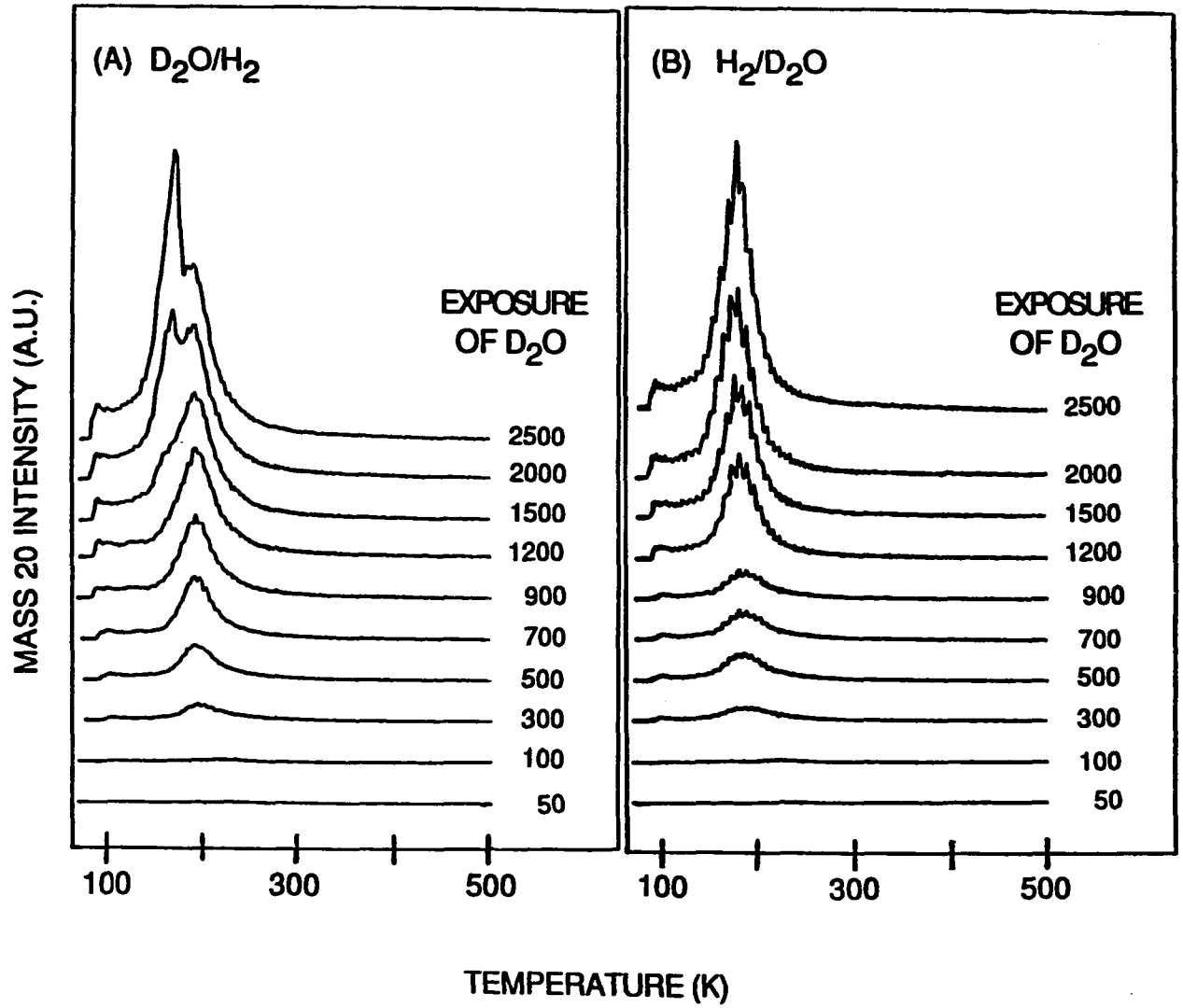

Figure 2. Thermal desorption results for water coadsorbed with hydrogen

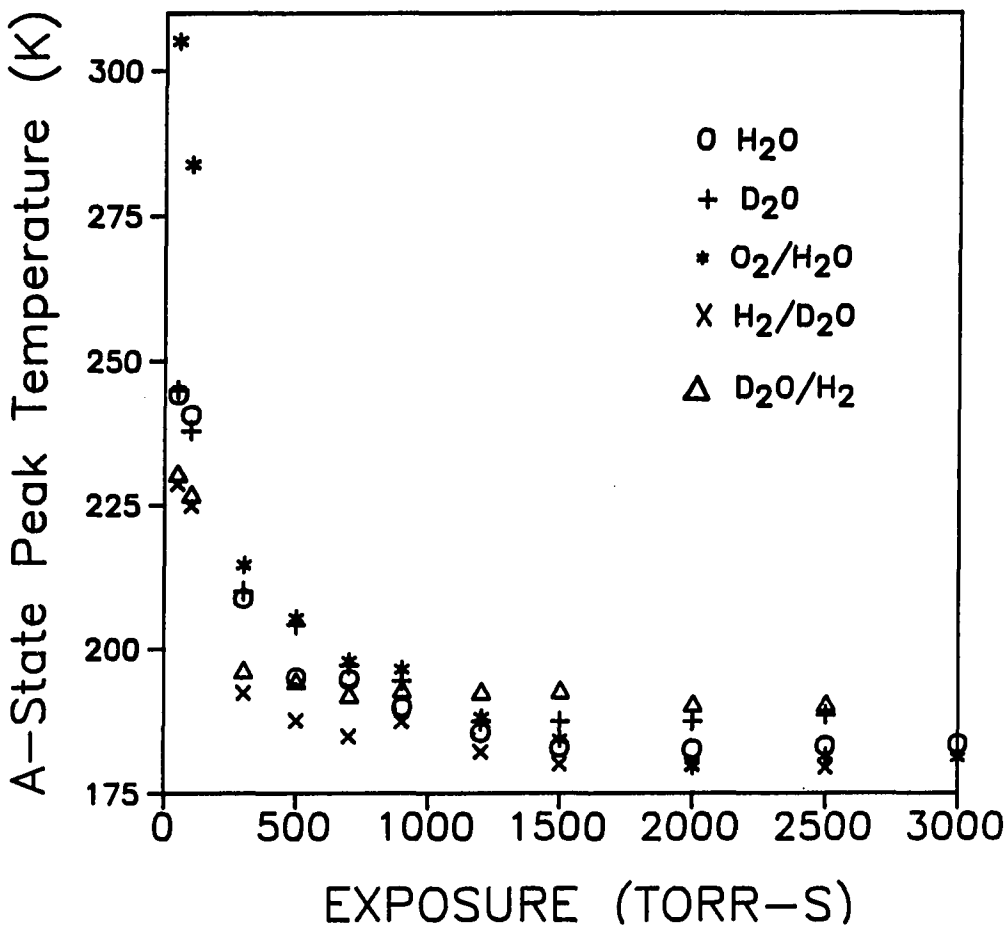

Figure 3. Peak temperature vs. water exposure for chemisorbed feature

Circles: H_2O.
Pluses: D_2O.
Stars: 0.5 L O_2/H_2O.
Crosses: 2 L H_2/D_2O.
Triangles: D_2O/2 L H_2.

dose and post-dose. Note that only the oxygen pre-dose induces this effect.

The thermal desorption results for water desorbing from Ru(100) with a 0.5 L oxygen pre-dose are presented in Fig. 4. The high exposure results are similar to those observed for the hydrogen pre-dose experiments--once again the multilayer state is forced up in temperature so that it is indistinguishable from the monolayer desorption feature.

Another trend in these spectra is not as apparent upon initial inspection. The full width at half maximum (FWHM) of the water feature appears to change in a reproducible fashion with changing water exposure. The FWHM increases with decreasing exposure from 3000 to 1500 Torr s. From 1200 to 500 Torr s the FWHM appears to be constant, and below 300 Torr s the FWHM decreases as the exposure is decreased.

The FWHM is also dependent upon the oxygen pre-dose. For water exposures less than or equal to 900 Torr s (~ 1 monolayer), the FWHM is greatest for oxygen pre-exposures of 0.1 and 0.25 L. The quarter Langmuir oxygen pre-dose appears to be an important value in these experiments as it was on several metal surfaces in which oxygen induced dissociation. Various oxygen pre-dose values were studied for water exposures of 300, 900 and 3000 Torr s. The increase in the temperature of the multilayer feature is observed at all oxygen pre-dose values studied. For the 300 and 900 Torr s water exposures with 0.25 L O_2 pre-dose, the FWHM is greatest. Figure 5 is a normalized plot of FWHM vs. oxygen pre-exposure for 300, 900, and 3000 Torr s exposures of water. The FWHM data were normalized at high oxygen coverages, so that they

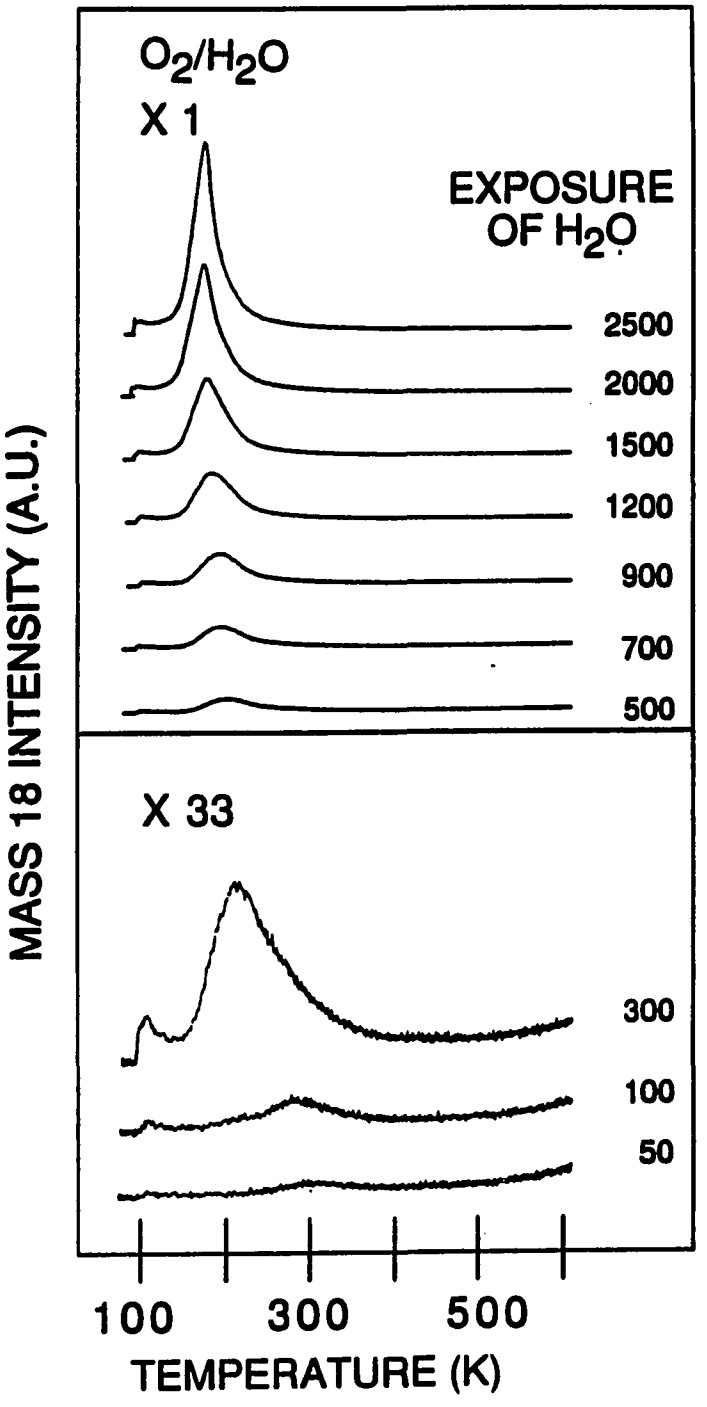

Figure 4. Thermal desorption traces of water on 0.5 L oxygen pre-dosed Ru(100)

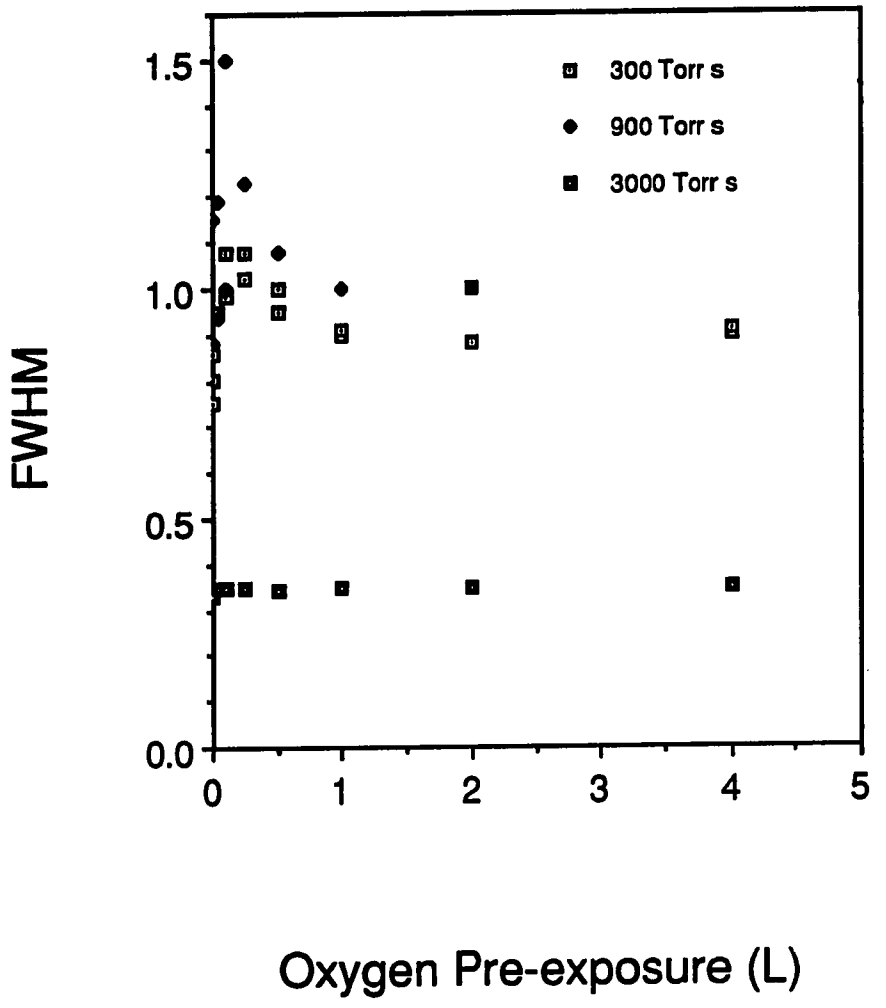

Figure 5. FWHM vs. oxygen pre-dose value for 300, 900 and 3000 Torr s water features

could all be displayed on the same graph. Above the 0.25 L oxygen pre-dose value, the high temperature hydrogen feature which is representative of the small amount of water dissociation which occurs on clean Ru(100) is also no longer observed. However, no corresponding increase in the area of the water feature is observed. (This may be a result of a lack of accuracy in measurement of peak areas, though.) For the 300 Torr s series, the 0.25 L oxygen pre-dose also results in the highest temperature desorption feature.

DISCUSSION

High Water Exposures

The following effects are observed due to coadsorption of hydrogen or oxygen with multilayer coverages of water on Ru(100):

1) The presence of 2 L of pre-dosed hydrogen forces the temperature of the multilayer up so that it is indistinguishable from the monolayer feature.

2) Reversing the adsorption order (i.e., adsorbing water first) eliminates this effect.

3) The presence of 0.5 L of pre-dosed oxygen also forces the multilayer peak temperature of water up to a point where it is indistinguishable with the monolayer feature.

4) Varying the coverage of pre-dosed oxygen from 0.1 to 4.0 L does <u>not</u> change the temperature of the observed desorption feature for greater than monolayer water exposures.

5) Pre-exposures of 0.1-0.25 L oxygen result in the highest peak temperatures and the broadest FWHM values for water exposures less than one monolayer. Above 0.25 L oxygen pre-dose, hydrogen resulting from dissociation of water is no longer observed.

The similarity in the effects of hydrogen and oxygen pre-exposures on the desorption of high coverages of water from Ru(100), lead one to believe that the mechanism for these effects is the same for the two coadsorbates. The difference between the desorption features for pre-dosed and post-dosed hydrogen indicates that a site-blocking effect is

probably occurring here, similar to that observed by Doering and Madey for water on oxygen pre-dosed Ru(001). This effect apparently is not due to thermodynamics since one would expect to see similar results upon reversing the adsorption order if this type of chemistry were involved. However, the fact that the temperature of the desorption feature observed for high water coverages does not change as the value of the oxygen pre-dose is varied, introduces doubt into the site-blocking model. Intuitively, one would predict that fewer water molecules would be affected due to site-blocking from oxygen if fewer oxygen atoms were present on the surface. The fact that this is not borne out experimentally is puzzling. One explanation that can be offered for this behavior is that one oxygen atom is influencing several water molecules, and that by a coverage of 0.1 L of oxygen the entire first monolayer of water is already affected, so no further effects will be observed as the oxygen pre-dose is increased. This explanation is plausible since one oxygen atom is known to influence the desorption characteristics of several water molecules from metal surfaces. It is interesting to note that this effect--shifting the multilayer temperature up due to the presence of hydrogen or oxygen coadsorbates--has not been observed previously.

Low Water Exposures

Coadsorbed hydrogen appears to have no effect on the thermal desorption of low exposures of water from Ru(100). Preadsorbed oxygen, on the other hand, has quite a strong effect on the desorption of small

amounts of water from this surface. Interestingly, pre-dosed oxygen appears to have its greatest influence on the desorption of low exposures of water from Ru(100) when present at a value of 0.25 L. This oxygen coverage is the value that induces the greatest degree of adsorbed OH formation on metal surfaces which dissociate water under the influence of oxygen pre-exposure. But Ru is not one of these metals! Furthermore, oxygen appears to have its greatest effect on the desorption of water from Ru(001) when it is pre-dosed at a value of 0.5 L. For a 300 Torr s exposure of water on Ru(100), 0.25 L of oxygen causes the most broadening of the FWHM and it also forces the desorption peak up to a higher temperature than any other oxygen pre-dose value. Above this oxygen exposure value, the hydrogen desorption feature indicative of the small amount of water dissociation on clean Ru(100) also disappears. One could surmise that this difference in the amount of oxygen required for its maximum effect is related to the number of available surface sites for water adsorption of the Ru(100) vs. the Ru(001) surface. Perhaps the more open Ru(100) surface has fewer surface sites available for water molecules to bond in a first layer, or perhaps water molecules prefer to form multilayer-like islands of water on this surface since the lattice match between the Ru(100) surface and the icosahedral structure of ice is much poorer than the match with the Ru(001) surface making formation of long-range hydrogen-bonded clusters more difficult on Ru(100). If either of these conditions are true, a decrease in the value of pre-dosed oxygen required to have its greatest influence on the adsorbed water molecules on Ru(100) is expected. Another explanation for this difference in the

"critical" amount of oxygen pre-exposure for Ru(100) vs. Ru(001) is simply that exposures can not be compared exactly from one vacuum system another. This is due to the fact that ion gauge sensitivities vary by a factor of two, giving rise to exposure variations from system to system since exposure rests on pressure measured by the ion gauge.

At very low water coverages (i.e., 50 Torr s), a 2 L oxygen pre-exposure pushes the water desorption temperature up by as much as 65 K. This indicates that the presence of coadsorbed oxygen strongly stabilizes the structure of low coverages of water on Ru(100). This effect is similar to the effects of preadsorbed oxygen on the desorption of water from Cu(110) reported by Bange et al. (4). They attribute this increased stabilization due to the presence of coadsorbed oxygen to a stable hydrogen-bonded structure in which pre-adsorbed oxygen plays a role.

Although many models could be proposed on the basis of the oxygen and water coadsorption results presented here, we describe a model which is consistent with all aspects of our data, and with what is known for some similar systems where water and oxygen were coadsorbed. We propose that oxygen is inducing water decomposition to H and OH at low water exposures (i.e., 50-100 Torr s). This results in the observed high-temperature desorption feature for water which is due to recombinative desorption. This assignment is in agreement with the general observation that water features desorbing above 250 K are due to recombination of H and OH (2). As water exposure is increased, we suggest that this reaction no longer occurs, but rather a stable hydrogen-bonded structure forms perhaps with oxygen acting as a "bridge" over the troughs of the

Ru(100) surface. This stable hydrogen-bonded structure containing water is similar to what Bange et al. propsed on Cu(110). Apparently, in this hydrogen-bonded structure, one oxygen atom will influence several water molecules, and there is a critical coverage at 0.25 L where oxygen is influencing as many water molecules as it can. Above this oxygen coverage, surface crowding evidently becomes a problem. As water coverage is further increased, this stable hydrogen-bonded structure is presumably prevented from forming, perhaps due to surface crowding again. The result is that the desorption temperature of the monolayer feature decreases rapidly just as we observed on clean Ru(100). This rapid decrease in peak temperature is correlated to an increase in hydrogen-bonding on the clean surface based on comparison of the electron energy loss and the thermal desorption data. We propose that this hydrogen-bonded structure is less stable than the structure that forms for low water coverages in the presence of oxygen.

It appears to be a coincidence that the hydrogen resulting from water dissociation disappears at the "critical" oxygen coverage of 0.25 L. We propose that the disappearance of this peak is simply due to recombination with the preadsorbed oxygen on the surface. It is interesting that this recombinative desorption of water does not present itself as a separate high-temperature feature. However, we expect that this feature would have very low intensity since only 5-10% of a monolayer of hydrogen is observed due to water dissociation on clean Ru(100) (1).

CONCLUSIONS

We have studied the interactions of preadsorbed hydrogen and oxygen with water on Ru(100) using thermal desorption spectroscopy. We observe an increase in the temperature of the multilayer feature for water due to the presence of preadsorbed hydrogen or oxygen. If the adsorption order is reversed in the hydrogen coadsorption experiment, this effect is not observed. Varying the amount of oxygen coadsorbed from 0.1 L to 4.0 L does not affect the degree of this shift. This shift in the temperature of the water multilayer due to the presence of hydrogen or oxygen coadsorbates has not been observed before to our knowledge.

At low water coverages, hydrogen has no effect on the water desorption. However, the oxygen pushes the water desorption temperature up by as much as 65 K at low oxygen exposures. The oxygen also appears to have its greatest effect on the water desorption at an exposure of ~0.25 L. This is interesting since the "critical value" for oxygen pre-dose on Ru(001) is 0.5 L, and since 0.25 L is the critical value for formation of OH on surfaces which are known to dissociate water in the presence of an oxygen pre-exposure. This difference in the critical pre-dose of oxygen for the two Ru surfaces may arise from a difference in the number of surface sites available for water adsorption, the difference in their ability to stabilize hydrogen-bonded structures, or simply the difference in exposure values between ultra-high vacuum chambers.

We have proposed a model which explains all of the experimental results for the oxygen coadsorption experiments, and which is also

consistent with results others have observed on similar systems. This model is certainly not the only model that could be proposed to explain the data available. More detailed experimental information is required to prove or disprove any models proposed.

ACKNOWLEDGEMENTS

We thank D.C. Johnson and L. Larew for supplying the purified H_2O used in this work. We thank D. Scott for experimental assistance in the D_2O purity studies. This research is supported by the Director for Energy Research, Office of Basic Energy Sciences. Ames Laboratory is operated for the U.S. Department of Energy by Iowa State University under Contract No. W-7405-ENG-82.

REFERENCES

1. P.K. Leavitt, J.L. Davis, J.S. Dyer and P.A. Thiel, Surface Sci. 218 (1989) 346.

2. P.A. Thiel and T.E. Madey, Surface Sci. Rep. 7 (1987) 211.

3. T.E. Madey and F.P. Netzer, Surface Sci. 117 (1982) 549; F.P. Netzer and T.E. Madey, Phys. Rev. Letters 47 (1981) 928.

4. K. Bange, D.E. Grider, T.E. Madey and J.K. Sass, Surface Sci. 137 (1984) 38.

5. E.M. Stuve, R.J. Madix and B.A. Sexton, Surface Sci. 111 (1981) 11.

6. M. Bowker, M.A. Barteau and R.J. Madix, Surface Sci. 92 (1980) 528.

7. K. Kretzschmar, J.K. Sass, A.M. Bradshaw and S. Holloway, Surface Sci. 115 (1982) 183.

8. D.L. Doering and T.E. Madey, Surface Sci. 337 (1982) 305.

9. P.A. Thiel, F.M. Hoffmann, W.H. Weinberg, Phys. Rev. Letters 49 (1982) 501.

PAPER III.

THE INTERACTION OF A FLUORINATED ETHER WITH A METAL SURFACE: EFFECTS OF SURFACE MORPHOLOGY AND WATER COADSORPTION

The Interaction of a Fluorinated Ether with a Metal Surface: Effects of Surface Morphology and Water Coadsorption

P. K. Leavitt and P. A. Thiel

Ames Laboratory, and Department of Chemistry
Iowa State University
Ames, Iowa 50011

ABSTRACT

We have investigated the interaction of perfluorodiethyl ether with Ru(100) using thermal desorption spectroscopy. The ether desorbs from the clean surface in three states: a multilayer at 120 K, and two additional states at 135 and 150 K. The latter states merge and move upward to 170 K as coverage increases. The corresponding low-coverage desorption energies are 37 and 39 kJ/mol, comparable to a value previously observed in perfluorodiethyl ether desorption from Ru(001). There is no detectable decomposition. We have also investigated the effect of water coadsorption. We find that water shifts both high-temperature states of the ether downward, to 125 and 130 K, respectively. Again, there is no detectable decomposition. The weakening of the ether-surface bond in the presence of water is discussed in terms of Lewis acid-base theory. Overall, we find that surface morphology does not strongly affect the ether-surface bond strength, but water coadsorption does.

INTRODUCTION

Perfluorinated polyethers such as Fomblin are commonly used as lubricants in the computer and aerospace industries. Their interaction with surfaces at a molecular level is not well understood, however. The purpose of this study is to model the interactions between metal surfaces and common lubricants by investigating the interactions of one simple fluorinated ether with a single-crystal metal surface in ultra-high vacuum. We purposely introduce water in order to simulate the effect of high humidity on these interactions.

Ethers are known to bond to transition metal surfaces via the lone pair electrons on the oxygen atom (1-4). The ethers donate electron density into the d-orbitals of the metal atoms. One expects that fluorination of the alkyl side chains may weaken this donation, since the electronegative fluorine atoms pull electron density away from the oxygen atom. In terms of Lewis acid-base theory, fluorination may weaken the Lewis basicity of the ether and thereby its adsorption bond strength. This expectation has been borne out by previous comparisons of fluorinated and hydrogenated ethers on Ru(001) in our laboratory (5-8).

Often, decomposition trends within a class of molecules can be used to predict the stability of particular molecules upon modification. Ethers, for instance, can be considered as modified alcohols, and the decomposition of alcohols at transition metal surfaces is fairly predictable. Most often an alkoxy species is formed, the stability of which appears to depend upon the stability of adsorbed CO, a major

decomposition product. Carbon monoxide forms a strong adsorption bond with surfaces such as Pd, Ni, Ru and W (9 and references therein). On these surfaces, alkoxy species are either not observed, or decompose below room temperature. However, on surfaces such as Cu and Ag, where CO is only weakly chemisorbed, the alkoxy species predominate to temperatures as high as 420 K (9 and references therein). There is much less information available regarding the decomposition of ethers at transition metal surfaces. Rendulic and Sexton have studied the adsorption of C_1-C_5 ethers on Pt(111) (4). They propose that these ethers form a first layer, distinguishable from the multilayer, and that 90% of this first layer desorbs molecularly. The decomposition pathway they propose for the remaining fraction involves a mechanism in which CO is formed, either in combination with adsorbed carbon and hydrogen or with alkane or unsaturated hydrocarbon fragments. This mechanism requires C-C bond scission and C-O bond scission. Basu and co-workers have studied the adsorption and decomposition of $(CF_2H)_2O$ on an Al_2O_3 surface (10). They observe C-F and C-O bond scission to form a surface formate species. Also from this group, Chen et al. have studied the decomposition of dimethyl ether on high-area alumina surfaces containing hydroxyl groups (3). They observe a surface methoxy species formed by C-O bond breaking.

It is difficult to predict the effect of fluorination on the degree of decomposition of the ethers since there is no clear decomposition pathway. However, it is clear that the C-O bond must be broken. One might guess that the fluorine atoms deplete electron density from the

molecule and thereby weaken the C-O bond, making it more prone to bond-breaking. This leads to the conclusion that decomposition may occur more easily for the fluorinated molecules. But the C-F bond is significantly stronger than the C-H bond [440 kJ/mol for C-F in C_5F_6 (11) vs. 410 kJ/mol for C-H in C_2H_6 (12)], so decomposition of the fluorinated ethers may be more difficult if C-F/C-H bond breaking is required. These competing effects make it difficult to predict the degree of decomposition for the fluorinated ethers.

The difference in the C-O bond strength for the fluorinated versus the hydrogenated ethers can be estimated by comparing the frequency of the C-O stretch in the ir spectra of these molecules. The gas-phase ir spectrum of perfluorodiethyl ether is shown in Fig. 1. This spectrum was acquired on an IBM IR-98 FTIR spectrometer. The background gas spectrum was subtracted from the ether spectrum, so the only bands appearing in this spectrum arise from vibrational stretches of perfluorodiethyl ether. The ir spectrum of perfluorodiethyl ether has been published previously, however, band assignments were not made (13). This is undoubtedly due to the fact that the bands in the region of the C-O stretch are extremely difficult to assign because the C-F stretches which also appear in the 1100-1300 cm^{-1} region of the spectrum are very unpredictable (13). There is little predictability in these stretches even within an homologous series of fluorocarbons. However, after much consideration and discussion with an expert in the field of fluorocarbon ir, we have decided to assign the 1108 cm^{-1} band to the C-O stretch of perfluorodiethyl ether (14). Assuming this assignment is correct, this

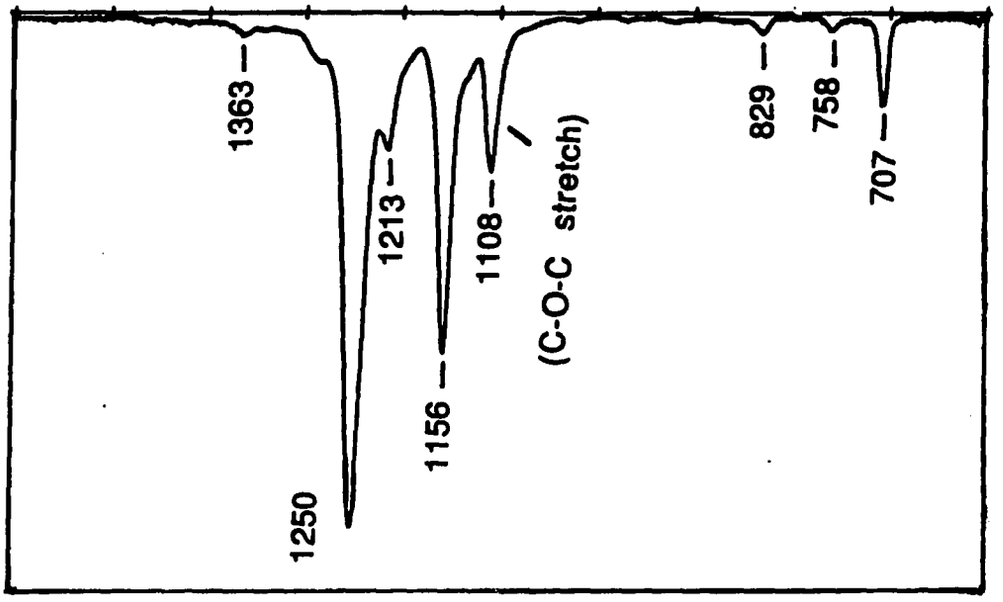

Figure 1. Infra-red spectrum of perfluorodiethyl ether

indicates that the C-O bond of perfluorodiethyl ether is slightly weaker than that of its hydrogenated analog. The C-O stretch of diethyl ether appears at 1120 cm^{-1} (15). This weakening of the C-O bond supports the supposition that fluorination pulls electron density away from this portion of the molecule, thereby weakening this bond as well as the ether-surface bond.

Previously, we have studied the interaction of several small oxygenated fluorocarbons, mainly ethers and ketones, with the atomically-smooth Ru(001) surface (5-8). In general, the fluorinated molecules form weaker bonds at the surface than their hydrogenated analogs, as predicted. We also observe significantly less decomposition of the fluorinated molecules in comparison to their hydrogenated analogs. In addition to the reason suggested above, this decrease in the degree of decomposition upon fluorination may be due to the fact that the fluorinated molecules desorb at lower temperatures than the hydrogenated ethers, and they may simply desorb before the temperatures required for bond scission can be reached. Finally, the bulkier fluorine atoms may sterically hinder the fluorinated molecules from approaching the surface closely enough to undergo the interactions necessary for dissociation.

If steric hindrance is indeed an important factor which influences decomposition of the fluorinated molecules, perhaps changing from an atomically-smooth to an atomically-rough surface morphology can affect the degree of decomposition of this important class of molecules. A main purpose of this study is to observe the effect of surface morphology on

the adsorption strength and degree of decomposition of perfluorodiethyl ether on Ru.

The Ru(100) surface is a row-and-trough type of surface, as opposed to the hexagonally-close-packed surface of Ru(001). The (100) surface is indistinguishable from the (010) surface by Laue X-ray techniques. Figure 2 is a representation of the Ru(100) and Ru(010) structures. Note that Ru(100) has a trough depth of 0.78 Å and Ru(010) has a trough depth of 1.57 Å. Presumably, surface-free-energy considerations favor one of these two surfaces over the other, but data to that effect are presently unavailable. For the duration of this manuscript, we refer to our surface as "Ru(100)", even though it is probably some combination of Ru(100) and Ru(010) faces, separated by single-atom steps.

Water and perfluorodiethyl ether are both Lewis bases. Since the electron density in the ether is more delocalized than in the compact water molecule, water is the harder of the two Lewis bases. One thus expects that these two molecules may compete for adsorption sites, and each may adversely affect bonding of the other. A second main objective of this paper is to investigate the interaction between these two adsorbates, with the practical goal of beginning to understand how water contamination or humidity may influence performance of lubricants which are in contact with metals.

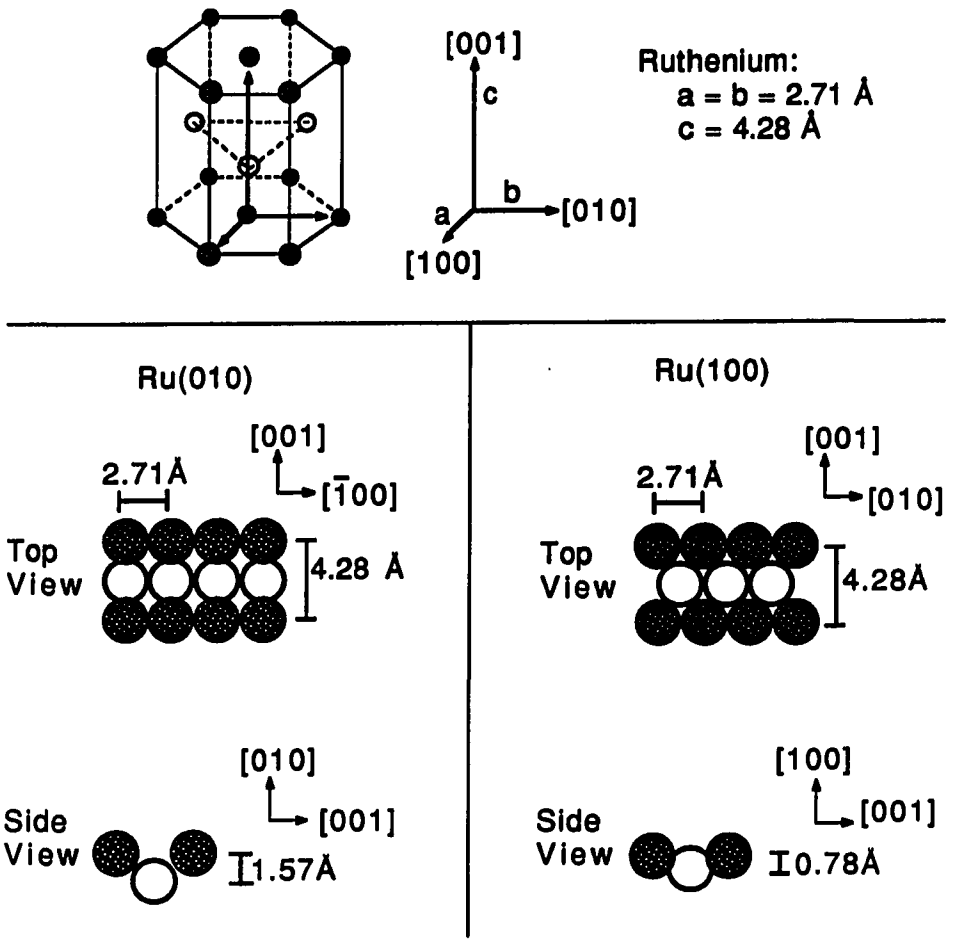

Figure 2. Representation of the atomic positions in and below the Ru(010) and Ru(100) planes

Although both are row-and-trough surfaces, the trough depth is deeper for Ru(010). Presumably the real surface (which we refer to as "Ru(100)" for brevity) is actually a mixture of the two.

EXPERIMENTAL PROCEDURES

The experimental apparatus, and the initial sample cleaning procedure, have been discussed extensively elsewhere (16). In short, the stainless steel chamber has a base pressure of 1 X 10^{-10} Torr, and is equipped with a UTI 100C mass spectrometer, a cylindrical mirror analyzer Auger spectrometer, an ion gun, and an effusive-flow gas doser. The perfluorodiethyl ether used in these experiments, purchased from Strem Chemical Co., is specified as 98% pure. The ether is introduced to the chamber via the effusive flow gas doser. The units of exposure for the ether are Torr-s, corresponding to pressure in Torr behind the conductance limiting aperture times the dose time. As a point of reference, a 900 Torr-sec dose of water using this doser corresponds to approximately 1 L exposure achieved by backfilling the chamber. The water is obtained in-house. The procedure used for its purification is described elsewhere (16). It is introduced to the chamber via a variable leak valve.

Between experiments, the sample is cleaned by exposure to 1 L of oxygen followed by monitoring mass 28 (for CO) as the sample is heated, to detect carbon residues on the surface. In general, no mass 28 signal is detectable when this procedure is used. This "titration" is followed by a one-minute anneal to 1650 K in vacuum, to remove adsorbed oxygen. After this procedure, no oxygen is observable in the Auger.

The sample is cooled to about 90 K prior to its exposure to water or ether. A heating rate of approximately 10 K/sec is used to induce

desorption. Typically, masses 19, 28, 31, 50, 69 and 119 are monitored when the ether is adsorbed alone, and masses 2 and 18 are added when water is co-adsorbed.

EXPERIMENTAL RESULTS

Desorption

Perfluorodiethyl ether

Three states are observed in the desorption of perfluorodiethyl ether from Ru(100). At low coverages, two states grow in simultaneously at ~135 K and ~150 K. We label these as α_1 and α_2. The corresponding desorption energies, calculated by the method of Redhead (17) and assuming a pre-exponential factor of 10^{13} s^{-1}, are 35 and 37 kJ/mol, respectively. These two states merge at high exposures, moving up to ~170 K. We assign these features to molecular chemisorption of perfluorodiethyl ether in a first or second layer, which is perturbed by the close proximity of the metal surface.

The third state observed in the thermal desorption spectra of perfluorodiethyl ether from Ru(100) grows in at high exposures and exhibits characteristics of a multilayer state. This peak, labelled γ, appears at ~120 K, similar to its position also on Ru(001) (5, 6). The thermal desorption spectra of perfluorodiethyl ether on Ru(100) are shown in Fig. 3.

Water Pre-adsorption

When water adsorption precedes that of the fluorinated ether, the desorption traces of both species are changed relative to those traces which would be obtained in the absence of the other adsorbate. Specifically, the water A-state (at 240 - 180 K) and the water

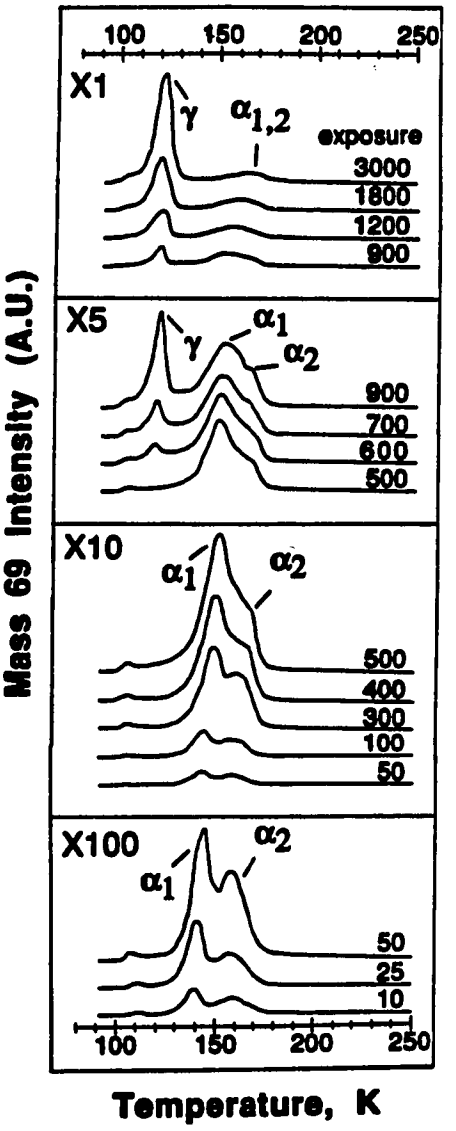

Figure 3. Thermal desorption traces of perfluorodiethyl ether on Ru(100), following adsorption at 90 K

multilayer, i.e., the C-state (at 160 K), remain unperturbed in position or shape (16, 18). Their relative populations do change, however, indicating that the ether displaces some H_2O from the A-state into the C-state. Here, we focus mainly on the traces of the fluorinated ether, which deviate more strongly from their clean-surface form. These traces are shown in Fig. 4, for two different water pre-exposures. Assuming a relative H_2O coverage of $\theta'_{H_2O} = 1.0$ at the point where the multilayer just begins to appear (16), these two H_2O coverages correspond to $\theta'_{H_2O} = 1.0$ and 1.4, as indicated in Fig. 4. The integrated area of the water desorption peaks is independent of the ether exposure, indicating that the ether does not displace the water from the surface, and these relative coverages of water are maintained in all the experiments represented by Fig. 4. The pre-adsorbed water has two main effects on ether desorption. First, the α_1 and α_2 states are less well-resolved at low coverage. Second, these states do not shift upward in temperature as coverage increases, unlike the situation for the clean surface. In other words, the presence of water shifts these peak positions downward in temperature by as much as 25 K, the shift being most pronounced at high ether exposures. Finally, the multilayer grows in at approximately the same exposure and temperature as it does in the absence of water.

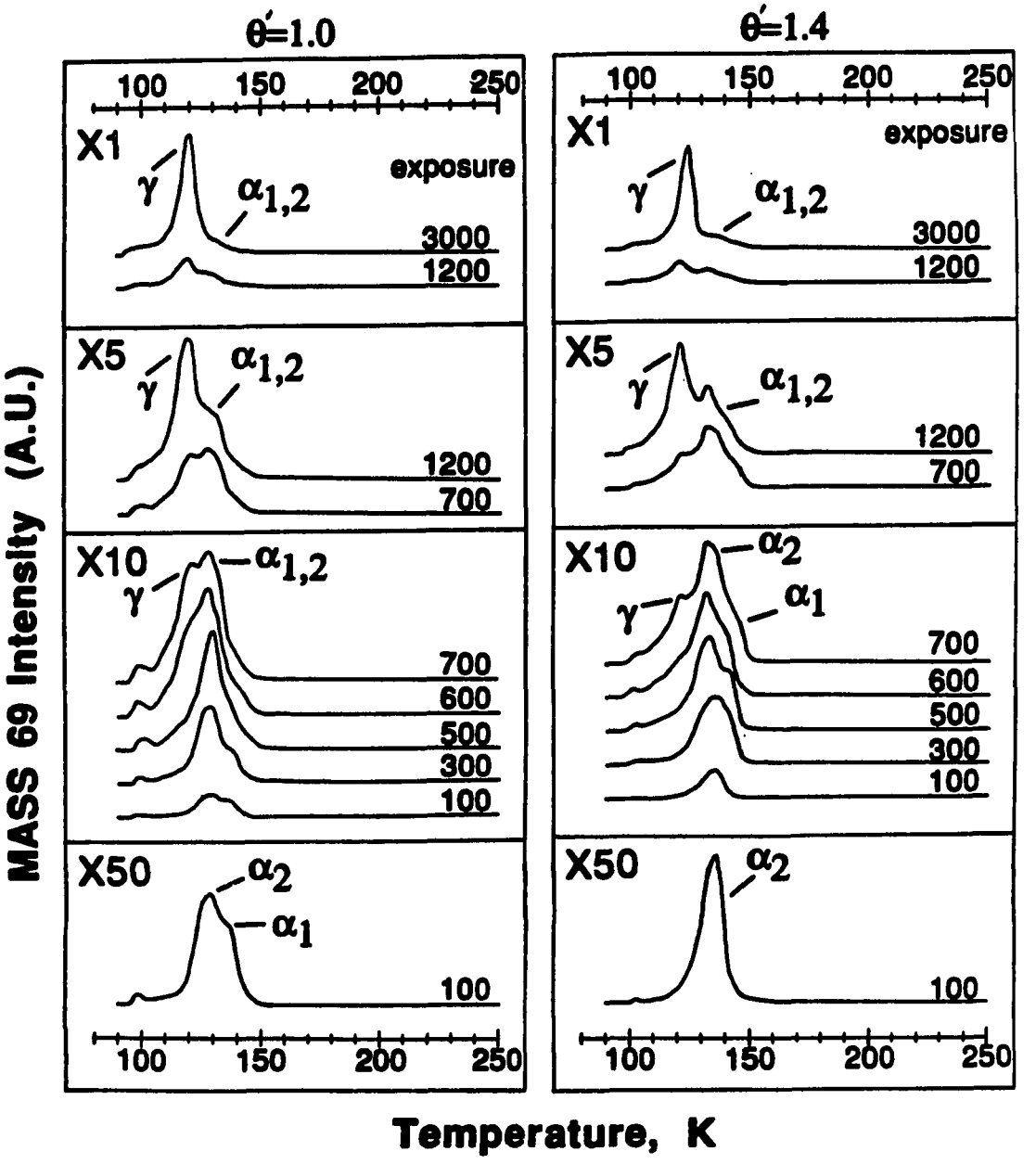

Figure 4. Thermal desorption traces for perfluorodiethyl ether/water coadsorption experiments

Decomposition

The best measure of the amount of decomposition of the perfluorodiethyl ether is in the integrated desorption peak area as a function of exposure. These data are plotted in Fig. 5 for perfluorodiethyl ether on clean and water pre-dosed Ru(100). In all cases, little or no decomposition of the ether occurs, based on the linearity of the data and the fact that the lines described by the data nearly intersect the origin. The slope of the area vs. exposure function is somewhat smaller for the water pre-dose experiments, indicating that the sticking coefficient of the ether is slightly lower in the presence of water. Also, the absence of any CO signal (i.e., absence of residual surface carbon) when the sample is titrated with oxygen between experiments is a very good indication that no decomposition occurs.

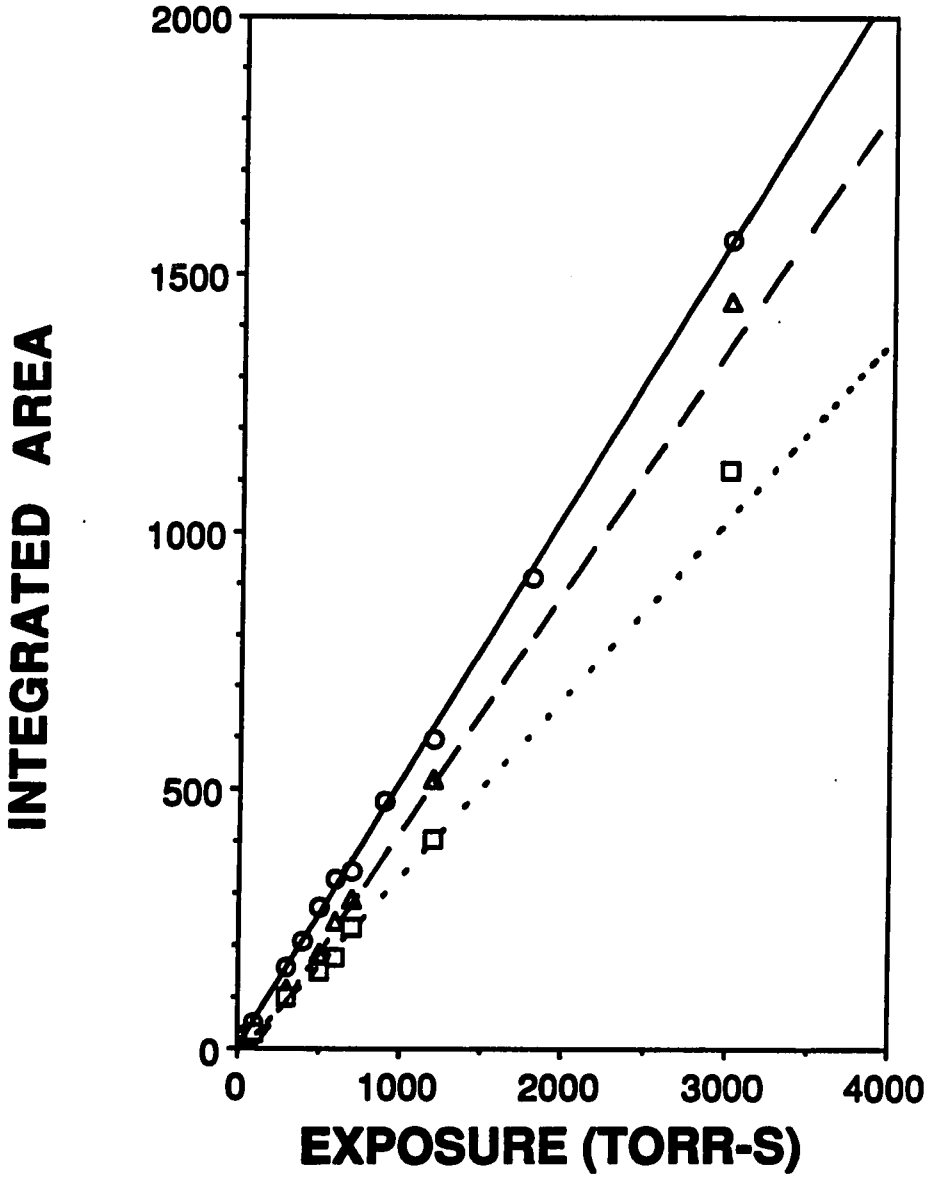

Figure 5. Integrated desorption area versus exposure for perfluorodiethyl ether on clean Ru(100) and on Ru(100) with water coverages of θ'_{H_2O}=1.0 and θ'_{H_2O}=1.4

Water is adsorbed first. The clean surface data are represented by circles and a solid line. The θ'_{H_2O}=1.0 data are represented with squares and a dotted line. θ'_{H_2O}=1.4 data are represented by triangles and a broken line.

DISCUSSION

The appearance of two sharp peaks in the desorption spectra of perfluorodiethyl ether from Ru(100) is interesting, since only one feature is observed on Ru(001) (5-8). The origin of these two peaks is unclear, but most certainly lies in the surface morphology. It is interesting to note that the relative population of the α_1 and α_2 states is not very reproducible, especially at low exposure. It may be that the number of surface sites available for the α_1 and α_2 states is variable. Recall that this surface is most probably a combination of Ru(100) and Ru(010) planes. We suspect that the number and/or size of the 'patches' of each type of crystallographic orientation may change when the sample is annealed between experiments, thereby making one state or the other prevalent in a given experiment. We expect that the ether will bond through the oxygen, and that the oxygen will sit on the more electropositive on-top sites so that it can freely donate electron density to the metal surface. This may then leave the perfluorinated side chains to fall into or above the troughs. The only difference between these two surfaces is the trough depth, as shown in Fig. 2. It may be that the (010) surface, with its deeper troughs, can allow the oxygen of the perfluorodiethyl ether to approach the surface more closely before the fluorinated side chains begin to be repelled by the electronegativity of the trough.

Note that the desorption energies of the α states, 37 and 39 kJ/mol, are similar to that of the single desorption state observed on Ru(001),

at 42-43 kJ/mol. We therefore conclude that surface morphology does not play a large role in the strength of the ether-surface bond.

The interaction between the fluorinated ether and coadsorbed water is complex. The ether displaces some chemisorbed water into the multilayer, while its own adsorption bond strength is weakened by the presence of water. It is clear that there is a competition between these two adsorbates, for adsorption sites and/or for more subtle electronic factors which influence the surface bond strength. One approach to understanding these data is to use Lewis acid-base theory. An important rule of thumb in Lewis acid-base theory is that hard acids prefer to bond with hard bases and soft acids prefer to interact with soft bases, where the adjectives "hard" and "soft" refer to the polarizability of the molecule (18). An important exception to this rule which may be relevant for the present work is a concept called symbiosis (19). This phenomenon occurs in metal ligand systems. Once a metal has formed a bond with a ligand, be it hard or soft, the metal tends to bond to only ligands of that kind.

According to Lewis acid-base theory, a metal surface can act as either a soft Lewis acid or a soft Lewis base (20). Several interactions must be considered when discussing this system in terms of Lewis acid-base theory. First of all, the surface and the ether are a soft acid and a soft base, respectively, making a strong interaction between the two likely. Secondly, water, which is a hard Lewis base, is stronger than the ether, and is also the preadsorbed ligand. We have determined experimentally that water weakens the ether surface bond strength. This

interaction can be explained in one of two ways; either the water, being the stronger base, donates enough electron density to the surface to make formation of the ether-surface bond more difficult, or the metal surface forms ether-surface bonds less readily due to the symbiosis effect. Since the water, a hard Lewis base, is preadsorbed, the surface may subsequently tend to bond only to other hard Lewis bases. Diethyl ether is also a hard Lewis base, which should be softened upon fluorination. Fluorination is known to increase the polarizability of hydrocarbons (2.85 A^3 for CF_4 vs. 2.60 A^3 for CH_4) (21), and increasing this parameter softens a molecule. Since polarizability values for both diethyl ether and perfluorodiethyl ether are not available in the literature, the extent of softening upon fluorination is unclear. However, the polarizability difference between CF_4 and CH_4 is small compared to the range of polarizabilities published (~0.2 to 14) (21) for various molecules ranging from hard to soft, suggesting that the polarizability difference alone between water and perfluorodiethyl ether is not enough to cause a symbiosis effect. We intend to continue this study with a series of water post-dose experiments, which should lend some insight into which of these two models is correct. If symbiosis is the dominating factor in this system, then preadsorbing the ether should show an ether-surface bond strength similar to that observed in the absence of water. However, if the strength of the two bases is the important factor in this system, the presence of the water may still weaken the interaction between the ether and the metal surface.

CONCLUSIONS

We have studied the desorption of perfluorodiethyl ether from clean Ru(100), and from water pre-dosed Ru(100). Perfluorodiethyl ether desorbs from the clean surface in two chemisorption features at 135 K and 150 K, with desorption energies similar to that of the single desorption state observed on Ru(001). Water decreases the desorption temperature of these chemisorption states by as much as 25 K. This is an example of a hard Lewis base (water) weakening the interaction between a soft Lewis base (the ether) and a soft Lewis acid (the metal).

Water is only slightly affected by the presence of the coadsorbed ether. Similar peak temperatures and peak shapes are observed. However, some of the water is displaced from the chemisorbed A-state into the multilayer C-state. This indicates that the interactions ocurring between these coadsorbates can not be explained with any simple model.

Little or no decomposition occurs on either the clean or the water pre-dosed surface. This stability against decomposition is a general property of the perfluorinated monoethers (5-8).

We conclude from this study that surface morphology does not affect the strength of the ether-surface bond for perfluorodiethyl ether, but water pre-adsorption does. The electronegative water coadsorbate weakens the ether-surface bond strength. On a more practical note, this study indicates that conditions of high humidity may weaken metal-lubricant interactions.

ACKNOWLEDGEMENTS

This research is supported by the Director for Energy Research, Office of Basic Energy Sciences. Ames Laboratory is operated for the U.S. Department of Energy by Iowa State University under Contract No. W-7405-ENG-82.

REFERENCES

1. H. Luth, G.W. Rubloff and W.D. Grobman, Surface Sci. 63 (1977) 325.

2. B.A. Sexton and A.E. Hughes, Surface Sci. 140 (1984) 227.

3. J.G. Chen, P. Basu, T.J. Ballinger and J.T. Yates, Jr., Langmuir 5 (1989) 352.

4. K.D. Rendulić and B.A. Sexton, J. Catalysis 78 (1982) 126.

5. M.M. Walczak, P.K. Leavitt and P.A. Thiel, J. Am. Chem. Soc. 109 (1987) 5621.

6. M.M. Walczak, P.K. Leavitt and P.A. Thiel, J. Vac. Sci. Technol. A 5 (1987) 539.

7. M.M. Walczak, P.K. Leavitt, and P.A. Thiel, in New Materials Approaches to Triblolgy: Theory and Applications, L.E. Pope, L.L. Fehrenbacher, and W.O. Winer, Eds. (Materials Research Society, Pittsburgh, PA, 1989) p. 417.

8. M.M. Walczak, P.K. Leavitt and P.A. Thiel, 1989 STLE-ASME Tribology Conference Proceedings, in press (1990).

9. B.A. Sexton, Surface Sci. 102 (1981) 271.

10. P. Basu, T.H. Ballinger and J.T. Yates, Jr., Langmuir 5 (1989) 502.

11. M. Stacey, J.C. Tatlow and A.G. Sharpe, Advances in Fluorine Chemistry (Butterworths, London, 1961).

12. V.I. Vedeneyev, L.V. Gurv'ich, V.N. Kondrat'yev, V.A. Medvedev and Y.L. Frankevich, Bond Energies, Ionization Potentials and Electron Affinities (Edward Arnold Ltd., London, 1966).

13. J.H. Simons, Ed., Fluorine Chemistry, Vol. II (Academic Press Inc., New York, 1954).

14. D. Deurst, Analytical Chemistry Division, 3M Corporation, St. Paul, MN, private communication, 1989.

15. R.L. Shriner, R.C. Fuson, D.Y. Curtin and T.C. Morrill, The Systematic Identification of Organic Compounds, 6th Ed. (John Wiley and Sons, New York, 1980).

16. P.K. Leavitt, J.L. Davis, J.S. Dyer and P.A. Thiel, Surface Sci., 218 (1989) 346.

17. P.A. Redhead, Vacuum 12 (1962) 203.

18. R.G. Pearson, Science 151 (1966) 172.

19. T.-L. Ho, Hard and Soft Acids and Bases Principle in Organic Chemistry (Academic Press, New York, 1977).

20. P.C. Stair, J. Am. Chem. Soc. 104 (1982) 4044.

21. C.J.F. Bottcher and P. Bordewijk, Theory of Electric Polarization, 2nd edition, Vol. II (Elsevier Scientific Publishing Company, Amsterdam, 1978).

CONCLUSIONS

In this dissertation we investigate the interactions of water and perfluorodiethyl ether with Ru(100) in an attempt to advance the understanding of the effects of surface morphology and humidity on the bonding of perfluoropolyether lubricants to metal surfaces. The main conclusions which can be drawn are summarized below:

a) Water bonds to Ru(100) primarily in a molecular fashion, only 5 -10% of a monolayer dissociates. Two thermal desorption features are observed-a feature attributed to the chemisorbed monolayer which appears at 240 K at low exposures and decreases in temperature to 180 K as exposure is increased, and a feature attributed to desorption from a water multilayer which appears at 160 K.

b) Electron energy loss data for water on Ru(100) are indicative of a fairly non-hydrogen-bonded species at low exposures with an increase in the amount of hyrdogen-bonding as exposure is increased.

c) Coadsorption of 0.50 L oxygen or 2 L hydrogen with water on Ru(100) pushes the water multilayer feature up in temperature so that it is indistinguishable from the monolayer desorption feature.

d) Coadsorption of 0.50 L oxygen with low coverages (i.e., 50-300 Torr s) of water on Ru(100) forces the peak temperature of the water monolayer feature up by as much as 65 K.

e) Perfluorodiethyl ether is molecularly adsorbed on Ru(100). It desorbs in three states-two states attributable to desorption from a

chemisorbed monolayer with desorption energies of 35 and 37 kJ/mol and desorption from a multilayer state at 120 K.

f) Comparison of the degree of decomposition and the desorption energies of perfluorodiethyl ether on Ru(100) with results from Ru(001) indicates that surface morphology does not affect the bonding of this molecule to metal surfaces.

g) Both perfluorodiethyl ether and water bind to Ru(100) more weakly in the presence of the other. The monolayer peak temperatures of perfluorodiethyl ether are shifted to lower temperatures by as much as 25 K due to the presence of a water monolayer. Small amounts (50 Torr s) of perfluorodiethyl ether force adsorbed water molecules from the monolayer to the multilayer state.

h) These investigations indicate that humidity may be an important consideration in the bonding of perfluoropolyether lubricants to metal surfaces, but surface morphology plays little role in their bonding.

REFERENCES

1. Y.Hu and F.E. Talke, in Tribology and Mechanics of Magnetic Storage Systems, Vol. V, B. Bhushan and N.S. Eiss, Jr., Eds. (Society of Tribologists and Lubrication Engineers, Park Ridge, IL, 1988) p. 43.

2. S. Mori and W. Morales, Wear 132 (1989) 111.

3. R.G. Gilson and M. Davies, in Symposium Proceedings Textbook: The Symposium on Memory and Advanced Recording Technologies (Magnetic Media Information Services, Chicago, IL, 1986) p. 26.

APPENDIX 1.

A WARNING CONCERNING THE USE OF GLASS CAPILLARY ARRAYS IN GAS DOSING: POTENTIAL CHEMICAL REACTIONS

A Warning Concerning the Use of Glass Capillary Arrays in Gas Dosing: Potential Chemical Reactions

P. K. Leavitt and P. A. Thiel

Ames Laboratory and Department of Chemistry
Iowa State University
Ames, Iowa 50011

This appendix appears in volume 8 of Journal of Vacuum Science and Technology A on page 148, 1990.

ABSTRACT

We have encountered complications using a glass, capillary-array gas doser in our laboratory. In this note, we discuss the possibility that chemical reactions occur on the glass surface.

TEXT

In any study of chemisorption on surfaces, it is necessary to expose the surface to the gas of interest in some controlled manner. Over the past ten years, effusive beam dosers have gained increasing popularity as a way of introducing reactive gases into ultra-high vacuum systems (e.g., 1-6). The reason for their popularity is that they are simple, yet they provide a spatially-collimated beam which can selectively impinge on the sample. Thus, the gas pressure (local flux) at the sample can be several times greater than that which prevails in the vacuum chamber. Enhancements of up to 10^2 have been reported relative to background pressure (6).

There are two main ways of collimating a gas beam doser. One is to use a single narrow tube, or small aperture, at the end of the gas doser, aimed at the sample (effusive source). The other is to use a glass capillary array, in which thousands of small orifices (typically 10 micron diameter) penetrate a glass frit, again aimed at the sample. The latter approach was first described by Goodman, Yates and Madey in 1978 (1). Campbell has discussed the relative merits of these two approaches, in terms of flux and spatial homogeneity of flux at the sample (5).

In this paper, we point out difficulties we have encountered in using the glass capillary array. We believe that these problems are due to reaction of the gas with the glass surface, exacerbated by the fact that the total surface area of the capillaries is extremely high. (For a glass frit which is 1 mm thick and 13 mm in diameter, with 10-micron

diameter capillaries, the total surface area is about 270 cm^2.) These difficulties have been obviated in our laboratory by the substitution of a simple metallic aperture.

Inconsistencies in thermal desorption spectra of perfluorodiethyl ether from Ru(100) lead us to suspect that the doser is chemically reactive. Early results from this system showed desorption states which were not reproducible, in spite of rigorous efforts to exclude all possible experimental problems, such as sample cleanliness. After replacing the glass doser with a metal aperture, several desorption states disappeared and the remaining desorption features have been completely reproducible over a period of several months.

Although ethers are generally unreactive molecules [cleavage takes place in solution only under vigorous acidic conditions (7)], we suspect that the silica surface of the glass frit may be acidic enough to induce cleavage. Silica surfaces are generally hydroxylated unless care is taken to dehydrate them. Small amounts of Al_2O_3 make silica strongly acidic (8). The glass frits commonly used in these dosers are obtained from Galileo (9) and are a Corning R-6-soda lime glass which contains primarily SiO_2 (73 wt. %), with about 1.7 wt. % Al_2O_3, among other additives (10). Therefore, the doser frit surface may be acidic enough to catalyze cleavage of the ether. In addition to the suspected reactions on silica, the sodium and potassium in these glasses may also promote chemical reactions.

In summary, we suspect decomposition of perfluorodiethyl ether at a glass frit of the type commonly used in capillary-array gas dosers. We

caution other users against the possible reactivity of glass capillary array dosers.

ACKNOWLEDGEMENTS

This research is supported by the Director for Energy Research, Office of Basic Energy Sciences. Ames Laboratory is operated for the U.S. Department of Energy by Iowa State University under Contract No. W-7405-ENG-82.

REFERENCES

1. D.W. Goodman, J.T. Yates, Jr. and T.E. Madey, Chem. Phys. Letters 53 (1978) 479; also D.W. Goodman, T.E. Madey, M. Ono and J.T. Yates, Jr., J. Catalysis 50 (1977) 279.

2. S.M. Gates, J.N. Russell, Jr. and J.T. Yates, Jr., Surface Sci. 159 (1985) 233.

3. M.J. Bozack, L. Muelhoff, J.N. Russell, Jr., W.J. Choyke and J.T. Yates, Jr., J. Vac. Sci. Technol. A 5 (1987) 1.

4. J.E. Deffeyes, A.H. Smith and P.C. Stair, Surface Sci. 163 (1985) 79.

5. C.T. Campbell and S.M. Valone, J. Vac. Sci. Technol. A 3 (1985) 408.

6. D.E. Ibbotson, T.S. Wittrig and W.H. Weinberg, Surface Sci. 110 (1981) 294.

7. R.T. Morrison and R.N. Boyd, Organic Chemistry, 3rd Ed. (Allyn and Bacon, Inc., Boston, 1973) p. 559.

8. B.C. Gates, J.R. Katzer and G.C.A. Schuit, Chemistry of Catalytic Processes (McGraw-Hill, Inc., New York, 1979) p. 48.

9. Part number C13S10M10; Galileo Electro-Optics Corp., Sturbridge, MA.

10. B. LaPrade, Channel Products Development, Galileo Electo-Optics Corporation, Sturbridge, MA, private communication, 1988.

APPENDIX 2.

COMPUTER PROGRAM AND INTERFACE FOR THERMAL DESORPTION STUDIES

INTRODUCTION

For convenience in obtaining and analyzing data, the instrumentation necessary for thermal desorption experiments has been interfaced to an IBM-AT computer. This interface allows essentially simultaneous monitoring of up to eight masses for each thermal desorption experiment. In this manner, the parent mass for the compound of interest as well as several fragment peaks and suspected decomposition fragments can be monitored in order to obtain information about the stability of a given molecule on the surface. For instance, if the compound of interest is perfluorodiethyl ether (PFDE), which has a parent peak at m/z=230, several masses of interest can be monitored.

First of all the parent peak may be monitored if it has enough intensity. In this case, mass 230 is not a very intense peak in the cracking pattern of PFDE. Therefore, a mass of more interest might be m/z=69, which is the most intense fragment in the cracking pattern of PFDE. The intensity of this mass can be monitored and compared to that of other masses in the cracking pattern to assimilate information concerning decomposition. For instance, m/z=69 can be ratioed to masses 31, 50 and 119, which are all abundant in the cracking pattern as well. These ratios, as well as thermal desorption data from suspected decomposition fragments (for instance, mass 28 for CO), provide us with information concerning the amount and mechanism of decomposition.

HARDWARE

The equipment necessary for a thermal desorption experiment includes a mass spectrometer and a temperature control circuit. In this laboratory, a UTI 100C quadrupole mass spectrometer and a Hertz temperature controller circuit (1) are used to perform the experiments. These are interfaced to an IBM-AT computer for multi-mass thermal desorption experiments. The AT is equipped with a Hercules card for high resolution graphics and a math coprocessor for use with IBM Professional Fortran software. Once obtained, the data can be plotted out on a Hewlett-Packard 7470A plotter or printed on a Star Micronics NX-1000 printer.

INTERFACE

The interface between the computer and the equipment used in acquiring data is accomplished with two interface boards, two voltage-to-frequency converters, and eight REED relays. The interface boards, a CTM-05 board and a DAC-02 board, are both manufactured by MetraByte. The CTM-05 board is a counter/timer and digital input/output expansion board. It has five independent 16-bit counters, and eight bits each of TTL/DTL digital input and output with latch. It is also equipped with a programmable frequency output. Digital output from the CTM-05 board is buffered using inverters and then used to control low current REED relays. The inverting buffers make it necessary to operate the relays in the negative logic mode. Therefore, to turn a relay 'on', the corresponding digital output bit must be set LO. Output ports 0-7 (OP0-OP7) carry the voltage signals from the CTM-05 board to the REED relays.

The UTI mass spectrometer is controlled by ports OP0-OP4. Output port zero controls the multiplier function (essentially turning the mass spectrometer on and off). Output ports 1-4 control the gain range on the mass spectrometer. Various combinations of HI and LO signals at these ports produce the different gain ranges. The necessary combinations of signals for each range are illustrated in Table 1. For example, to set the mass spectrometer to a range setting of 10^{-8} amps full scale, a LO must be sent to OP2 and OP3. This is essentially equivalent to grounding pins 5 and 14 at the UTI interface connector.

Table 1. UTI pin number settings for various gains

Range	Output Port	State	UTI Pin Number
10^{-5}	OP4	LO	16
10^{-6}	OP3	LO	14
	OP4	LO	16
10^{-7}	OP2	LO	5
10^{-8}	OP2	LO	5
	OP3	LO	14
10^{-9}	OP1	LO	3
10^{-10}	OP1	LO	3
	OP3	LO	14
10^{-11}	OP1	HI	3
	OP2	HI	5
	OP3	HI	14
	OP4	HI	16
10^{-12}	OP1	HI	3
	OP2	HI	5
	OP3	LO	14
	OP4	HI	16

The Hertz temperature controller is controlled by OP5-OP7. A momentary LO at OP5 starts the temperature ramp, a momentary LO at OP6 stops the ramp, and a momentary LO at OP7 resets the controller.

The relays used to carry the signal from the output ports of the CTM-05 board to the mass spectrometer or temperature controller are low current, 32 volt, TTL compatible, REED relays. The relays that control the mass spectrometer functions are located in the interface box which is located near the computer, and those that control the temperature controller are located inside the chassis of the Hertz temperature controller.

The DAC-02 board consists of two 12-bit digital to analog converters (DA0 and DA1). Only one of these is presently used (DA0) to set the AMU via the external program input of the mass spectrometer.

Once the signals have been sent to the mass spectrometer and the temperature controller, the experiment is running and its progress must be monitored and the appropriate data values must be collected. This is accomplished with a combination of the two voltage to frequency converters and the five counters found on the CTM-05 board.

Counter number 1 on the CTM-05 board provides a waveform which triggers counters 2, 4 and 5. This waveform is designed by the operator when the experimental parameters are set. The waveform begins by arming counter 1. Then the "delay" time is allowed to pass. This is a parameter set by the operator (generally 10-20 msec) which allows the mass spectrometer picoammeter time to settle when the gain is changed. At least 10 msec of settling time are generally required. Following the

delay, counter 1 signals the first gate edge, and counters 4 and 5 are armed and begin counting. The count interval, which is also set by the operator as the "dwell", is then passed. This value can be anywhere from 10-99 msec, and defines the length of time a signal will be averaged for each data point. Once the dwell time has passed, counter 1 signals the second gate edge which stops the count at counters 4 and 5 and signals them to transfer their count to a hold register. When counter 1 has signaled both the first and second gate edge, it then has a count of 2 (one for each gate edge) in its hold register. This value of two at counter 1 signals a high at counter 2, which is being used as a comparator, indicating that the conversion is complete (i.e., one data point has been taken). Counter 2 is wired to the digital input port as INPO, so this HI input signal from counter 2 triggers the software to restart the count for the next data point. Counter 3 is loaded and armed at the beginning of the experiment, and simply keeps track of the elapsed time (1 count=10 msec).

The two voltage to frequency converters (both are Burr Brown VFC 320's with 65,000 counts per 10 volts full scale) are used to convert the analog output from the mass spectometer and the temperature controller into frequencies that can be counted. Counters 4 and 5 are tuned to read the frequencies of the mass spectrometer and the temperature controller voltage to frequency converters, respectively.

SOFTWARE

The software utilized in this program includes Professional Fortran, version 1.2, No Limit Fortran Library, version 3.0, and Graphics Development Toolkit. The TESTTDS.FOR program was originally written by J. A. Polta with documentation by B. S. Nielsen, and major modifications by J. W. Anderegg and J. S. Dyer. The SLOWTDS.FOR version of the program was developed from the original program by J. S. Dyer. The program is structured such that one major program (TPP.FOR) introduces and initializes the main variables in the program and calls a series of subroutines to carry out the necessary functions in the program. Many of these subroutines are included in other programs which were set up to carry out specific tasks in the thermal desorption experiment. For instance, the AMASS.FOR program is a unit which acquires the mass data. It contains the subroutine ACQUIRE. Table 2 is a tabulation of the Fortran programs utilized in the TESTTDS.FOR program along with a listing of the subroutines found in each of them, and the main purpose of the program.

Some subroutines, which are required to carry out relatively simple operations (such as converting a real number to an integer) are located in a library titled MYSUP1.LIB. The programs (and the subroutines therein) which are included in MYSUP1.LIB are denoted by an asterisk in Table 2.

A second library has been constructed for use with the TESTTDS.FOR program. This library, called MYSUP.LIB, contains four programs which

Table 2. Fortran programs used in TESTTDS.FOR program

Program	Purpose	Subroutines
TPP.FOR (TDS)	-Main TDS program -Sets default values -Allows operator to change parameters	SHOW
TA1P.FOR	-Acquires time and temperature data	TDSRUN TDSACQ GETDAT
T2TP.FOR	-Converts Kelvin temperatures to mV using an empirical fit with 3rd-order polynomials	KTOMV ITOK MVTOK MVOCT ITOKR
EMASS.FOR	-Sets up the screen for taking mass spec data	MS
AMASS.FOR	-Acquires the mass data	ACQUIRE
MMASS.FOR	-Plots mass spec data on the screen	MONPLT
HMASS.FOR	-Plots TDS data on the Hewlett Packard plotter	HPLOT
NEWM2P.FOR	-Plots TDS data on the screen, plotter, or printer	M2
AREAP.FOR	-Calculates the area under a designated peak	AREACALC
INTCHAR5.FOR	-Converts an integer to a character * 5	INTCHAR5

Table 2 (Continued)

Program	Purpose	Subroutines
T1P.FOR[a]	-Consists of a series of subroutines which set up the operating parameters for a TDS experiment	FNAMEP DATEP MENU ERASE ABSCSR VIDATR MESSON MESSOFF AMUP COP DELAYP OFFP SMP1SP YSCP OPRARP ATRNG DWELP SLOPEP ITEMPP FTEMPP NMASSP
CMASS.FOR[a]	-Consists of a series of subroutines and functions which change variables from reals to integers and vice versa, and similar operations	INTCHAR INTCHAR4 REALCHAR RCHAR5 RCHAR11 CHARINT CHARINT4 WAIT FXR FYR FXTR FYTR
CMASSTM.FOR[a]	-Calls subroutine CTMSP to set up the counters and timers on the CTM-05 board	CTMSP
INOUTP.FOR[a]	-Consists of subroutines to store and load data and send it to the DEC printer	STORE LOAD DPRINT

[a]Programs appearing in MYSUP1.LIB.

are written in assembler language, and are required to input and output data. These programs and their functions are listed in Table 3. Table 4 is a list of all the subroutines in the program, a short description of the function of each one, and its location.

Table 3. Programs appearing in MYSUP.LIB

Program	Purpose	Function
TIME(G)	-Reads the system clock	Not used in program
IPEEK	-Looks at a number at a specific memory location	Not used in program
IPOKE	-Places a number at a specific memory location	Not used in program
INPRT[a]	-Inputs a value to the computer	Used in program
OUTPRT[a]	-Outputs a value from the computer	Used in program

[a]These two programs are found on a floppy disk labelled MISCELLANEOUS1.

Table 4. Subroutines in the TDS program

Subroutine	Description	Location
ABSCSR[a]	-Sets the position of text on the screen	T1P.FOR[b]
ACQUIRE	-Acquires data for the mass spectrum -Init. range and AMU -Increments DOUT	AMASS.FOR
AMUP[a]	-Accepts and displays the AMU information for each mass peak as entered by the operator	T1P.FOR[b]
AREACALC	-Calculates the area under a designated peak -Displays the value of time, temperature and intensity at any chosen cursor point	AREAP.FOR
ASZRO	-Calls a series of MEF Fortran subroutines to perform simple commands	NLVR3TS2.FOR[c]
ATRNG	-Accepts and displays the ranging mode	T1P.FOR[b]
CHARINT	-Converts a character*3 to an integer (I5)	CMASS.FOR[b]
CHARINT4	-Converts a character*4 to an integer (I5)	CMASS.FOR[b]
CHKDRV	-MEF Fortran routine that checks a drive for errors or status	MEF FORTRAN.LIB

[a]Subroutine uses the ascii character set.

[b]Program located in MYSUP1.LIB.

[c]Program located in FORTRAN\LIBRARY.

Table 4 (Continued)

Subroutine	Description	Location
#COP	-Accepts and displays four comment lines of up to 40 characters each	T1P.FOR[b]
CTMSP	-Sets up all the timers on the CTM-05 board	CMASSTM.FOR[b]
DATEP[a]	-Accepts and displays the date for the current data file	T1P.FOR[b]
DELAYP	-Accepts and displays the delay time	T1P.FOR[b]
DPRINT	-Allows data to be printed on the DEC printer	INOUTP.FOR[b]
DSKINF	-MEF Fortran routine that locates free disk space	MEF FORTRAN.LIB
DWELP	-Accepts and displays the counting time (dwell)	T1P.FOR[b]
ERASE[a]	-Clears the screen	T1P.FOR[b]
FILINF	-MEF Fortran routine to obtain information about a file	MEF FORTRAN.LIB
FILSTG	-MEF Fortran routine to fill a string with characters or bytes	MEF FORTRAN.LIB
FNAMEP[a]	-Accepts and prints the filename, device and extension of the current data file across the top of the screen	T1P.FOR[b]
FRANDW	-MEF Fortran routine to perform a logical AND on two words	MEF FORTRAN.LIB

Table 4 (Continued)

Subroutine	Description	Location
FRSHRW	-MEF Fortran routine to perform a logical "shift right" on a word	MEF FORTRAN.LIB
FTEMPP	-Accepts and displays the final temperature	T1P.FOR[b]
FXR	-This is a function that converts a real % into an x-axis graphics unit	CMASS.FOR[b]
FXTR	-This is a function that converts an integer % into an x-axis graphics unit	CMASS.FOR[b]
FYR	-This is a function that converts a real % into a y-axis graphics unit	CMASS.FOR[b]
FYTR	-This is a function that converts an integer % into a y-axis graphics unit	CMASS.FOR[b]
GETDAT	-Obtains count from counters 3, 4 and 5 (total elapsed time, intensity and temperature)	TA1P.FOR
HPLOT	-Plots mass spectra acquired by MS subroutine on the Hewlett-Packard plotter	HMASS.FOR
INKEY	-MEF Fortran routine to read the keyboard one key at a time	MEF FORTRAN.LIB
INSTR	-MEF Fortran routine to find a string match	MEF FORTRAN.LIB
INTCHAR	-Converts an integer to a character*3	CMASS.FOR[b]

Table 4 (Continued)

Subroutine	Description	Location
INTCHAR4	-Converts an integer to a character*4	CMASS.FOR[b]
INTCHAR5	-Converts an integer to a character*5	INTCHAR5.FOR
ITEMPP	-Accepts and displays the initial temperature	T1P.FOR[b]
ITOK	-Converts counts to mV -Calls MVTOK to convert from mV to Kelvin	T2TP.FOR
JUSTL	-MEF Fortran routine to left justify a character string	MEF FORTRAN.LIB
KTOMV	-Converts Kelvin temperatures to mV using an empirical fit with 3rd-order polynomials -Calls MVTOK to convert from mV to Kelvin	T2TP.FOR
LINEA	-MEF Fortran routine to draw a line, a box, or a filled box	MEF FORTRAN.LIB
LOAD	-Loads TDS or MS data from drives A: or D: to drive C: into the program	INOUTP.FOR[b]
M2	-Uses Graphics Development Toolkit routines to open the workstation and plot TDS data to the screen, plotter or printer	NEWM2P.FOR
MENU[a]	-Arranges the menu on the screen	T1P.FOR[b]

Table 4 (Continued)

Subroutine	Description	Location
MESSOFF[a]	-Shuts off the blinking message on the screen	T1P.FOR[b]
MESSON[a]	-Prints a blinking message on the bottom of the screen	T1P.FOR[b]
MONPLOT	-Plots mass spectra acquired by MS subroutine on the screen	MMAS.FOR
MS	-Sets up the screen for taking mass spectral data -Turns on mass spectrometer -Acquires mass spectral data -Displays mass spectrum on screen -Calls various subroutines to carry out menu functions such as load, store, erase, etc.	EMASS.FOR
MVOCT	-Converts mV to counts using an empirical fit with an 8th-order polynomial	T2TP.FOR
MVTOK	-Converts from mV to Kelvin using the calibration from a Re 5%-26% thermocouple and a 5th-order polynomial	T2TP.FOR
NMASSP	-Accepts and displays the number of mass peaks observed	T1P.FOR[b]
OFFP	-Accepts and displays the y-offset value for the current data on the screen	T1P.FOR[b]

Table 4 (Continued)

Subroutine	Description	Location
OPRARP	-Accepts and displays the name of the current operator (up to 24 characters long)	T1P.FOR[b]
OUTPRT	-Subroutine written in assembler language to output data from the computer	MYSUP.LIB
PUTCUR	-MEF Fortran subroutine to put an alphanumeric cursor on the screen	MEF FORTRAN.LIB
RCHAR5	-Converts a real number (F5.2) to a character*5	CMASS.FOR[b]
RCHAR11	-Converts a real number (F11.2) to a character*11	CMASS.FOR[b]
REALCHAR	-Converts a real number (F4.2) to a character*4	CMASS.FOR[b]
SCROLL	-MEF Fortran routine used to scroll a window portion of the screen	MEF FORTRAN.LIB
SEAGAP1	-MEF Fortran routine used to set an individual EGA palette register	MEF FORTRAN.LIB
SEGAAL	-MEF Fortran routine used to set all EGA palette registers and border	MEF FORTRAN.LIB
SHOW	-Sets the initial screen display -Updates screen for the TDS experiment	TPP.FOR

Table 4 (Continued)

Subroutine	Description	Location
SLOPEP	-Accepts and displays the slope of the heating ramp	T1P.FOR[b]
SMPLSP	-Accepts and displays the sampling interval	T1P.FOR[b]
STORE	-Stores TDS or MS data from the program in drive C: to drives A: or D:	INOUTP.FOR[b]
TDSACQ	-Acquires current, time and temperature data -Turns on temperature controller -Sets AMU -Sets mass spectrometer gain -Loads and arms all timers -Stops temperature ramp and turns mass spectrometer off -Allows early abort using 'shift s'	TA1P.FOR
TDSRUN	-Initializes gain and AMU values -Determines final temperature in counts -Calls TDSACQ to acquire the TDS data	TA1P.FOR
VIDATR[a]	-Sets the video attributes of the screen	T1P.FOR[b]
WAIT	-Wastes time	CMASS.FOR[b]
WCHARS	-MEF Fortran routine that writes a string of characters	MEF FORTRAN.LIB
YSCP	-Accepts and displays the y-scale for the current data	T1P.FOR[b]

PROGRAM OPERATION

The program (presently, TESTTDS) is a menu-driven thermal desorption program. It is relatively simple to use. When called, the program prints the initial 'default' menu on the screen. A copy of this menu is given in Fig. 1. To the left of the screen, all of the experimental parameters, with the exception of the masses and their respective gains, are displayed. These parameters can be changed by typing in the first two letters of the desired parameter, and then typing in the new choice for that particular parameter. The CAPS LOCK must be on for the program to accept user commands.

The 'drive' parameter is used to choose the drive at which the current data set should be stored, or loaded. To change the drive choice, simply type in the letter of the desired drive (only drives C, D and A are accessible.) Note that drive D is a random-access memory (RAM) drive which is cleared every time the computer is booted.

The 'date' is simply the date on which the current data set is acquired. The form of this parameter is not rigidly set by the program (i.e., both 1/29/62 and 1-29-62 are acceptable). The date is simply formatted as an 8-character string.

The 'operator' parameter allows a 24-character long string to be input describing the current operator. No spaces or punctuation can be used in this string.

The 'filename' is set up in a manner similar to the 'operator' except that only 10 characters are permitted in this parameter. The

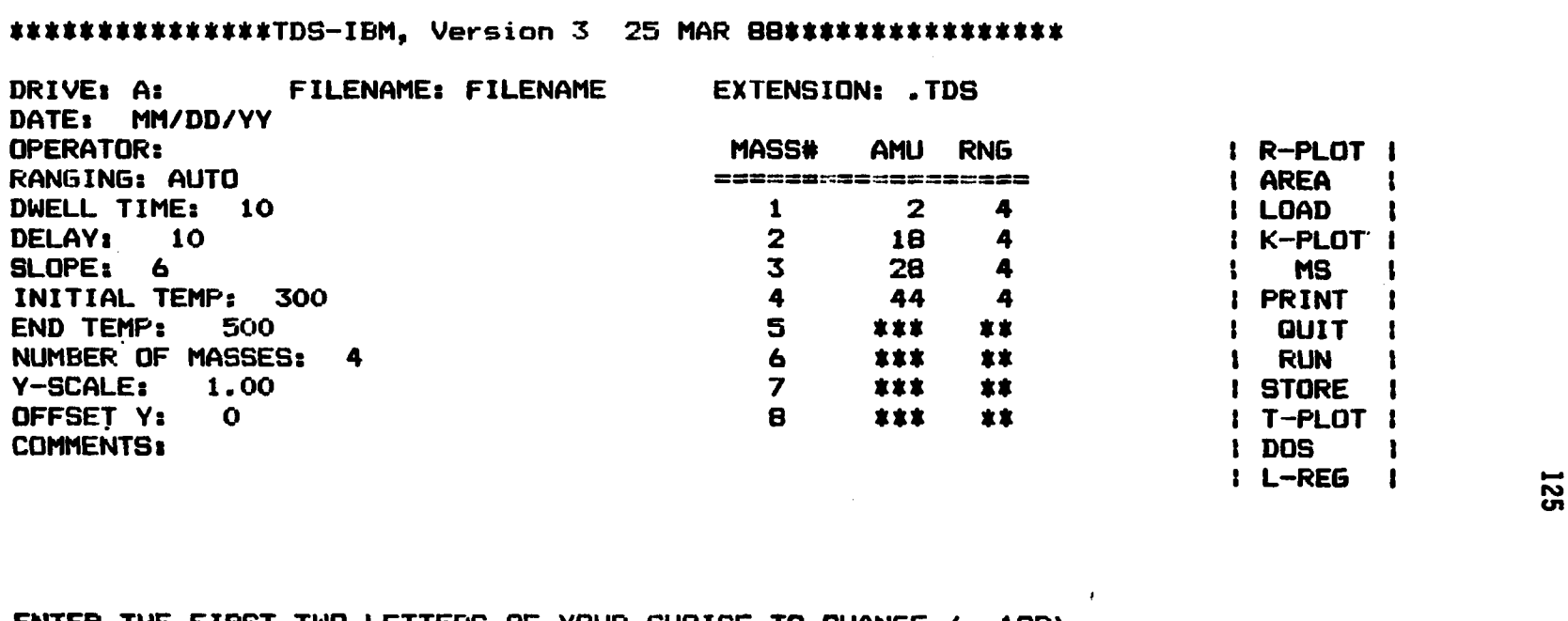

Figure 1. Default menu for TDS program

filename will have the 'extension' that is chosen for that parameter. The default characters for 'extension' are .TDS. Note that only 3 characters are accepted for this parameter.

The program was originally designed to set the mass spectrometer ranges independent of the operator. However, the autoranging section of the program has never functioned properly. As a result of this original setup, a parameter called 'ranging' still exists in the program. The possible choices for this parameter are 'auto' and 'manual'. Since the autoranging does not work, the 'manual' choice is necessary.

The 'dwell' is the number of milliseconds that the computer collects data for a given mass and a particular data point. This value can range from 5 to 100 milliseconds. Closely related to this value is the 'delay'. This parameter describes the amount of time the computer should sit at a given mass before it begins collecting data for a particular data point. The default for this parameter is 10 milliseconds, and common values are between 10 and 30 milliseconds for a dwell of 10 to 20 milliseconds, and a slope of about 10 K/s. The delay can be varied from 10 to 85 milliseconds. When setting these values, one should also consider the slope at which the experiments will be run. The 'slope' can be varied from 1 to 10 on the Hertz temperature controller. This corresponds to a variation in heating ramp from .1 to 100 mV/min, or about .2 to 200 K/sec at room temperature. Generally slopes between 4 and 7 are used. Once the slope has been chosen for a particular experiment, the dwell and delay values can be set. For "slow" slopes (<5), the dwell (and possibly the delay) should be set to relatively long

times (>30) so that numerous data points will not be taken at each temperature in the range. Taking too many points at a particular temperature value will fill up the data arrays quickly making long temperature ramps inaccessible at slow slopes, and it will also make the data look rather "noisy".

The 'initial temp' is the temperature at which the computer will begin collecting experimental data and the 'end temp' is the temperature at which the computer will halt data acquisition. These temperatures should be entered in Kelvin. The computer will convert these values to mV and finally to their corresponding counts, so that these values can be compared to those obtained at the voltage-to-frequency converter in the Hertz controller.

The 'number of masses' parameter allows the operator to choose the number of masses the computer should monitor. From 1 to 8 masses can be monitored essentially simultaneously for any given experiment. The masses to be monitored, and their corresponding gain values are displayed near the middle of the screen. To set a given mass, the mass number (i.e, 1 to 8) is entered, and then the desired AMU value can be entered. The 'rng' can be set for each mass by choosing the 'ranging' parameter. When 'manual' ranging is chosen, the computer will ask the operator to input the range for each AMU requested.

The 'y-scale' and 'offset y' parameters allow the data to be scaled or moved in the y direction on the screen or plotter. Y-scale values can range from 0 to 99. The plot can be moved up or down on the screen or plotter by adjusting 'offset y' to an integer value between +9 and -9.

These values correspond to screen units. The plotting screen is set up into 10 units on the y-scale. This is simply an equal division of the plotting box on the screen or plotter into 10 parts.

The 'comments' parameter allows the operator to write any pertinent comments to the data file. Up to 4 lines of 40 characters each are available for comments. This parameter can either be accessed by entering C0 or by entering C1, C2, C3, or C4 for the appropriate comment line.

On the right side of the menu are the choices of operations that can be performed. The 'R-PLOT' option gives a plot of time vs. temperature. This plot is useful for determining the heating rate at a given temperature to a first approximation.

The 'AREA' option allows the operator to determine the area under a selected plot. Once the area option is chosen, the operator is asked to choose which mass to integrate. In the area routine, the operator may choose to take the area of the chosen mass or determine the signal intensity, temperature, point number and time at any particular point in the spectrum. The latter is accomplished by entering 'V' for value. The area, taken after the first and last point are chosen and the operator requests to have the area calculated, is given in Amp seconds.

The 'LOAD' and 'STORE' options load the data set chosen in 'FILENAME' from, or store it to, the specified 'DRIVE'.

The 'K-PLOT' option plots out a spectrum for a particular mass, specified by the operator, to the screen, printer, or plotter. The spectrum plots intensity vs. temperature. The 'T-PLOT' option is very

similar to 'K-PLOT', except that the data is plotted as intensity vs. time. This is the plotting function called in the area routine, so that a time-integrated area is obtained. When plotting to the plotter from either the k-plot or the t-plot option, note that the left pen is pen #1 and the right pen is pen #2.

The 'MS' option allows the operator to take a computer controlled mass spectrum. This option calls a new menu to the screen with many of the same options found on the main TDS menu. In this case, the operator must set the initial and final AMU values defining the scan region.

The 'PRINT' option prints the current data set to the printer designated lpt1. The print routine is designed for the wide carriage of the DEC printer.

To run the thermal desorption experiment, the operator chooses the 'RUN' option after all of the experimental parameters have been chosen. This option turns the mass spectrometer and the temperature controller on and off at the appropriate times and obtains the time, temperature, and intensity data for the experiment. The data file will consist of data arrays (of up to 5000 points) for time, temperature, and intensity at each mass observed. Note that the mass spectrometer must be in the external mode with the standby option chosen, and it must be set to a gain of 10^{-11}. The temperature controller should be set at the appropriate slope and should have the heater switch in the on position. Also, as always when running a temperature ramp, the power supply for heating the sample must be on. Finally, note that whenever using the

computer to set values at the mass spectrometer or the temperature controller, the interface box must be on.

To exit the program, two options are available. These are 'QUIT' and 'DOS'. The quit option is somewhat faster, but it does not store the data or the current parameters. When the program is exited through DOS, the current data set and parameters are stored on drive D, and are reentered when the program is called next (assuming the computer is not rebooted before the program is called again).

SUPPLEMENTAL PROGRAMS

There are two programs on the IBM that are useful in combination with the thermal desorption program. These are the 'FIXDATA1' program for obtaining instantaneous heating rate data, and the 'DACSWEEP' program for determining the appropriate DAC values for each mass to be observed in the thermal desorption experiments.

The 'DACSWEEP' program was written in basica by J. S. Dyer, and is found in the basicpgm directory. Choosing the 'TUNE' option of this program, allows the operator to enter a DAC value. This DAC value will be output to the mass spectrometer. By observing the mass spectrometer intensity in the region of the masses of interest, the operator can choose the appropriate DAC units to use in the experiment (that is, the DAC unit with greatest signal intensity for each mass). One can vary the DAC values by one unit at a time using the F9 and F10 keys as stated in the program. Note that the mass spectrometer must be in the external mode when using this program, but the operator must turn the mass spectrometer on and set the range value.

Once the best DAC values have been obtained for each mass, the operator must fit the AMU vs. DAC data to two straight lines, one for masses <5 and one for masses >5. Once the slopes and intercepts of these lines are obtained, they must be entered into the program. The lines in the program that set the DAC units are found in program TA1P.FOR. The linear equations in the program read as follows:

DOUT=(m/z)*13.xxxx +(-) xxxx.

These equations can be accessed by searching the TA1P.FOR program, using MS WORD, for DOUT. Once these equations have been set for the desired experimental values, the TA1P.FOR program must be re-compiled and finally re-linked to the thermal desorption program.

The second supplementary program of interest is the FIXDATA1.FOR program. This program is found in the PROGRAMS subdirectory of the TDS-NOW directory. It is useful for determining the instantaneous heating rate at a given temperature for a particular experiment. This value is necessary for determining the desorption energy using the Redhead equation.

To use this program, simply call it from the TDS-NOW\OBJECT directory. The program will begin by asking the operator to input a filename with drive specification and extension. Then the program will smooth the data in the temperature domain by applying linear least squares fits to 15 point segments. The least squares fit removes any "wobble" (fluctuations) in the temperature domain caused by inaccuracies in the temperature signal that is output from the voltage to frequency converter. Once the data has been entered and manipulated, the computer will request a new filename, again including drive specification and extension. This new data file will contain 5 columns of numbers. These are, from left to right, the smoothed time, the smoothed temperature, the instantaneous heating rate, the inverse of the smoothed temperature multiplied by 1000, and the original temperature.

A modification of this program, FIXDATA3.FOR, replaces the new temperature with the intensity data for the first mass in the TDS file.

The files generated in this program can be transferred into the GRAPHER program for plotting, if needed.

APPENDIX 3.

THE ADSORPTION OF HYDROGEN ON RU(100): THERMAL DESORPTION RESULTS

The Adsorption of Hydrogen on Ru(100): Thermal Desorption Results

P. K. Leavitt and P. A. Thiel

Ames Laboratory and Department of Chemistry
Iowa State University
Ames, Iowa 50011 USA

ABSTRACT

We have investigated the interaction of hydrogen with Ru(100) using thermal desorption spectroscopy. Hydrogen desorbs from the clean surface in two states which appear at 189 and 332K at low exposures and move to lower temperatures as exposure is increased, finally appearing at 170 and 269 K, respectively. A second-order desorption energy has been calculated by the method of Redhead for the lowest-exposure feature. A pre-exponential of 5×10^{-8} $cm^2/(H$ atoms s) and a desorption energy of 42 kJ/mol are obtained. These results are compared to recently published results of Lauth and co-workers (1).

INTRODUCTION

An understanding of the interactions of hydrogen with transition metal surfaces is important for many reasons. In particular, these interactions are of interest in surface electrochemical and fusion studies. Our interest in studying the interactions of hydrogen with Ru(100) is to characterize its interactions alone so that comparison can be made when hydrogen is coadsorbed with water on this surface. There are numerous studies in the literature detailing the interactions of hydrogen with Ru (1-16). Most of these studies were carried out on the basal plane.

Until recently, there were no published studies of the adsorption of hydrogen on the Ru(100) surface. However, Lauth and co-workers recently published a very thorough study of the adsorption of hydrogen on Ru(100), in which this system was studied using LEED, HREELS, TDS and work function measurements (1). We have studied this system using only thermal desorption spectroscopy, and our results are not in agreement with those of Lauth and co-workers. In this paper, we present our results, point out the discrepancies between our results and those of Lauth and co-workers, and finally present possible explanations for these discrepancies.

EXPERIMENTAL PROCEDURES

The stainless steel chamber used in these experiments has a base pressure of 1 X 10^{-10} Torr, and is equipped with a UTI 100C mass spectrometer, a cylindrical mirror analyzer Auger spectrometer, an ion gun, and an effusive-flow gas doser (17). The hydrogen used in these experiments, purchased from Matheson Gas Products, is specified as 98% pure. The hydrogen is introduced to the chamber via the effusive flow gas doser or a variable leak valve. The units of exposure for the doser are Torr-s, corresponding to the product of pressure in Torr behind the conductance-limiting aperture and the dose time. As a point of reference, a 4200 Torr-sec dose of hydrogen using this doser corresponds to approximately 1L exposure achieved by backfilling the chamber. Between experiments, the sample is cleaned by annealing to 1695 K in vacuum to remove any oxygen that may adsorb when the sample is at 90 K. After this procedure, no oxygen is observable in the Auger spectrum.

The sample is cooled to about 90 K prior to its exposure to hydrogen. A heating rate of approximately 10 K/sec is used to induce desorption. Typically, masses 2 and 28 are monitored. The mass 28 signal is recorded as a monitor of the amount of background gases coadsorbing with the hydrogen. In general, no mass 28 signal is observed.

EXPERIMENTAL RESULTS

Two states are observed in the desorption of hydrogen from Ru(100). At low coverages, an assymetric peak appears at ~332 K. This peak shifts down in temperature as exposure is increased, finally appearing at 269 K at high exposures. Assuming second-order desorption kinetics, and a pre-exponential factor of ~5 X 10^{-8} cm^2/(H atoms s), and using the method of Redhead (18), a desorption energy of 42 kJ/mol is obtained at low coverages.

The thermal desorption spectra are plotted in Fig. 1. The high and low temperature features are labelled β and γ, respectively. The spectra in Fig. 1 are all obtained following hydrogen exposure via the effusive flow gas doser.

Mass 2 area vs. hydrogen exposure is plotted in Fig. 2. At low exposures the area vs. exposure curve climbs rapidly. At approximately 3800 torr sec (or about 0.9 L) this curve rolls over, and increases very slowly as exposure is further increased, indicating a marked change in sticking coefficient at this coverage.

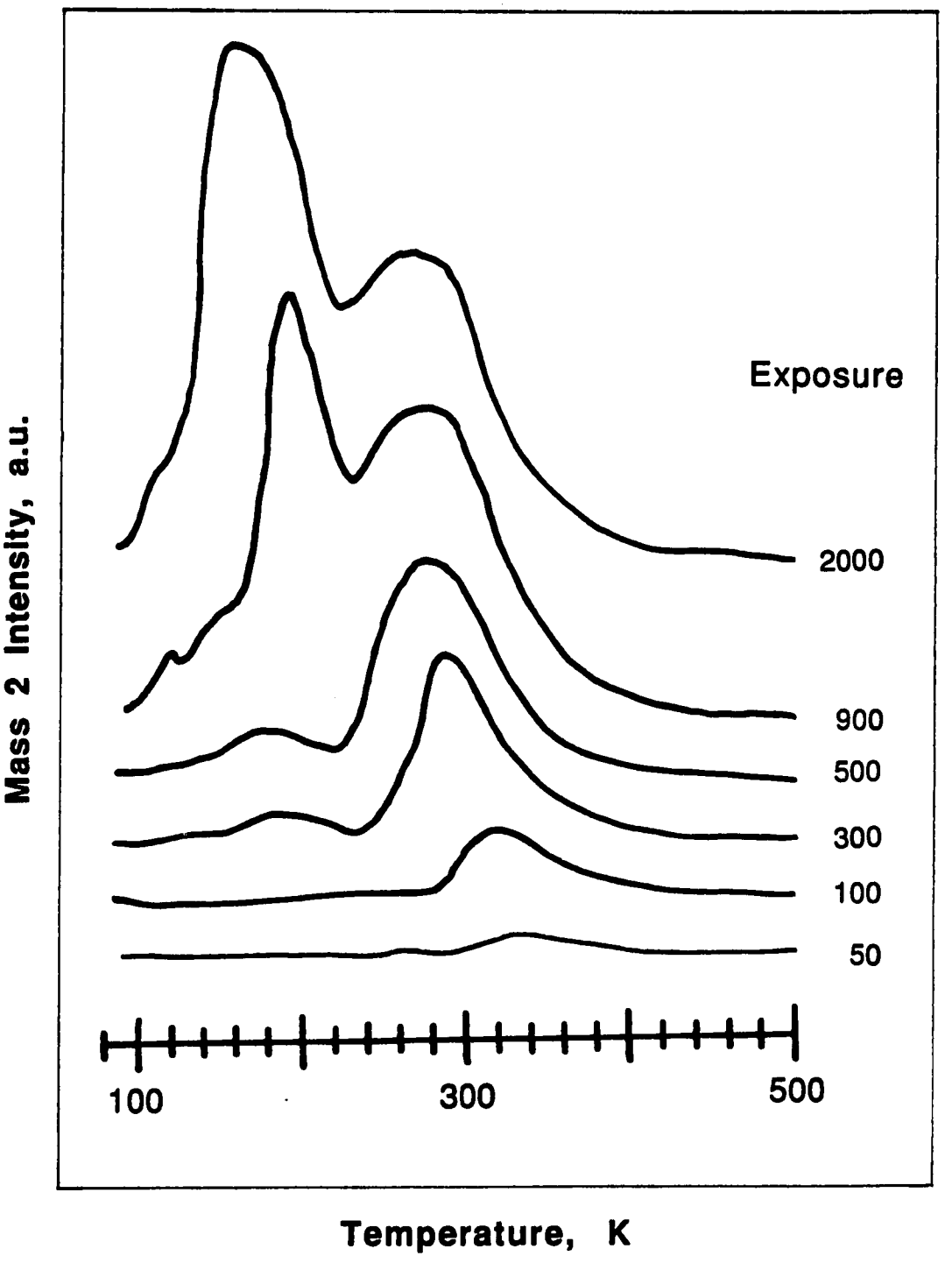

Figure 1. Thermal desorption of various coverages of hydrogen from Ru(100)

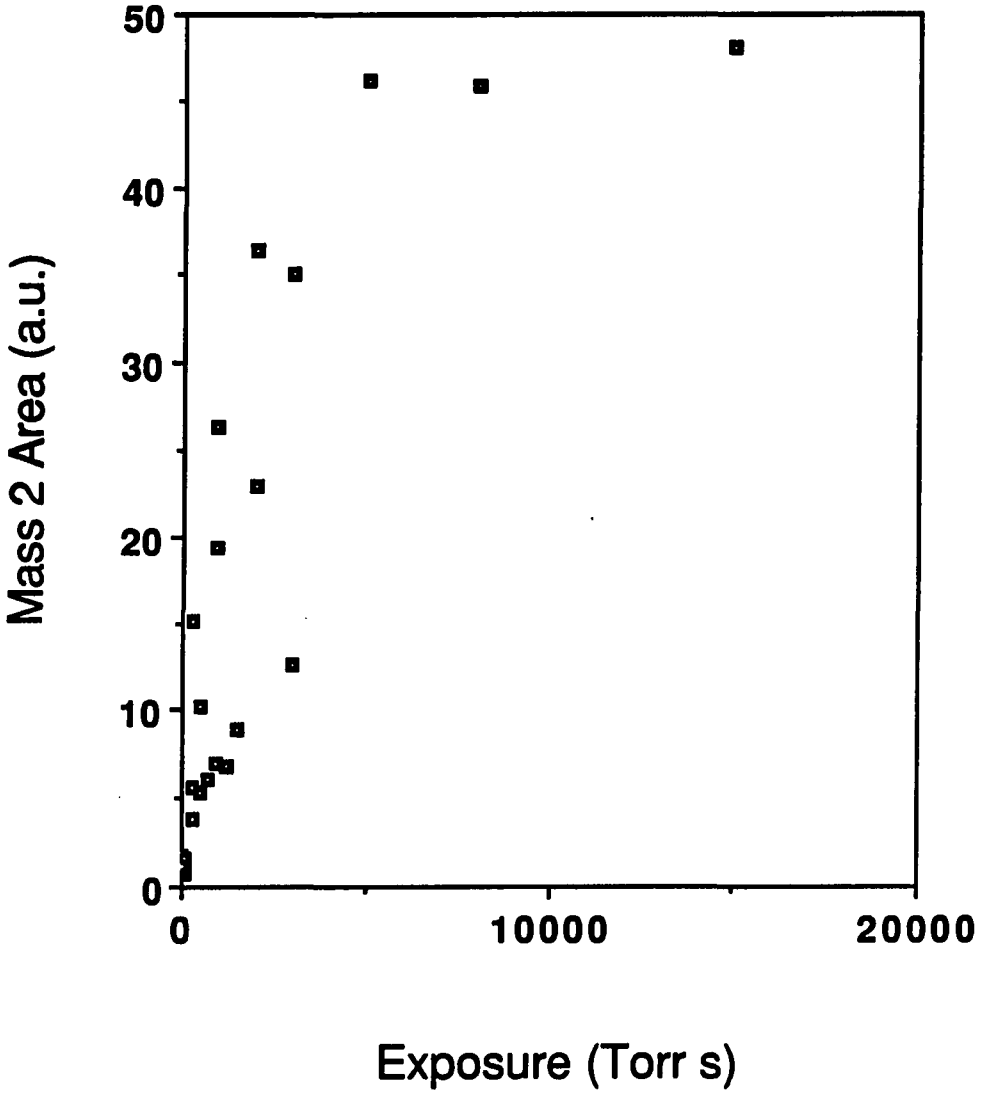

Figure 2. Mass 2 area vs. hydrogen exposure for desorption of various coverages of hydrogen from Ru(100)

DISCUSSION

The thermal desorption data presented in Fig. 1 differ significantly from those recently published by Lauth and co-workers (1). They observe a total of four hydrogen desorption features in this system. Initially, they observe one symmetrical state which appears at 385 K and shifts down to 350 K as coverage increases. After exposures of about 0.25 L, a second weak desorption feature is observed at about 287 K. This feature also shifts to lower temperatures as exposure is increased, indicative of second-order desorption. A third peak, with somewhat more intensity, grows in simultaneously with this 287 K feature. This third feature desorbs at about 258 K. At high exposures (2-6 L), a very intense fourth state grows in at 220 K. The peak temperature of this state does not shift with increasing exposure indicating first-order desorption kinetics. Using the method of Redhead (18), desorption energies were calculated for the high temperature and the low temperature states. Lauth and co-workers obtained a desorption energy of ~80 kJ/mol with a pre-exponential of 9×10^{-3} $cm^2/(H\ atoms\ s)$ for the second-order high temperature state. A value of 50 kJ/mol is reported for the low temperature feature assuming a pre-exponential of 10^{14} s^{-1} for first-order desorption.

If one is willing to dismiss the two mid-temperature features in the data of Lauth and co-workers which are fairly weak in intensity as possible artifacts or as desorption from defect sites, the remaining two features can be compared to the features obtained in our desorption

spectra. These data seem to be at odds upon initial inspection. We obtained our pre-exponential value and desorption energy using a fitting routine (19) to model the low-exposure chemisorption feature. The plot of the fitted data is presented in Fig. 3. The pre-exponential of 5 X 10^{-8} results in a deviation in the full width at half maximum between the experimental and the modelled peak of only 2%. The goodness of this fit indicates that the values of υ and E_d chosen for our data are reasonable. Using this fitting routine, we were unable to find a reasonable value for E_d for our experimental data using the pre-exponential value of 9 X 10^{-3} reported by Lauth and co-workers. However, we could vary the pre-exponential over a range of four orders of magnitude (10^{-6}-10^{-9}) with less than or equal to 20% error in the value of the full width at half maximum.

Another point of contention between these two investigations lies in the shape of the low-exposure desorption feature. We ovserve a much more asymmetric chemisorption peak than Lauth and co-workers. The asymmetry that we observe is typical for first-order desorption. The highly symmetric peak of Lauth and co-workers is more indicative of a second-order desorption state. First-order desorption is physically unreasonable for this particular desorption state, though. Hydrogen dissociates upon adsorption on transition metal surfaces, particularly at low coverages. Recombinative desorption must then take place, making this desorption process necessarily second-order.

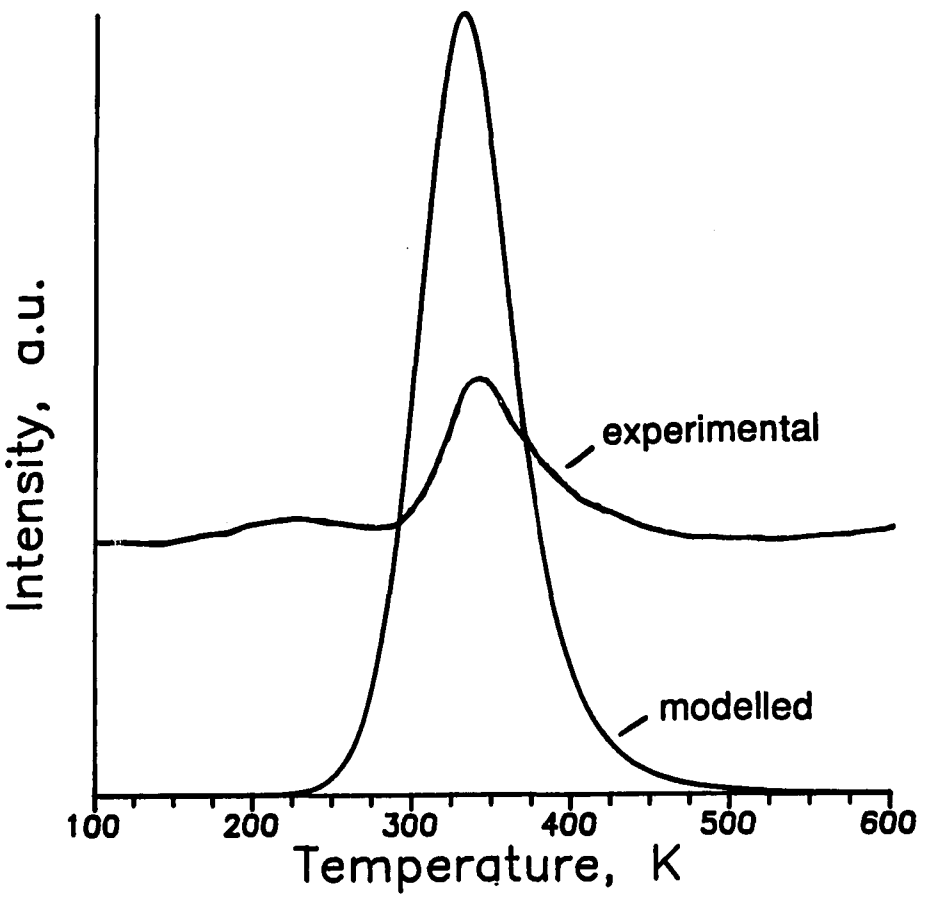

Figure 3. Comparison of experimental and modelled peaks

Both the desorption energy and the pre-exponential factor obtained by Lauth and co-workers are also typical for second-order desorption of hydrogen from transition metal surfaces.

Typical values for E_d range from 40-120 kJ/mol and pre-exponentials range from 10^{-2} to 10^{-6} $cm^2/(H\ atoms\ s)$. Our desorption energy of 42 kJ/mol falls at the lower end of this range, and our pre-exponential factor of 5×10^{-8} $cm^2/(H\ atoms\ s)$ is smaller than those commonly reported for these systems. However, the pre-exponential factor we report is still within the realm of physical possibility for second-order desorption.

Our pre-exponential value of 5×10^{-8} indicates that hydrogen atoms have a longer surface lifetime in our experiments than in those of Lauth and co-workers. Perhaps this is reasonable considering the difference in the preparative techniques for the crystals in the two investigations. We anneal our sample to 1695 K for 3 minutes between experiments. At this temperature, one can certainly imagine that many Ru atoms can move around in 3 minutes. Previously, we have discussed the possibility that terraces of both Ru(100) and Ru(010) exist on our surface (20). We expect that large terraces of Ru(100) and Ru(010) are formed during the 3 minute anneals to 1695 K. This surface preparation should be compared to that of Lauth and co-workers. They never anneal their surface above 1200 K. Therefore, one might conclude that the step density is much higher on their surface than it is on ours. This increased step density may explain the much larger pre-exponential value (and hence, shorter desorption times) they observe. Atoms prefer to adsorb at step sites, so if one assumes a mobile pre-cursor model for the adsorbate, the atoms are

expected to gather at the steps thereby making recombination and desorption a much faster process on a highly-stepped surface. But aside from the pre-exponentials, an energy difference still exists between these two systems. This too may be explained by the difference in the number of steps on the surface. The steps are the preferred binding sites because they are the most energetically favorable binding sites (i.e., the strongest chemisorption bonds can be formed there). Therefore, Lauth and co-workers should observe a higher binding energy for hydrogen than we do, and this is indeed the case.

As an aside, apparently the reason that these investigators chose not to anneal their surface above 1200 K is because they believe that Ru undergoes a bulk phase transition at ~1400 K (21). We find no evidence to support this phenomemon, though. In 1931, Jaeger and Rosenbohm reported transition points of Ruthenium at 1308, 1453, and 1773 K based on specific heat measurements (22). In 1957, Hall and Crangle contradicted the two low-temperature transition points based on powder diffraction results (23). And recently published phase diagrams for ruthenium indicate that no phase transitions are observed (24, 25).

Comparison of the low temperature states for this system is more complicated. Lauth and co-workers assign their low temperature state to a first-order desorption feature whereas our low temperature feature appears to exhibit second-order characteristics. The first-order behavior reported by Lauth and co-workers and the second-order behavior we observe are both physically reasonable. Both first-order and second-order desorption states have been observed for desorption of high

coverages of hydrogen from transition metal surfaces. We have not modelled the high-exposure feature in our data as interaction energies become important at these coverages. However, based on rough calculations, we estimate that the desorption energy for the feature we observe is similar to the energy reported by Lauth and co-workers (50 kJ/mol), but the pre-exponential value is obviously different by orders of magnitude since the desorption orders are different.

Finally a comparison of area vs. exposure data is in order. A significant change in the sticking coefficient is observed in both studies. However, even the point at which this appears to occur is different in our study than it is in the work of Lauth and co-workers. By comparing Figs. 1 and 2, one can see that the sticking coefficient changes drastically in our system at a coverage of about 3800 Torr sec. This corresponds to a point at which the β state is basically filled and the γ state is partially filled. Lauth and co-workers observe this change in sticking coefficient before their high temperature desorption state is even filled! Perhaps this too is related to the difference in step density between the two surfaces. The change in the sticking coefficient in the data of Lauth and co-workers at such a low exposure may indicate that this change is occurring as soon as the step sites are filled, whereas this "roll-over" does not occur in our investigation until all of the surface sites are actually filled.

CONCLUSIONS

We have studied the desorption of hydrogen from Ru(100). In this paper, we have reported the results of this investigation along with results of a recently published study by Lauth, Schwarz and Christmann. The differences in the results of these two studies have been highlighted and discussed in terms of possible differences in the surface structure which arise from differences in the preparative surface cleaning techniques. We suggest that the higher annealing temperature utilized in our investigation gives rise to larger terraces which allow different desorption kinetics than those that are observed by Lauth and co-workers. In general, we observe much smaller pre-exponential values and smaller desorption energies, indicating that hydrogen atoms must remain on our surface longer before recombination is accomplished, and that the adsorption sites available on our surface are less energetically favorable than those available on the Ru(100) surface of Lauth and co-workers. All of these results can be explained in terms of an increased step density on the surface of Lauth and co-workers, and this increased step density is easily explained in terms of their low-temperature surface preparation. One can conclude from these observations that the adsorption of hydrogen on Ru is extremely sensitive to surface structure.

ACKNOWLEDGEMENTS

This research is supported by the Director for Energy Research, Office of Basic Energy Sciences. Ames Laboratory is operated for the U.S. Department of Energy by Iowa State University under Contract No. W-7405-ENG-82.

REFERENCES

1. G. Lauth, E. Schwarz and K. Christmann, J. Chem. Phys. 91 (1989) 3729.

2. L.R. Danielsen, M.J. Dresser, E.E. Donaldson and J.T. Dickinson, Surface Sci. 71 (1978) 599.

3. H. Shimizu, K. Christmann and G. Ertl, J. Catalysis 61 (1980) 412.

4. P. Feulner and D. Menzel, Surface Sci. 154 (1985) 465.

5. M. Lindroos, H. Pfnür, P. Feulner and D. Menzel, Surface Sci. 180 (1987) 237.

6. M. Lindroos, H. Pfnür and D. Menzel, Surface Sci. 192 (1987) 421.

7. P. Hoffmann and D. Menzel, Surface Sci. 152/153 (1985) 382.

8. M.A. Barteau, J.Q. Broughton and D. Menzel, Surface Sci. 133 (1983) 443.

9. H. Conrad, R. Scala, W. Stenzel and R. Unwin, J. Chem. Phys. 81 (1984) 6371.

10. J.T. Yates, Jr., C.H.F. Peden, J.E. Houston and D.W. Goodman, Surface Sci. 160 (1985) 37.

11. C.H.F. Peden, D.W. Goodman, J.E. Houston and J.T. Yates, Jr., Surface Sci. 184 (1987) L405; 194 (1988) 92.

12. P.J. Feibelman and D.R. Hamann, Surface Sci. 179 (1987) 153.

13. P. Feulner, H. Pfnur, P. Hofmann and D. Menzel, Surface Sci. 184 (1987) 1411.

14. D.W. Goodman, T.E. Madey, M. Ono and J.T. Yates, Jr., J. Catalysis 50 (1977) 279.

15. Y.-K. Sun and W.H. Weinberg, Surface Sci. 214 (1989) L246.

16. M.Y. Chou and J.R. Chelikowsky, Phys. Rev. Letters 59 (1987) 1737.

17. P.K. Leavitt, J.L. Davis, J.S. Dyer and P.A. Thiel, Surface Sci. 218 (1989) 346.

18. P.A. Redhead, Vacuum 12 (1962) 203.

19. J.S. Wang, Proc. Cambridge Phil. Soc. 34 (1938) 238.

20. P.K. Leavitt and P.A. Thiel, J. Vac. Sci. Technol. A, in press (1990).

21. H. Pfnür and K. Christmann, Institute for Physical and Theoretical Chemistry, The Free University of Berlin, Berlin, Germany, private communication, 1989.

22. F.M. Jaeger and E. Rosenbohm, Proc. Acad. Sci. Amst. 34 (1931) 808.

23. E.O. Hall and J. Crangle, Acta Cryst. 10 (1957) 240.

24. P. Villars and L.D. Calvert, Pearson's Handbook of Crystallographic Data for Intermetallic Phases, Vol. 3 (American Society for Metals, Metals Park, OH, 1985) p. 3108.

25. T.B. Massalski, Ed. in chief, Binary Alloy Phase Diagrams, Vol. 2 (American Society for Metals, Metals Park, OH, 1986) p. 1987.

APPENDIX 4.

ULTRA-HIGH VACUUM CHAMBER DESCRIPTION

INTRODUCTION

All of the experiments discussed in this thesis were performed in a standard ultra-high vacuum chamber, which required assembly before experiments could be started. The chamber was designed by Dr. P. A. Thiel and constructed by Norcal Products, Inc., Yreka, CA. The chamber was fabricated out of 1/8" cross-forged, 300 series stainless steel, allowing a typical base pressure of 1×10^{-10} Torr.

Table 1 describes the location and use of each of the ports in the top half of the chamber. The angle θ describes the angle of each port with respect to the 8" view port located at the "front" of the chamber. Positive angles are taken clockwise from this port, and negative angles are counter clockwise. The angle Φ describes the angle of each port with respect to the focal plane of the chamber: positive angles for those ports above the focal plane and negative angles for those below. Figure 1 is a schematic of a top-view of the chamber. The dotted circle in the center of this drawing is the focal point circle. Along this focal point circle, there are several "clusters" of ports aimed at a particular point on the focal point circle. Figure 2 is a schematic of a side-view of the chamber. Note that a cluster of ports appears on the right side of this figure. The numbers that appear on the flanges in these figures correspond to the flange numbers in Table 1.

Table 1. Location and use of ports on the top half of the vacuum chamber

Number	Flange-face to focal point distance	Current use	θ Angle of focal point	Φ Angle with respect to focal plane	Flange outer diameter
1	10.000"	view port	-75°	0°	8.000"
2	8.000"	electron gun	-75°	30°	2.750"
3	8.000"	ion gauge	-75°	-30°	2.750"
4	5.000"	empty	-37.5°	0°	4.500"
5	4.000"	view port	0°	0°	8.000"
6	5.250"	mass spectro-meter	60°	0°	4.500"
7	4.500"	view port	60°	45°	2.750"
8	4.500"	low pressure doser	60°	-45°	2.750"
9	4.375"	high pressure doser	60°	0°	2.750"
10	4.000"	EELS	115°	0°	10.000"
11	8.000"	empty	115°	-25°	2.750"
12	10.000"	view port	180°	30°	2.750"
13	4.000"	Auger	180°	0°	8.000"
14	5.250"	empty	-90°	0°	4.500"
15	4.500"	view port	-90°	45°	2.750"
16	4.500"	empty	-90°	-45°	2.750"
17	4.375"	ion gun	-90°	0°	2.750"

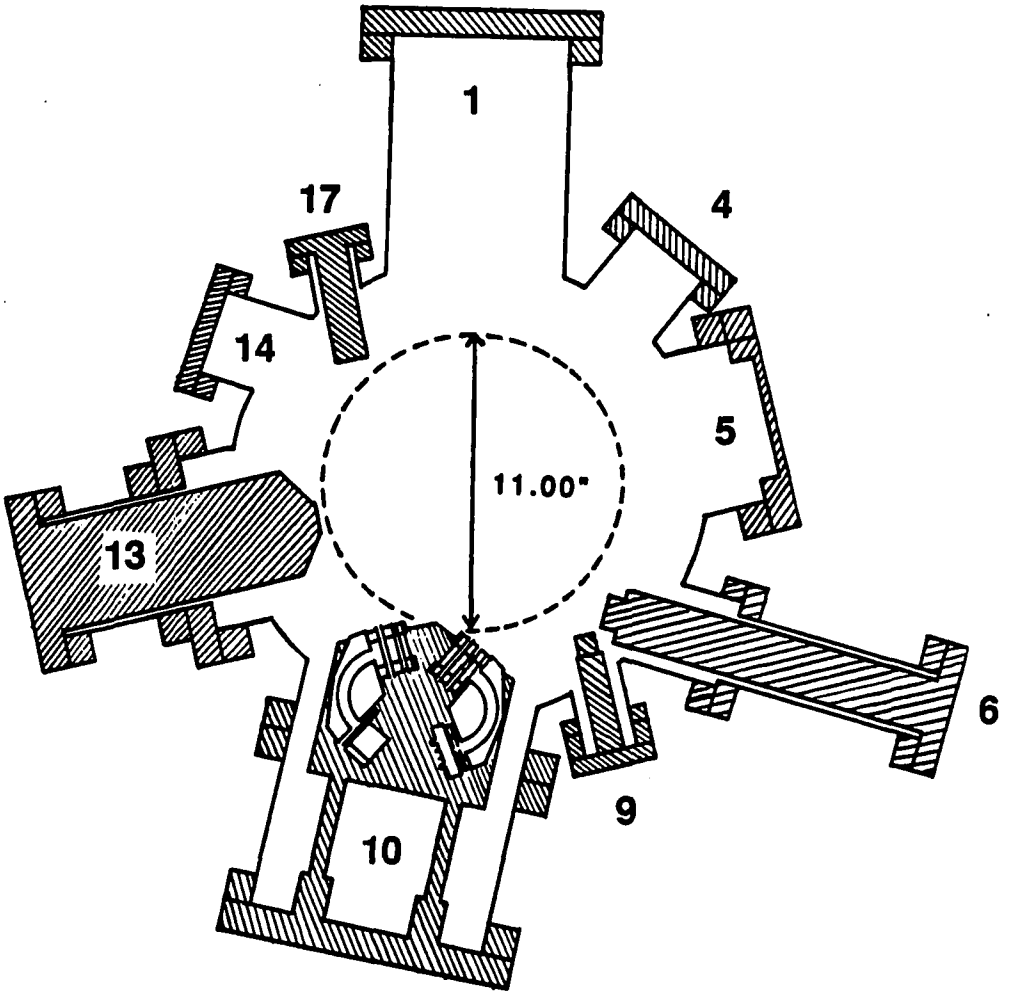

Figure 1. Schematic of the top-view of the chamber

The dotted line in the center represents the circle of focal points. The numbers on the flanges correspond to the flange numbers in Table 1.

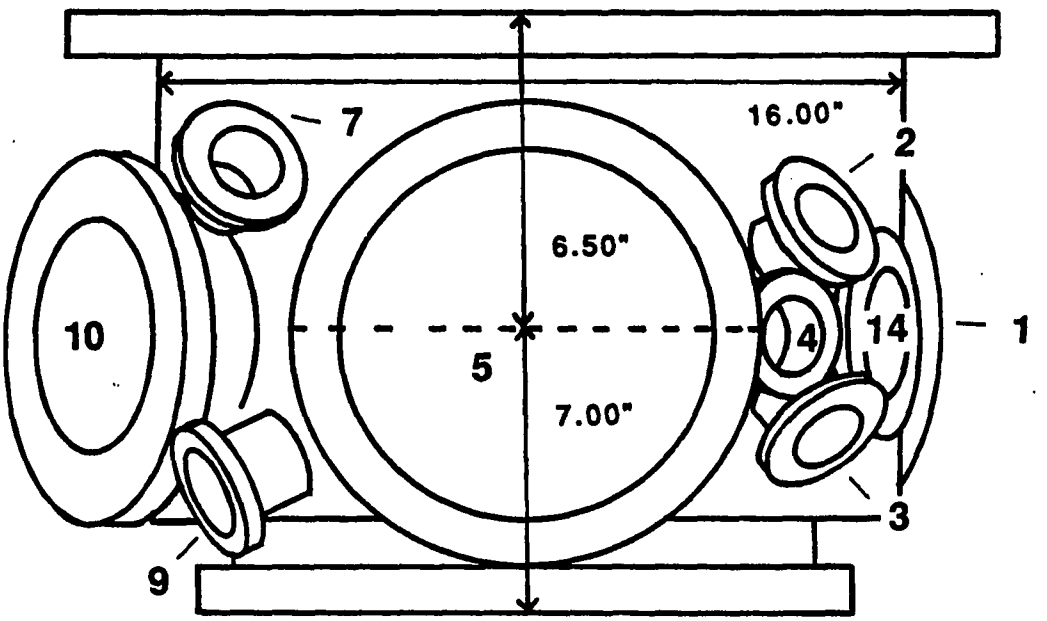

Figure 2. Schematic of a side-view of the chamber top

Note that a cluster of ports appears on the right side of the figure. The numbers on the flanges correspond to the flange numbers in Table 1.

The bottom portion of the chamber connects to all of the pumps used in the chamber, as well as the leak valves used to backfill the chamber with low pressures of various gases. Figure 3 is a top-view of the chamber basewell. Note that there are three large ports, ninety degrees from one another, and on the fourth side of the basewell there are several smaller ports. The main pumps for the chamber are installed on the three large ports of the basewell. Figures 4 and 5 are side views of the chamber basewell. Some of the small ports shown in Fig. 5 are inlets for various gases. In the following paragraphs, the location of various components in the vacuum system and their typical operating condition is discussed.

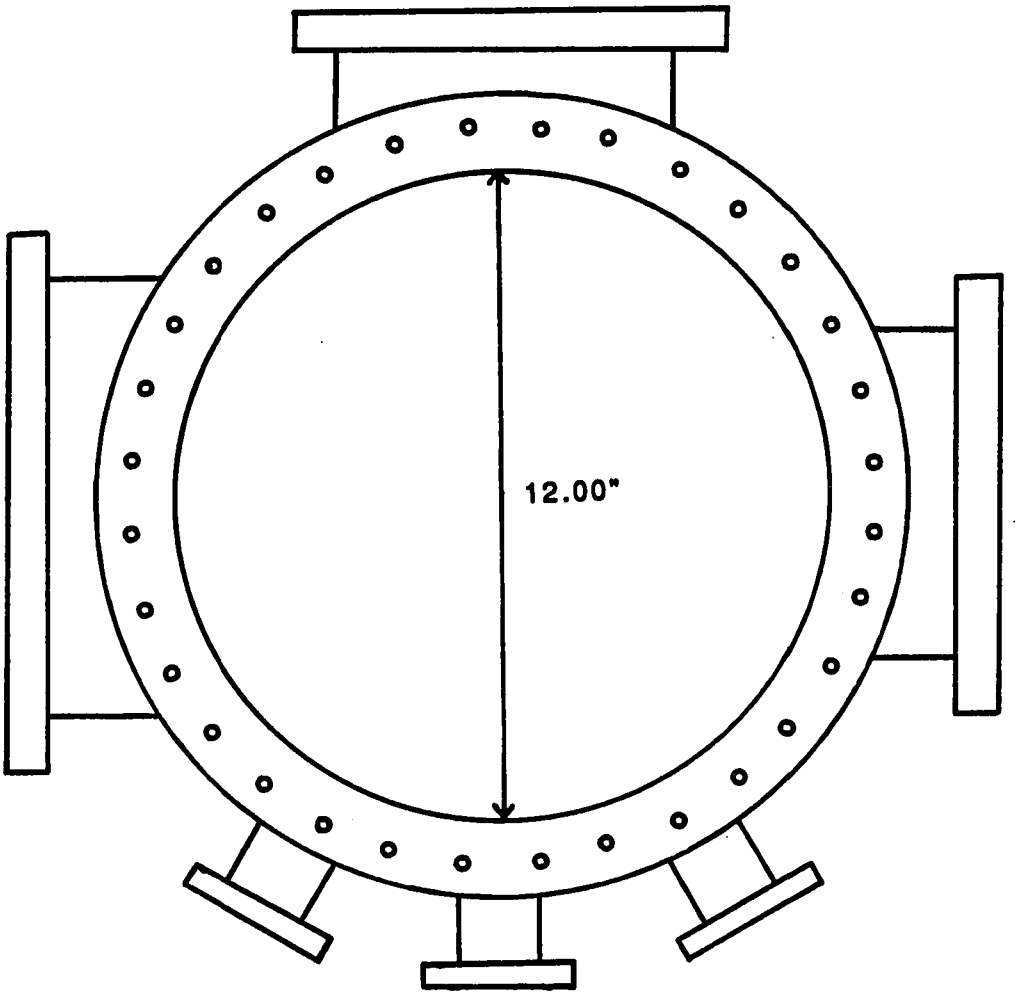

Figure 3. Top-view of the chamber basewell

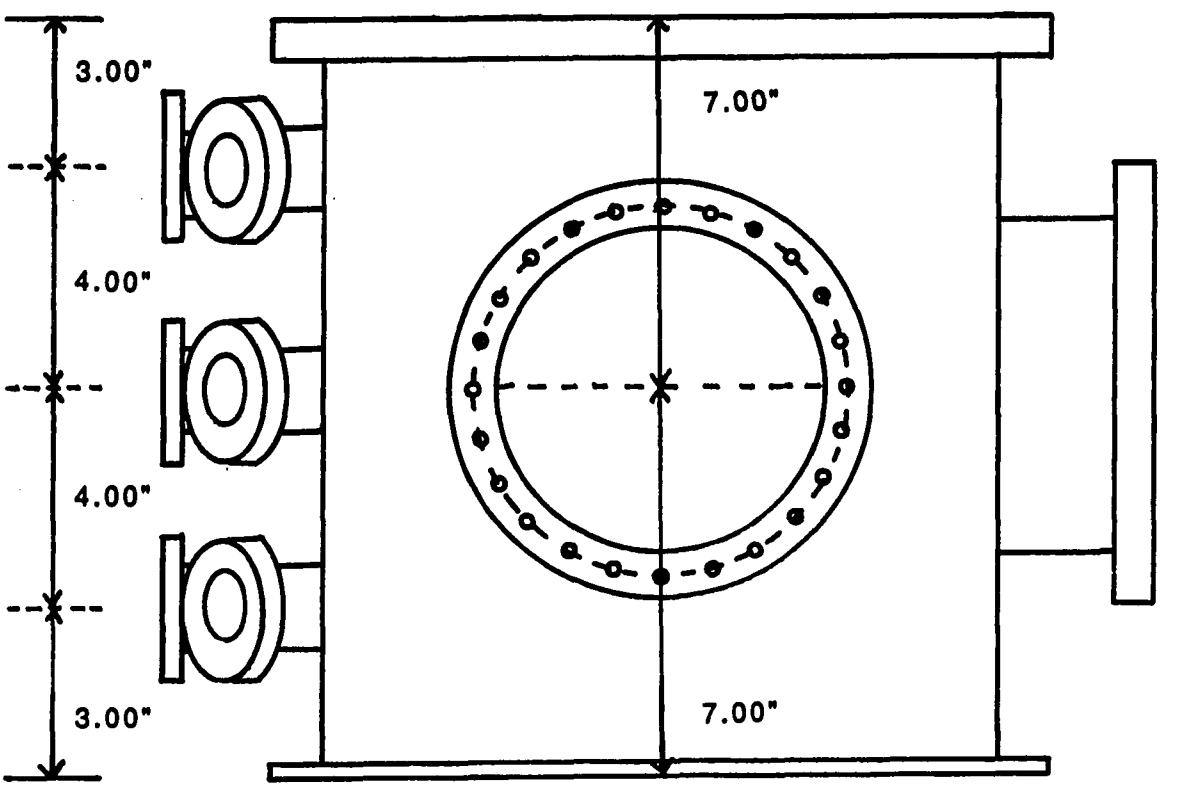

Figure 4. Side-view of the chamber basewell

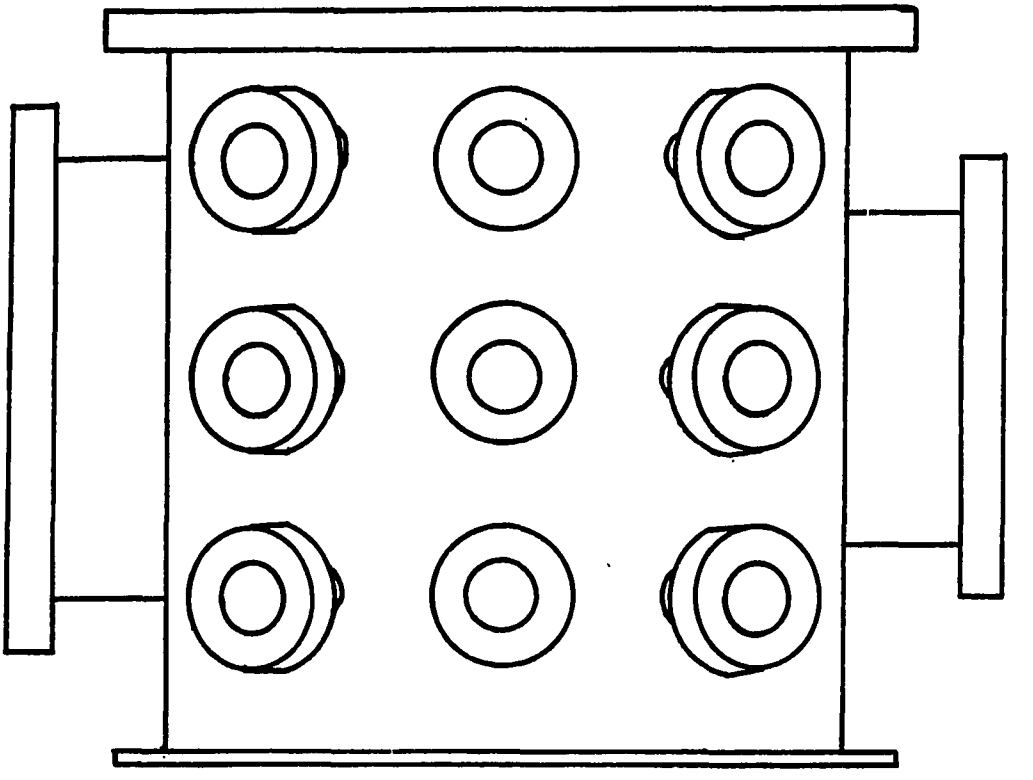

Figure 5. Side-view of the chamber basewell showing the configuration of the small ports

CHAMBER TOP

Spectrometers

Mass Spectrometer

The mass spectrometer is located in port number 6. It is a UTI model 100C quadrupole mass spectrometer with a mass range of 0-300 amu and an electron impact ionization source. The distance from the top of the ionizer of the mass spectrometer to the focal point circle of the chamber is 0.9375". Typically, the mass spectrometer is operated with an emission current of 2.00 mA and a multiplier voltage of ~2200 V. Recently, this multiplier voltage was increased to 2340 V. However, all of the data included in this thesis was recorded with the multiplier voltage at the former value. The mass spectrometer has been modified after Johnson (1) to reduce the electron current at the sample surface from 10^{-5} to 10^{-11} A. This modification decreases the amount of electron stimulated desorption and decomposition at the sample surface. For all of the experimental data reported in this thesis, no spatially-limiting aperture was present at the front of the ionizer. The mass spectrometer is interfaced to an IBM-AT computer so that up to eight masses can be monitored essentially simultaneously for thermal desorption experiments.

Electron Energy Loss Spectrometer

The electron energy loss spectrometer (EELS) is a McAllister model PS200 spectrometer in the double-C configuration with angular resolution. It is located in port number 10, and the distance from the monochomator output to the focal point circle is 2.875". The EELS is enclosed in a μ-

metal shield shaped like a coffee can. The bottom of this "coffee can" can be opened to allow movement of samples into the focal point of the spectrometer. The spectrometer is typically operated with a beam current of 1.9 A and a beam energy of -4.9 V. These settings result in typical resolution of 10-12 meV and count rates of ~1-200,000 cps. For further details on the EELS spectrometer see Ref. 2.

Auger Spectrometer

The Auger spectrometer is a PHI model 10-155 single pass cylindrical mirror analyzer (CMA). It is located in port number 13 with a distance of 3.25" from the end of the spectrometer to the focal point circle. Typical operating conditions for the Auger spectrometer are an emission current of 1.2 mA, a beam voltage of 2 kV, modulation voltage of 1 V peak-to-peak, and modulation frequency of ~7 kHz. These conditions result in a resolution greater than 5%.

Miscellaneous Components

Ion Gun

The ion gun is located in port number 17, with a filament-to-focal point distance of 0.6875". It is a home-made gun fabricated after the design of Bermudez and Thomas (3). The ion gun filament is constructed of 0.5 mil W wire, and the anode is fabricated from 10 mil Ta foil. Typically, the gun is operated with a filament current of 2.1 A and an accelerating voltage of 400 V. This results in an emission current at the sample surface of approximately 5×10^{-5} A for 5×10^{-5} Torr Ar pressure.

Ion Guage

The hot filament ion guage, located in port number 3 is a Varian model CVT 844. Typically, at a pressure of approximately 1 X 10^{-10} Torr, the grid voltage is -184 V, the ion collector current has a value of -3.68 X 10^{-7} A, and the emission current is -4.4 X 10^{-5} A. The gauge is calibrated by electronically supplying a simulated ion collector current to the controller.

Electron Gun

A Cliftronics model CE406W electron gun is located in port number 2. This gun is currently not in use.

Dosers

One collimated molecular beam gas doser is located in port number 9. This doser was used for all of the experiments reported in this thesis. The end of this doser is located 1.125" from the focal point. The doser consists of a 2 μ conductance-limiting aperture followed by a 0.5 mm directional aperture. Exposures reported through this doser are defined in Torr s corresponding to the product of pressure behind the conductance-limiting aperture and the dose time. Typical pressures behind the conductance-limiting aperture for dose times of about 50 s are 3 to 20 Torr. A schematic of this doser is shown in Fig. 6.

Originally, this particular doser was designed with a microcapillary array instead of the 0.5 mm aperture at the front of the doser. However, we suspect that this silica microcapillary array induced decomposition of the perfluorinated ether, so it was replaced with the stainless steel aperture. See Appendix 1 for more details.

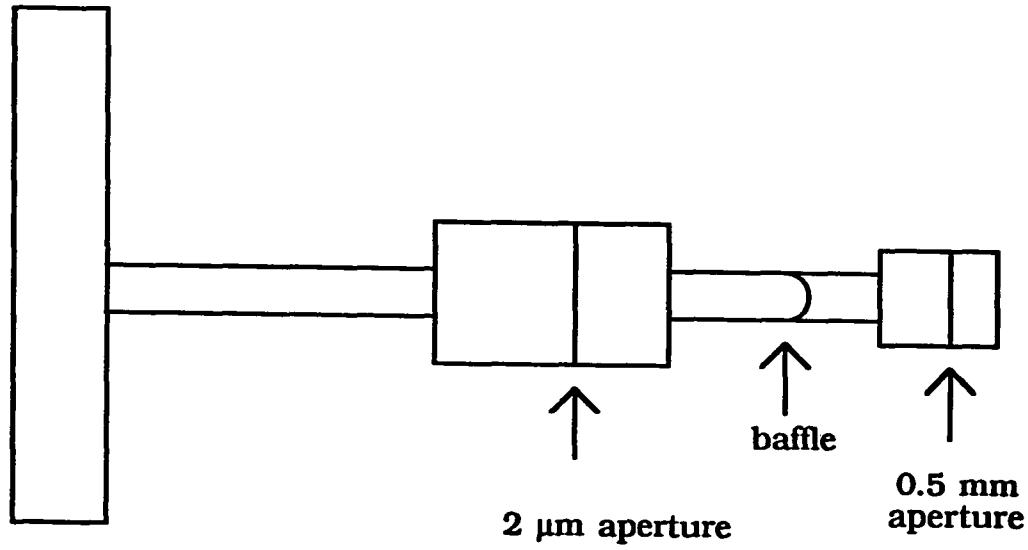

Figure 6. Schematic of the high pressure doser

A second gas doser is located in port number 8. This doser is also located approximately 1" from the focal point, but this doser is located about 0.25" above the plane of focal points as well. So the sample must be raised from the focal point circle to access this doser. Since this gas doser is designed to be used with much lower pressures behind it (~10 mTorr range), a much larger conductance-limiting aperture can be used (20 μ). Finally, a 0.5 mm directional aperture is again utilized at the end of the doser.

Others

All other ports in the top half of the chamber are either currently blanked off or they contain view ports as indicated in Table 1.

CHAMBER BASEWELL

Pumps

Ion Pump

The ion pump is located -90° from the front of the chamber. It is a Varian 110 L/sec triode ion pump.

Titanium Sublimation Pump

The titanium sublimation pump (tsp) is located 180° from the front of the chamber. It is a Varian model 0017 tsp cartridge which is enclosed in a liquid-nitrogen-coolable shroud.

Turbo Molecular Pump

The turbo molecular pump is located 90° from the front of the chamber. It is a Balzar's model TCP300 with a pumping speed of 330 L/sec.

Valves

There are three Varian model 5106 variable leak valves located on the front of the chamber basewell, on the top three small ports pictured in Fig. 5. These valves are used to back-fill the chamber with various gases.

Others

The other ports located on the front of the basewell are either empty or they contain valves necessary for venting the chamber or pumping it down.

REFERENCES

1. A.L. Johnson, Ph.D. Dissertation, University of California at Berkeley, 1986.

2. M.R. Columbia, Ph.D. Dissertation, Iowa State University, to be published.

3. V.M. Bermudez and R.E. Thomas, J. Vac. Sci. Technol. A 1, (1983) 1557.

ACKNOWLEDGEMENTS

I would like to thank my research advisor, Dr. Patricia Thiel, for her unending patience and support throughout my graduate career. In particular, I would like to express my appreciation for her role in my development of a better self-image and a marked improvement in my speaking abilities.

My thanks also goes out to the past and present members of the Thiel group. During my stay in Ames, this group has been like a second family to me. In particular, I would like to thank Mike Columbia, with whom I have worked closely for the past five years. Together, we managed to assemble and upkeep the vacuum chamber used for the experiments in this thesis. I am also grateful for fruitful discussions with and constructive criticism from Dr. Mary Walczak, Diane Sanders, Barb Nielsen and Rochelle Lockridge.

I appreciate the companionship of my friend and critic, Ray Garant. He has helped me to maintain my sanity and my perspective on life for the past three years.

Finally, I would like to acknowledge my family for their love and support. Home has been a refuge from the anxieties of graduate school in the past few years. The rest and relaxation I enjoy in the company of my family have not been matched elsewhere.

This work was performed at Ames Laboratory under contract No. W-7405-eng-82 with the U.S. Department of Energy. The United States government has assigned the DOE Report number IS-T-1416 to this thesis.